N79-22619

NASA CR-150296

cy 1

SPACE-BASED SOLAR POWER CONVERSION AND DELIVERY SYSTEMS STUDY

VOLUME III

MICROWAVE POWER TRANSMISSION STUDIES

(NASA-CR-150296) SPACE-BASED SOLAR POWER CONVERSION AND DELIVERY SYSTEMS STUDY. VOLUME 3: MICROWAVE POWER TRANSMISSION STUDIES Final Report (Raytheon Co.) 195 p HC A09/MF A01

N79-22619

Unclas
CSCL 10B G3/44 19217

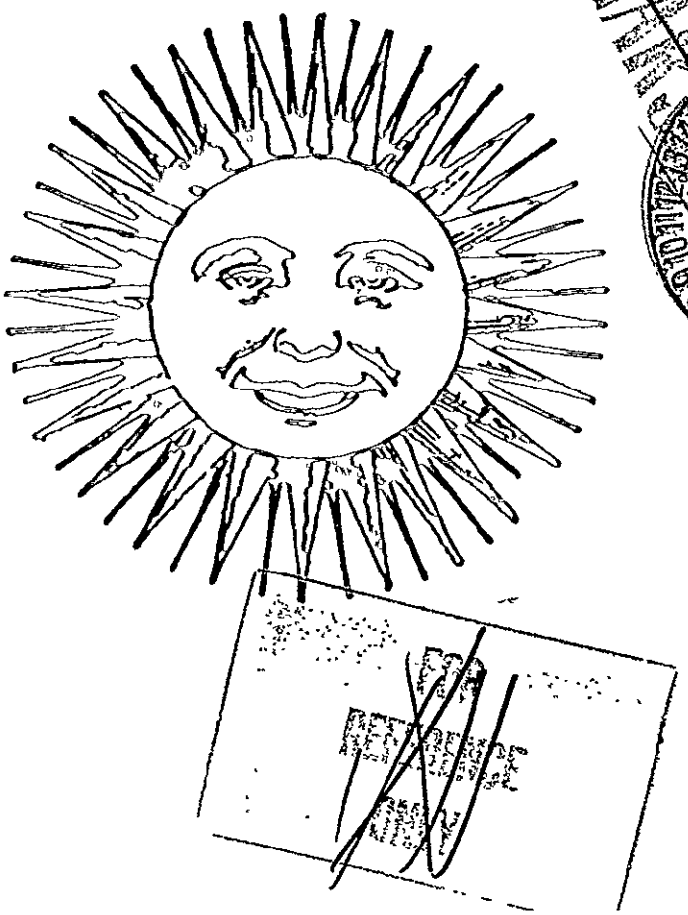

SPACE-BASED SOLAR POWER CONVERSION & DELIVERY SYSTEMS STUDY

VOLUME III

MICROWAVE POWER TRANSMISSION STUDIES

Prepared for

NATIONAL AERONAUTICS AND SPACE ADMINISTRATION
GEORGE C. MARSHALL SPACE FLIGHT CENTER

Under Subcontract ECON-0003 from

ECON, INCORPORATED
Princeton, New Jersey

Prepared by

Raytheon Company - Equipment Division
Wayland, Massachusetts

1 MARCH 1977

ABSTRACT

A study of the Microwave Power Beam Ionosphere effects and critical interfaces between the Microwave Power Transmission System (MPTS) and the Satellite was conducted by Raytheon as part of the NASA/MSFC continuing studies on the feasibility of power transmission from geosynchronous orbit. Theoretical predictions of ionospheric modifications produced by the direct interaction of the MPTS on the earths' upper atmosphere are used to determine their impact on the performance of the Microwave Power Beam and Pilot Beam System as well as on other RF systems effected by the ionosphere. A technology program to quantitatively define these interactions is developed.

Critical interface areas between the MPTS and the satellite which could have a major impact on cost and performance of the power system are identified and analyzed. The areas selected include; use of either a 20 kV versus 40 kV Amplitron, thermal blockage effects of Amplitron heat radiation by the satellite structure, effect of dielectric carry-through structure on power beam, and effect of material sublimation on performance of the Amplitron in Geosynchronous Orbit.

FOREWORD

This volume is the final report on Raytheon's portion of the "Space-Based Solar Power Conversion and Delivery Systems Study", Phase III, on Microwave Power Transmission. The study was performed for the NASA Marshall Space Flight Center under prime contract NAS 8-31308 to ECON, Incorporated of Princeton, New Jersey. Raytheon carried out their portion of the study under Subcontract ECON-0003. The Microwave Power Transmission Study was carried out under the overall cognizance of C. A. Wendell.

The Microwave Power Beam Ionospheric Effects portion of the study was directed by A. H. Katz. Participating in the ionospheric analysis were L. Holway and G. Meltz.

The critical interface portion of the study was directed by J. J. Rossi with the power distribution analysis done by J. Haley.

Special acknowledgement and thanks go to Mr. Walter Whitacre of NASA for his guidance and critical contributions, and to Mr. Owen Maynard of Raytheon for sharing his experience to assure the study complemented but did not duplicate prior work.

TABLE OF CONTENTS

TABLE OF CONTENTS
(CONTINUED)

TABLE OF CONTENTS
(CONTINUED)

TABLE OF CONTENTS
(CONTINUED)

LIST OF FIGURES

LIST OF FIGURES
(CONTINUED)

LIST OF TABLES

LIST OF TABLES
(CONTINUED)

1.0 INTRODUCTION

This volume describes Raytheons' contribution to the Space Based Solar Power Conversion and Delivery Systems Study. The study consists of two distinct areas although both are related to the MPTS. The areas of study are:

1. Power Beam Ionospheric Effects
2. Analysis of Critical Interfaces between the Satellite and the MPTS

In addition, the impact of these studies on the cost model utilized by ECON was evaluated and the results can be found in Section 4.0 of this volume.

1.1 POWER BEAM IONOSPHERIC EFFECT

The first area involves a study of the effects of the power beam on the earth's upper atmosphere, specifically, the ionosphere. Previous studies have indicated that the effects of the MPTS on the ionosphere are likely to have enough impact to warrant an experimental verification program before a commitment to a full scale prototype SSPS could be made. As such, Raytheon was requested to initiate an in-depth study which would:

1. Identify the ionospheric modifications caused by the power beam
2. Determine the resultant performance limitations these effects would have on both the MPTS (Pilot Beam) and other RF systems which are affected by ionospheric phenomenology.
3. Establish a technology program which by the mid 1980's would provide the necessary data on which to base a decision on whether and how to proceed with the full scale prototype vis-a-vis ionospheric effects.

Section 2.0 of this volume describes the Power Beam Ionospheric Effects. Further, Section 2.1 provides a description of the objectives, method of approach, key results, and an overview of the recommended technology program.

1.2 ANALYSIS OF CRITICAL INTERFACES BETWEEN THE SATELLITE AND THE MPTS

The second study area consisted of the investigation of four critical interface areas which had indicated having the most impact on the cost and performance of the MPTS. The four areas investigated are:

1. The potential cost and performance advantages of using a 40 kV distribution system for the Amplitron in lieu of the 20 kV system which is the current evident baseline configuration.

2. Detailed evaluation of the thermal blockage from the rear of the Amplitron by the satellite mast, flex joint and antenna subarray structure to determine if the thermal blockage exceeds 5%, the current baseline design specification.

3. Effect of the dielectric material connecting the solar panels on the satellite on the microwave power transmissions to determine if significant perturbations in the either the power beam, sidelobe or phase control system will occur.

4. To determine if sublimation products local to the Amplitrons would have any effect on the performance of the Amplitrons.

Section 3.0 of this volume describes the investigations of the critical interfaces between the MPTS and the satellite where Section 3.1 provides a discussion of the key results and an overview of the recommended technology program.

2.0 POWER BEAM IONOSPHERIC EFFECTS

2.1 INTRODUCTION

2.1.1 GENERAL

A series of studies have and are being conducted to identify and analyze critical areas which are related to the economic aspects and the risk involved in the design, construction and operation of the SSPS. One of the most sensitive of these areas is the environmental impact. This includes the environmental effects of the launch vehicles, the interaction between the microwave transmissions from GEO to the earth and the earths' atmosphere, and the distribution of RF energy at and near the earths' surface. Raytheon, in a previous NASA study[14], identified and analyzed the effects of the microwave transmissions through the earths' atmosphere which included the effects on the ionosphere, the effects of the ambient and disturbed ionosphere on the microwave beam, and the effects of the lower atmosphere on the microwave transmissions. Table 2.1 lists the areas addressed by that study and also provides a brief synopsis of the results. In that study, it was recognized that one of the most critical aspects was the potential effects the microwave transmissions would have on the ionosphere. It was recommended that a further study, specifically related to the ionospheric effects be undertaken.

As a result, the current study described in this report was conducted. It was also recognized that the study of atmospheric processes is such a broad and complicated discipline that the present effort should be concentrated on what was believed to be the most critical issues so as to be most productive. Therefore, areas such as the following were not addressed by the study: a) chemistry of the upper atmosphere; b) neutral gas heating and related phenomena; c) optical emission phenomena; d) excitation of neutral winds and of atmosphere gravity waves; and e) generation of harmonic radiation, or in general, of RFI. It is recognized that further effort must be directed toward each of these areas and in fact as will be shown, a significant technology program will be required to more fully assess the ionospheric impact alone. The study on ionospheric effects paid particular attention to the possible impact the resultant ionospheric changes would have on systems which are known to be affected by the identified ionospheric

phenomenology. The results of this study show that the ionospheric effects are potentially of great significance and could seriously constrain development of the SSPS Program unless a technology program is implemented to quantify the impact and establish acceptable limits of the ionospheric changes brought about by the microwave transmissions from the SSPS. As such, a multi-year development program has been defined with the objective being to quantify the risks associated with the ionosphere and allow tradeoffs to be made with respect to the economic benefit associated with high power densities versus the results of adverse ionospheric effects.

TABLE 2.1 ENVIRONMENTAL EFFECTS - PROPAGATION
RESULTS OF PREVIOUS STUDY

I. For the atmosphere at frequencies below 3 GHz:
   a. Absorption and scattering effects are small except for wet hail.
   b. Refraction changes and gradients cause negligible displacement or dispersion of the high power beam and do not degrade significantly a ground based pilot beam phase front as seen at the transmitting antenna. (NOTE: Current study indicates statement still valid, however, risk is sufficiently significant to warrant experimental verification.)

II. For the ionosphere at frequencies above 1 GHz:
   a. Refraction changes and gradients cause negligible displacement or dispersion of the high power beam, and do not degrade significantly a ground based pilot beam phase front as seen at the transmitting antenna.
   b. Absorption and scattering effects are negligible.
   c. Faraday rotation has only a small effect for a linearly polarized receiving antenna.
   d. Changes in electron density caused by power densities of 20 mW/cm^2 and above at 2.45 GHz need to be investigated for possible effects on other ionosphere users.
   e. Possibility of harmonic radiation from the ionosphere (radio frequency interference effects) should be investigated.

2.1.2 TECHNICAL OBJECTIVES

The effects of the Microwave Power Transmission System (MPTS) power beam on the ionosphere are of importance because of the possible interactions between the induced ionospheric disturbances and phase control system as well as the power beam itself. Of similar importance is the impact on "other users" by the ionosperic modifications caused by the power beam. Systems affected by ionospheric modifications, exclusive of the MPTS itself, will be defined as "other users". These include navigation systems such as Omega and HF communication systems, for example.

The specific subtasks of this study are to:

1. Assess the MPTS ionospheric potential changes and resultant effects on other users as well as the microwave power beam and its phase control system;
2. Outline a technology and demonstration program designed to establish quantitative information on these effects to guide the selection of limiting values for power density and thus approach a near optimum SPS System with controlled impact on the ionosphere and its other users.

Three questions were posed which this study has addressed:

1. Are ionospheric modifications significant and, if so, what is the critical range of power densities (i.e., power level of SSPS system) that must be examined during an experimental program?
2. Are the potential effects on "other users" significant enough to cause high risk during operation of SSPS systems and warrant an experimental program to quantitatively assess the risks?

3. Do we need an experimental verification program to minimize risk of SSPS with respect to the ionosphere and, if so, what are the requirements for this experimental program?

Section 2.1 of this report will describe the technical approach and provide a summary of the key results of this study. Sections 2.2 and 2.3 describe in detail Raytheon's assessment of the ionospheric modifications and effects on other users, respectively. Finally, Section 2.4 establishes the requirements of a technology and demonstration program as well as briefly describes the implementation of this program and its Rough Order of Magnitude (ROM) costs.

2.1.3 TECHNICAL APPROACH

The first task of this study was to provide an assessment of the ionospheric effects caused by the MPTS. Based on theoretical models of ohmic heating, the magnitude of the ionospheric effects in both the F-layer and D-layer have been calculated at 20, 80 and 320 mW/cm^2 power densities for both a southwest and northeast U. S. site. These are representative of the densities to be associated with 5, 10 and 20 GW output SSPS respectively. Results of this analysis indicate the occurrence of large electron temperature increases (several thousands of degrees) and electron density decreases (10 to 40%) in the F-layer (the F-layer is the height range where the peak ionospheric electron densities are observed). Two sites were evaluated because the orientation of the earth's magnetic field and elevation angle from the ground station to the array in space depends on site location, and it was found that F-layer effects will vary with site location. In addition to the F-layer effects, simulations indicated that D-layer effects (where maximum absorption of radio waves occurs) showed large temperature increases accompanied by increases in the electron density. At frequencies below 20 MHz, this results in an increased absorption of radio waves which pass through the disturbed region. The D-region effects are not site dependent because the motion of the electrons is not restricted to magnetic field lines, as is the case in the F-region.

Theoretical predictions have not yet advanced to the point of providing a complete picture of the effects on the ionosphere. Because of the complex nature of the power beam interactions with the ionosphere, an experimental program will be required to more fully assess the ionospheric effects. To determine the impact of the ionospheric modifications on other users, it was necessary in this study to assume that the induced perturbations would be similar to ionospheric perturbations that occur naturally. Knowledge of how the naturally occurring ionospheric perturbations affect these users exists in the literature and can be used to estimate the impact of the MPTS on similar users. Two issues will have to be resolved by any proposed technology program before this assumption can be validated:

1. Are the power beam ionospheric effects more or less intense than the naturally occurring phenomena and do they increase the occurrence statistics of these phenomena?

2. Are the power beam effects limited to the region that the power beam intersects the ionosphere or will the effects occur over larger geographical regions?

The first issue is important because ionospheric effects, such as geomagnetic storms or periods of intense scintillations, do occur which significantly degrade performance of many systems. They occur infrequently enough so that the percentage of time that significant degradation occurs is small. However, continuous heating by a power beam could produce these effects a large percentage of the time.

The second issue needs to be addressed because natural phenomena occur over large and dispersed geographical regions, while the power beam effects, where they occur, would be over particular regions. A further point is that although one power beam might not cause significant perturbations in terms of the region disturbed, the total system involves the use of over 100 power beams which significantly increase the regions disturbed and thereby increase the probability of adverse interactions with other users.

A preliminary assessment of these issues was made by comparing the ionization depletion in the F-layer predicted by theoretical models of ohmic heating with disturbances caused by naturally occurring magnetic storms. The magnitude of the power beam disturbance compares in magnitude with the natural phenomena caused by magnetic storms. It is not yet known how the geographical distribution of the MPTS disturbance compares with the naturally occurring disturbance. However, the comparison does show that the effects of the MPTS are not insignificant when compared to naturally occurring phenomena and that this natural phenomena is known to cause serious disturbances to users which interact with the ionosphere.

The next task was to assess the potential effects of the ionospheric modifications on other users. The number of systems which potentially are affected by the ionosphere is too large to be fully explored here. The approach taken was to select specific examples which span the RF domain in generic systems such as navigation, communication and DOD radars. Clearly only the systems currently in use or envisioned to be in use over the next ten years can be included. Systems that might be utilized when the SSPS is operational can only be speculated upon. The purpose of the approach used was:

1) to indicate the extent of the interaction with other users;

2) to establish requirements of a technology program which includes evaluation of the effects of the ionospheric modifications on other users;

3) to establish a framework within which the design of future systems can accommodate the ionospheric effects of the power beam.

Based on the above studies, it was determined that an experimental program would be required to fully define the ionospheric effects of the MPTS. Requirements were established based on several criteria:

1. Power output with associated power densities required to establish an economically viable system;

2. Maximum power output and power densities allowed by environmental considerations, including ionospheric effects as well as limited consideration of biological effects.

It was determined that the likely range of system power output was from 4 to 7 GW, which corresponds to peak power densities from 14 to 43 mW/cm^2 and associated sidelobe power densities $\simeq$ 0.06 to 0.17 mW/cm^2.

2.1.4 SUMMARY OF KEY RESULTS AND RECOMMENDATIONS

1. Ionospheric modifications by the power beam are not insignificant and enough uncertainty exists in current models and predictions to warrant an experimental verification program.

2. A large number of systems ("other users") could be adversely affected by the ionospheric modifications and the impact of the MPTS on these systems has to be quantitatively specified.

3. The power density threshold where ionospheric modifications become significant is as low as 15 mW/cm^2, which corresponds to a 4 GW MPTS. Current theoretical studies indicate increased risk at power densities above approximately 50 mW/cm^2 (depends on site location), which corresponds to a 7 GW system, and the likelihood of a viable SSPS system above 7 GW is small (also supported by increased biological risks).

4. Economic studies by ECON have indicated that there is a decreasing economy of scale below 4 GW output power (See Volume V of this study).

5. Based on Items 3 and 4 above, the likely range of operation is from 4 to 7 GW and a technology program has been developed which will quantitatively assess the ionospheric impact of a 4 to 7 GW SSPS.

Based on the above results, a three-pronged technology program is recommended:

1. Theoretical Studies

   A. Establish a two-dimensional steady state theoretical model of the ionosphere under the influence of microwave power transmissions. Include in the model the effects of horizontal motions.

   B. Include the effects of plasma instabilities caused by ionospheric modifications by the power beam.

   C. Continue evaluation of potential ground based heating experiments at 2.45 GHz, particularly to determine the viability of small scale experiments to validate extrapolation of heating experiments performed at lower frequencies 20 - 60 MHz to 2.45 GHz.

2. Experimental Program: Ground Based Heater

   A. Establish a ground based heating facility which simulates the MPTS heating due to power densities over a geographical region similar to that of an operational MPTS. A ground based heater at a frequency of 20 MHz is recommended.

   B. Establish diagnostics to fully evaluate effects of heating on other users. Include operation of other user systems where feasible.

3. Orbital Experimental Program for MPTS Phase Control

The approach to establishing the earliest MPTS test antenna configuration at GEO (Geosynchronous Earth Orbit) is as follows:

Configure prototypical MPTS antenna elements to be tested at GEO such that a minimum beam width will result in spot size in the ionosphere and on the ground which approaches the size of the operational system. The spot size is inversely proportional to the array dimension so that a 100m array will give a

spot size about ten times that of a 1000m array. First order effects of the ground based pilot beam phase front disturbances by the ionosphere should then be measurable in terms of power density distribution on the ground with a 100 meter power transmitting array at GEO and ground based command system requirements to compensate for these disturbances should be able to be determined. A 100 meter linear power transmitting phased array at GEO should be sufficient to provide meaningful data on one axis for a minimum of power at GEO. Ionospheric disturbances, due to natural causes, of the power beam would be measurable in terms of power density distribution changes at the ground; however, the disturbances due to power beam heating of the ionosphere would not be present. Simulation of the power beam heating from the ground would properly influence the pilot beam and its effects on the power beam; however, the power beam itself would not be properly influenced unless the simulated heating were over a region approximately ten times that of the operational configuration. The orbital experimental program for MPTS phase control technology development and demonstration is therefore currently recommended as follows:

A. Establish a small scale system at GEO. For the mid 1980's a linear array 100 meters in length is recommended for the microwave transmission subsystem. During the early 1990's it may be prudent to place a 1 km linear array at GEO before full commitment to the prototype.

B. Establish a ground based pilot beam whose transmission path traverses the ionosphere region being modified by the ground based heater.

C. Establish a ground based monitoring system which measures the received power density distribution of the power beam from the linear array at GEO.

This experiment will determine the following:

1) Feasibility of retrodirective phase control of a phased array in space using a ground based pilot beam as the primary means of keeping the power beam focused and pointed on target;

2) effect of ionosphere, both ambient and ground based as modified by heater, on pilot beam system;

3) effect of ambient ionosphere on location of power beam and power spreading.

2.2 IONOSPHERIC PHENOMENA

2.2.1 GENERAL

Since an S-band microwave transmitter has a frequency that exceeds the maximum plasma frequency in the ionosphere by more than two orders of magnitude, the amount of power that can be absorbed from a beam transmitting microwave power from a geostationary satellite to the ground is a negligible fraction of the total transmitted power. However, this energy is absorbed directly by the free electrons in the ionosphere, and, as the calculation to be presented here will show, the temperature of these electrons can be raised to levels which are thousands of degrees hotter than the temperatures which exist in the undisturbed ionosphere.

In order to see this clearly, we write down the following formula for the wave number of microwave radiation passing through a region of the ionosphere in which the electron density is n.

$$k = \frac{\mu \omega}{c} + j\alpha \quad , \tag{1}$$

where the index of refraction is

$$\mu = 1 - (e^2/2\epsilon_o m)\left(\frac{n}{\omega^2}\right) \tag{1a}$$

and the absorption coefficient is

$$\alpha = (e^2/2\epsilon_o mc)\left(\frac{n\nu}{\omega^2}\right) \tag{1b}$$

These formulas assume that the (angular) microwave frequency ω is much larger than either the plasma frequency, $\omega_p = (ne^2/m\epsilon_o)^{1/2}$, or ν, the effective collision frequency for electrons with heavy particles.

Equation (1a) shows that the change in refractivity is largest where the plasma density is greatest, and this occurs at the peak of the F-region near 300 km altitude. On the other hand, Equation (1b) shows that the maximum absorption occurs at the altitude where the product $n\nu$ is largest. Since ν decreases exponentially with altitude, this occurs at a much lower altitude. During the daytime, when substantial ionization exists in the D-region (60-90 km) the peak absorption occurs near 70 km.

The microwave power beam has too high a frequency for attenuation to be significant. For example, the power flux, which is attenuated at the rate $e^{-\beta x}$ where $\beta = 2\alpha$, is reduced at the insignificant rate of 5×10^{-6} dB/km. The D-region absorption can be increased by more than an order of magnitude in the region where the electrons are heated, due to an increase in both ν and n as we show below, but even then the absorption will still be insignificant for the power beam. However, it is necessary to look more carefully at the possibility of effects upon communication systems which interact with the D-region, such as HF systems and VLF navigation systems such as Loran and Omega.

For the 2450 MHz microwaves, the change in the index of refraction caused by an electron density of 5×10^5 at the F-region peak is only $\mu - 1 = -3.4 \times 10^{-6}$ which amounts to a phase change of 17 radians over a path length of 100 km.

The dissipation per unit volume in watts/m^3 is

$$Q = \beta \langle S \rangle = 2\alpha c \epsilon_o \langle E^2 \rangle = \frac{e^2 \nu n}{m \omega^2} \langle E^2 \rangle \qquad (2)$$

where $\langle S \rangle$ is the Poynting flux in watts/m^2 and the brackets indicate that the quantity is averaged over an RF cycle.

According to Equation (2), the ohmic heating for different frequencies and power densities will be proportional to S/f^2. Because of this relationship it is possible to duplicate the ohmic heating due to microwave transmissions from a solar powered satellite with much lower power densities, provided a lower frequency is used. In particular, a large body of experimental information has been developed during HF ionospheric modification experiments[1], carried on at Platteville, Colorado and at Aerecibo.

Figure 2.1 shows typical powers obtained from a 5 MHz transmitter producing 2 MW of power with an antenna gain of 17 dB. Such a transmitter produces a power density of 88 $\mu W/m^2$ at 300 km which dissipates as much heat as a power density of 2.2 mW/cm^2 at 2450 MHz. In the D-region, the HF transmitter produces a higher power flux of 2200 $\mu W/m^2$ which is equivalent to 53 mW/cm^2 in the power beam.

The HF beam is not correctly described by Equation (1) when the plasma frequency or the collision frequency is comparable to the HF frequency, and it suffers additional refraction, focussing and deviative absorption. In particular, near the reflection height for the HF beam, Airy "swelling" effects take place which amplify the beam power. One can picture this occurring as the result of the group velocity of the wave decreasing in the vicinity of the reflection point. The effect is to increase the effective power density by more than an order of magnitude, so that the HF ohmic heating in a narrow height interval (on the order of 1 - 2 km) becomes equivalent to the heating at 2450 MHz which is caused by power fluxes in the range of 20 - 100 mW/cm^2. In the HF modification experiments, these power fluxes were sufficient to trigger instabilities, to cause chanced airglow at 6300 Å and to produce field aligned structures which scatter radiation in the VHF and UHF bands. Although some of these instabilities, such as the parametric decay instability,[3-4] will not be excited as effectively by the microwave radiation as by the HF radiation, it seems reasonable to expect that 20 mW/cm^2 of 2450 Hz radiation may produce effects comparable to those observed during the ionospheric modification experiments. It is also appropriate to remind the reader that the history of the ionospheric modification experiments[1] showed many un-

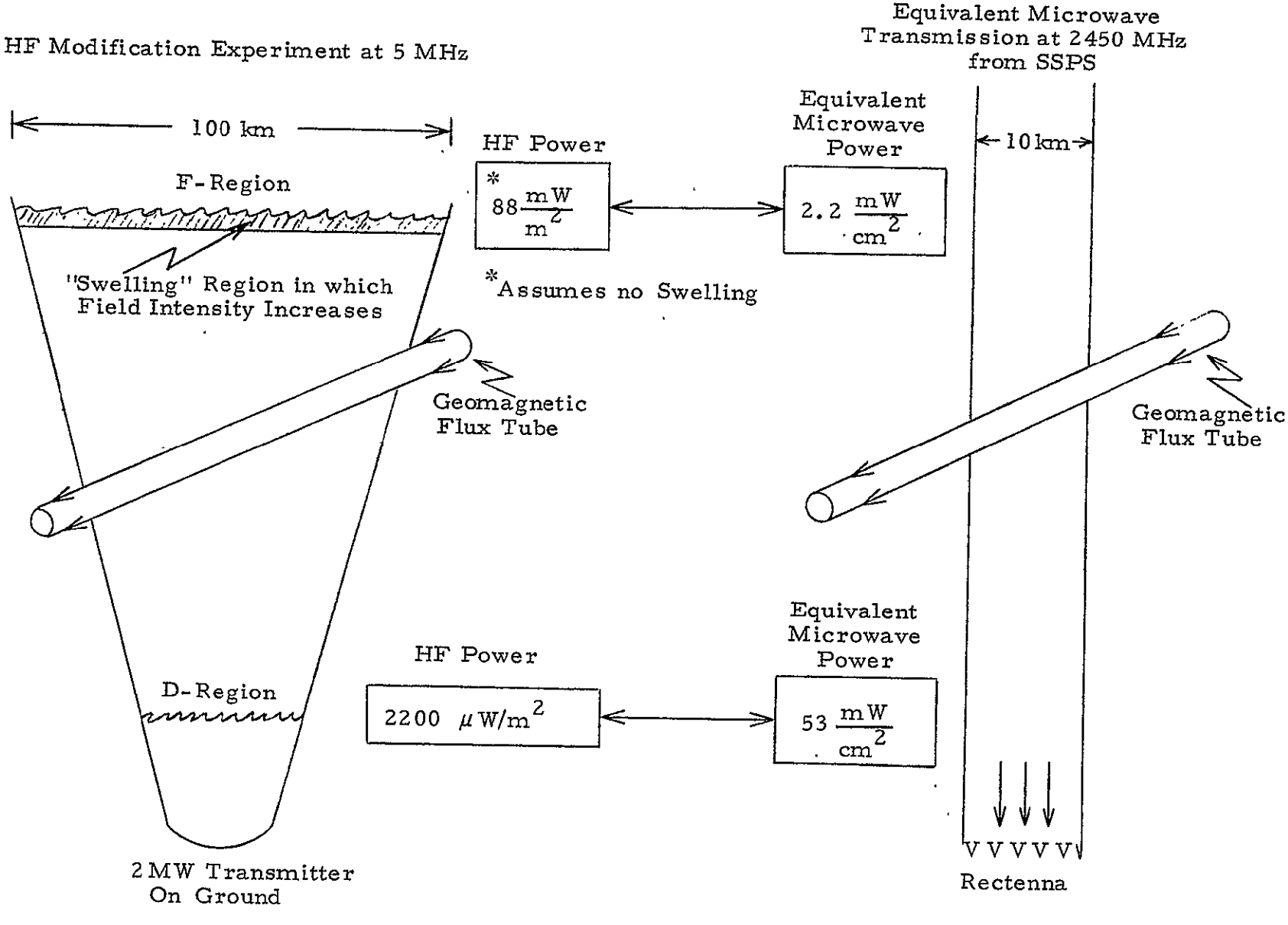

FIGURE 2.1 Equivalent HF and Microwave Ohmic Heating

anticipated effects observed during the experiments that were not predicted by theoretical analyses. In large part, these effects were difficult to predict because, in contrast to the ohmic-heating calculations which we are about to describe, these plasma instabilities involved nonlinear interactions which are able to affect the plasma in many and varied ways.

The most important differences between the HF modifications experiment and the microwave transmissions are the effects near the reflection point in the HF experiment. In the F-region, power fluxes equivalent to the microwave transmissions exist over a narrow altitude range below the reflection point. In this narrow range, the intensity oscillates, having several maxima, each of which are separated by distances less than 1 km. Another important difference is that the HF interaction region has a much greater horizontal extent, since the beam width in the F-region has a diameter of about 100 km, compared with a power beam diameter of 10 km or less.

2.2.2 F-REGION HEATING

The ohmic heating in the F-region changes both electron temperature and electron density. Although only the electron density directly affects the index of refraction, at high frequencies where Equation (1) is valid, the electron temperature is also important because it forces the expansion of the electronic fluid and also because it provides an indication of the amount of energy which is available to drive instabilities.

The most important feature of plasma motion above 120 km is that the plasma is forced to flow along the earth's magnetic field, and so the fluid motion can be treated as one-dimensional. However, an electro-dynamic drift with velocity $(\vec{E} \times \vec{B})/B^2$ exists at these altitudes which causes electrons and ions on each line of force to drift perpendicular to the earth's field. The drift varies with time of day, altitude, sunspot cycle and geographical location but has an average value near 50m/sec which causes the plasma to drift across a 10 km diameter power beam in about 200 seconds.

The electron temperature has been calculated by a computer program which numerically solves the coupled differential equations (1 - 3) given in a paper by Meltz and LeLevier[5]. In the model described in that paper, space charge effects cause the electrons and ions to move together so that they satisfy a single continuity and momentum equation, although separate equations are required for the temperatures T_e and T_i. Electrons gain energy directly from the power beam at the rate given by Equation (2) and, in the F-region, the most important cooling mechanism is thermal conduction by the electrons along the magnetic field. Although some heat is transferred to ions and neutral particles at all altitudes, the amount of heat deposited by the power beam is so large that most of it must be conducted down to lower altitudes near 200 km where collisions with neutral particles are frequent enough to cool the electrons. The thermal conductivity increases as $T_e^{5/2}$ so that, as the electronic temperature rises, the amount of heat which can diffuse downward increases. At night, a larger temperature increase will be caused by the power beam because there are fewer electrons to transport heat away from the dissipation region.

If the magnetic field makes an angle α with the power beam, a field line which passes through the center of the beam will be heated over a length $D/\sin\alpha$ where D is the beam diameter, so the temperature increase will be largest when the beam is nearly parallel to the field line.

For our examples, we assume that the satellite is on the equator, at a height $h = r_o/x$ above the center of the earth (where r_o is the earth's radius) and the power beam is transmitted in the meridian plane. Therefore, at a latitude θ, the beam will make an angle ψ with the horizontal, where

$$\psi = 90^\circ - \theta - \arctan\left(\frac{x \sin\theta}{1 - x\cos\theta}\right) \qquad (3a)$$

so that, when ϕ_D is the dip angle of the magnetic field

$$\alpha = \left|\phi_D - \psi\right| \qquad (3b)$$

Our calculations were made for both a Northeast site where $\phi_D = 72^\circ$ and $\theta = 42.48^\circ$ corresponding to conditions near Bedford, Massachusetts, and for a Southwest site where $\phi_D = 60^\circ$ and $\theta = 32^\circ$ corresponding to conditions near White Sands, New Mexico. The resulting angles were $\alpha = 31.5^\circ$ at the Northeast site as illustrated by Figure 2.2, and $\alpha = 7.6^\circ$ at the Southwest site, illustrated by the near-grazing angle shown in Figure 2.3.

The calculations have been carried out for S = 20, 80 and 320 mW/cm^2 for systems which have beam diameters of 10, 7.1 and 5 km respectively. These numbers have been associated with systems producing 5, 10 and 20 GW of total power and it is assumed that the higher power systems have larger antennas which allows smaller beam diameters to be achieved. The parameters used in the example are summarized in Table 2.2. Since the heat dissipation is proportional to $n\nu$, where ν is the total collision frequency for electrons colliding with neutrals and ions, it is useful to give the normalized dissipation $Q/n\nu$ in joules.

TABLE 2.2 Parameters for F-Region Heating

Location	Power Density (mW/cm^2)	$Q/n\nu$ (joules)	Beam Diameter (km)	Length of Field Line Heated by Beam (km)
Northeast	20	8.98×10^{-24}	10	19.2
	80	3.59×10^{-23}	7.1	13.5
	320	1.44×10^{-22}	5	9.6
Southeast	20	8.98×10^{-24}	10	75.6
	80	3.59×10^{-23}	7.1	53.5
	320	1.44×10^{-22}	5	37.8

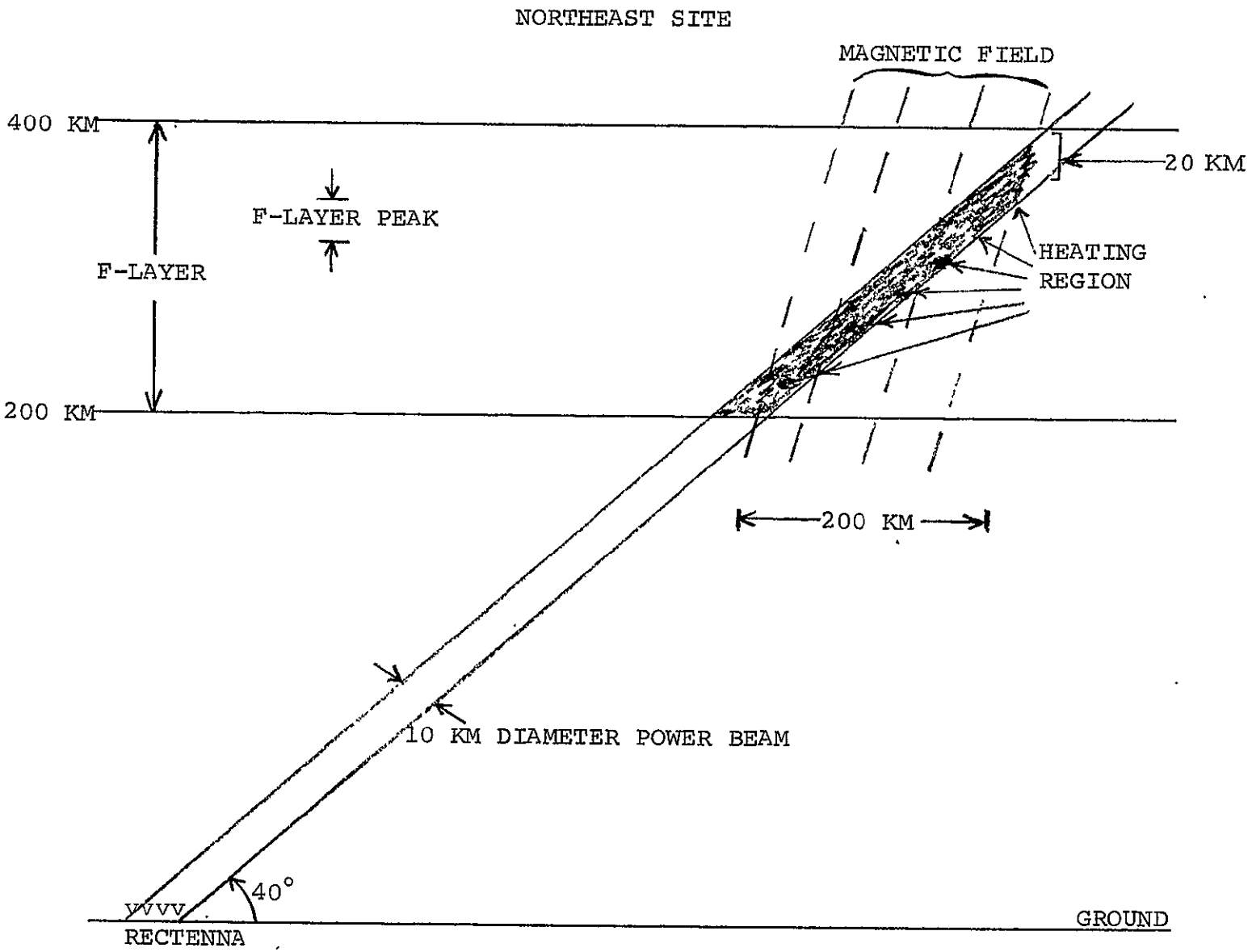

FIGURE 2.2 Relationship of the Earth's Magnetic Field and the Power Beam at a Northeast Site Near Bedford, Massachusetts.

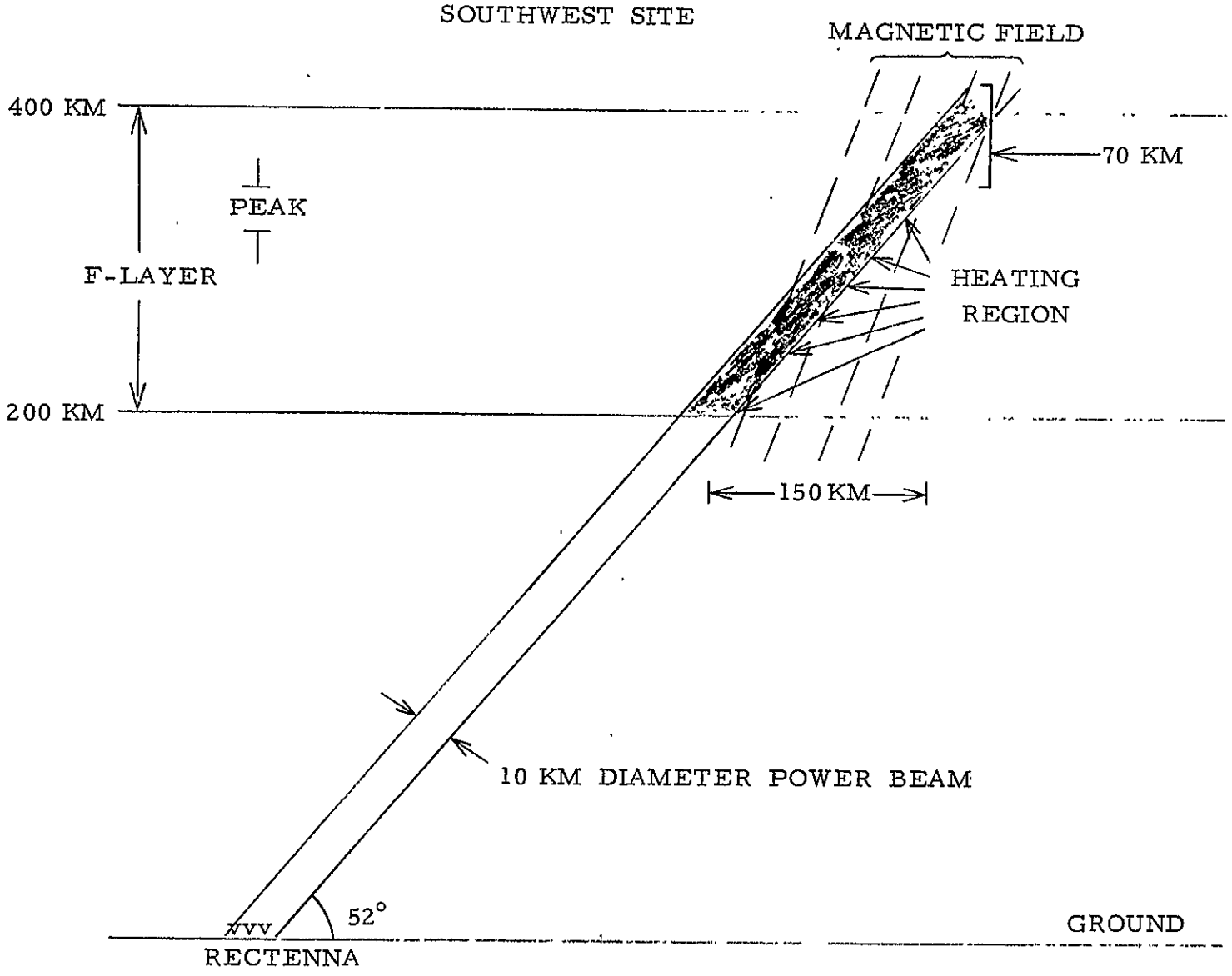

'IGURE. 2.3 A Near-Grazing Angle Between the Power Beam and the Geomagnetic Field at a Southeast Site, Near White Sands, New Mexico.

In order to describe the computer results, we will be able to orient ourselves most effectively if we begin by describing the time behavior of the electron temperature at the peak of the F-region when the beam is suddenly turned on. In these calculations, we have used atmospheric and ionospheric properties consistent with a night-time profile over Colorado, but we will use the beam orientation and magnetic field for the Northeast site. The temperatures, which are shown in Figure 2.4 for the three different power levels, increase from their undisturbed night-time temperature of 1200° K and approach a steady temperature after 20 - 30 seconds of heating. These steady temperatures are considerably higher than the increases of about 35 percent which occur in the HF modification experiments. The reason for this is that, even in the 20mW/cm^2 case, the power beam heats each field line over a distance of 19 km while the HF experiment produces a comparable magnitude of heat dissipation only over a narrow height range near the reflection height. However, we note that the high temperatures produced by the power beam will only occur in a slab about 10 km thick and parallel to the meridian plane containing the axis of the power beam.

The effect of continuing the heating over 3000 seconds is shown in Figure 2.5. The electron temperature increases rapidly and reaches a steady-state value about twice its undisturbed value in about 30 seconds. However, the electron density decreases much more slowly and requires about 2000 seconds before it reaches a steady-state value about 45 percent below the ambient. Physically, the reason the plasma expands so slowly is that it takes time for the heavy ions to physically move large distances as the thermal expansion pushes the plasma into the upper atmosphere. However, the heat is transmitted by the electrons and the thermal diffusion time is very fast. Even though the electron density is changing for 2000 seconds, the temperature can remain nearly constant because both the gain in heat from the beam and thermal conduction are proportional to the plasma density. Thus the absolute magnitude of the density does not change the temperature, although the manner in which the plasma is distributed as a function of altitude does.

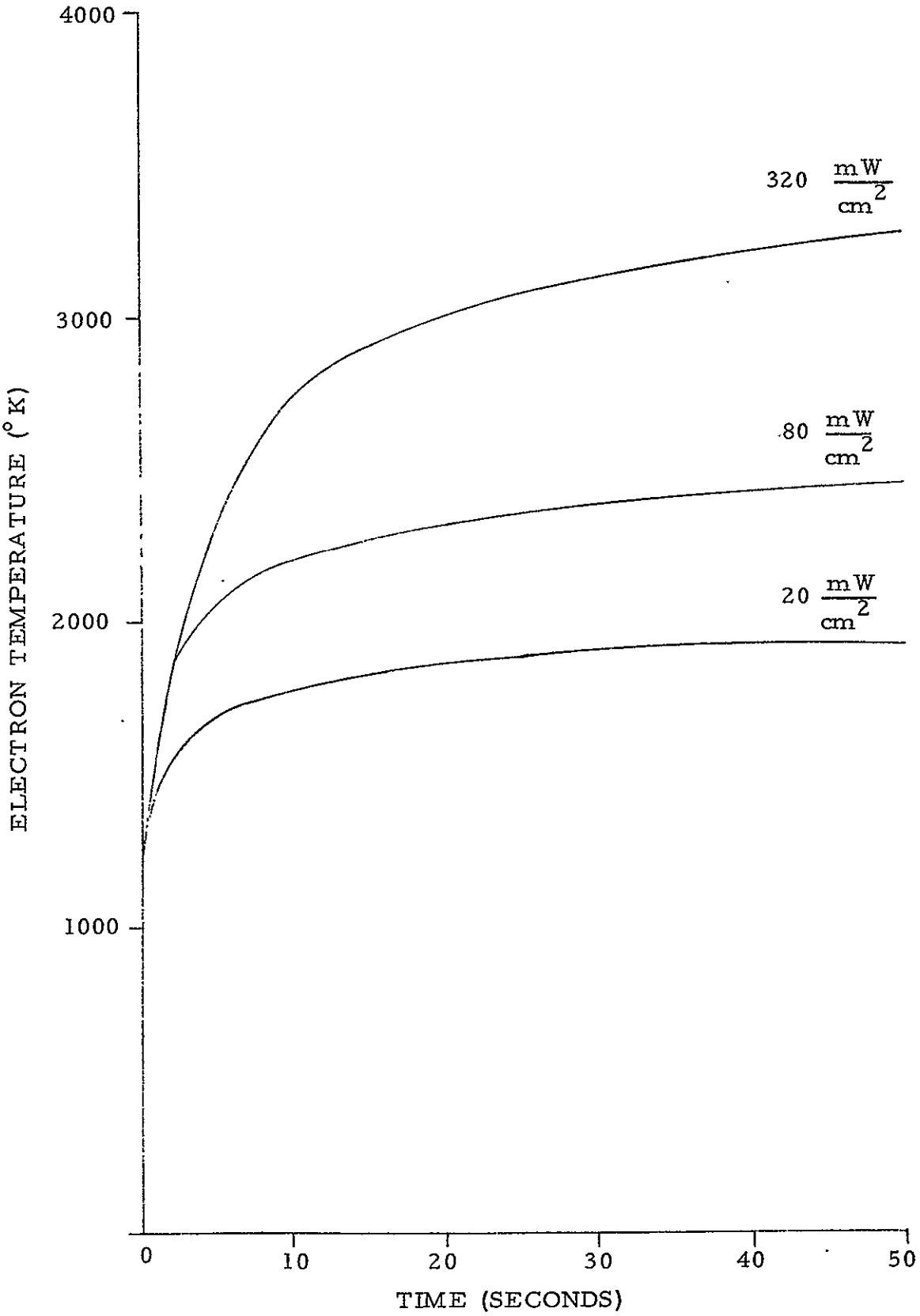

FIGURE 2.4 Time Behavior of the Electron Temperature at the Northeast Site at the Point Where the Power Beam is Heating the Peak of the F-Region at 300 km.

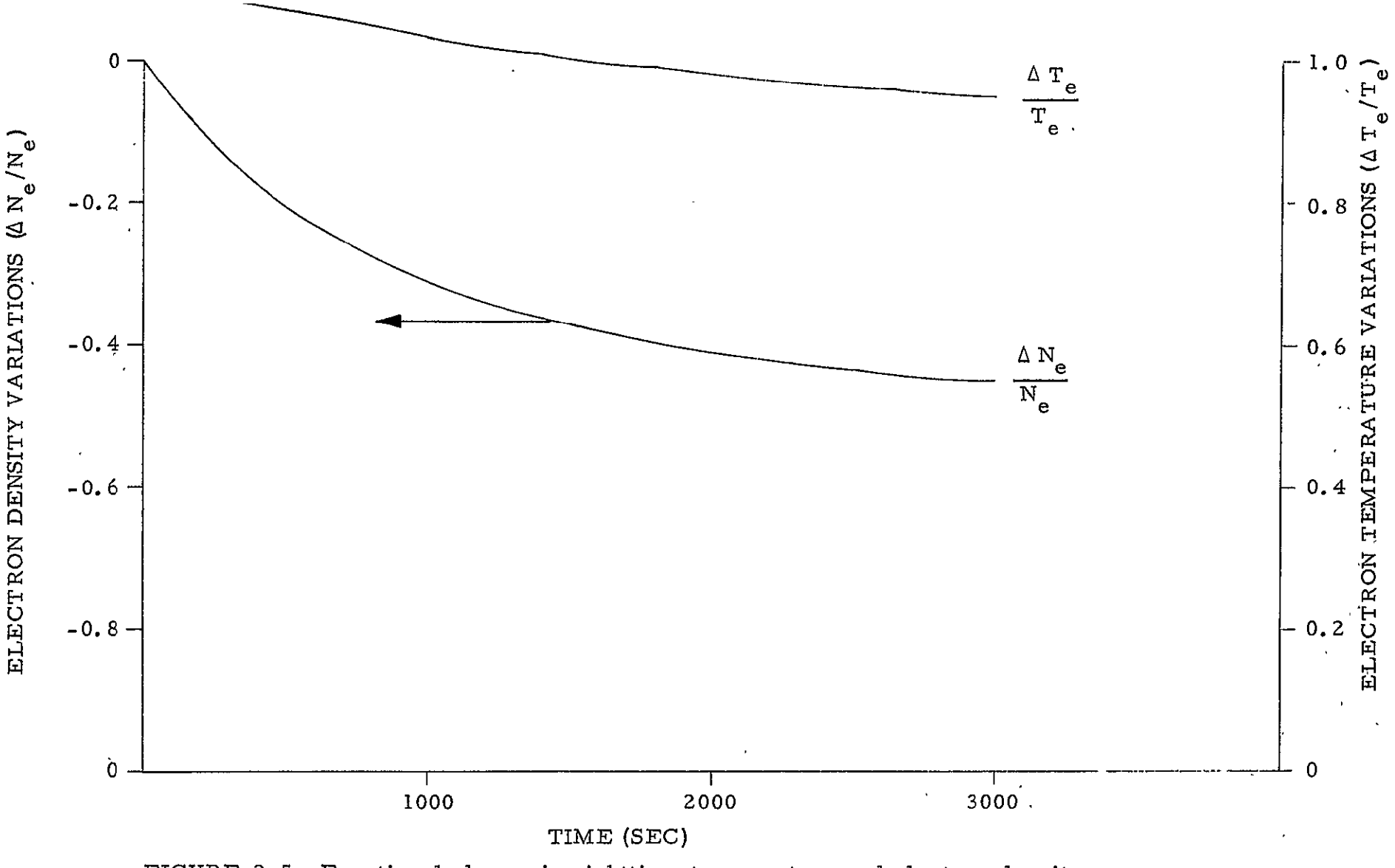

FIGURE 2.5 Fractional change in nighttime temperature and electron density over White Sands when 20 mW/cm^2 is applied to a line of force over a long period of time and over a height range from 260 to 325 km.

In interpreting these long-term results, it is necessary to remember the electrodynamic drift has a magnitude on the order of 50 m/sec. The best way to picture the effect is to imagine each line of magnetic flux moving perpendicular to itself, so that any given flux line will move through a 10 km beam diameter in about 200 seconds. Thus, the electron density will decrease for about 200 seconds reaching a level about eight percent below ambient and then increase toward ambient in a comparable time, because it will take the same time for ions to drift back into the "hole" as it took them to expand. Although we have not carried out this calculation, the temperature should decay back toward ambient in a time comparable to 30 seconds. These time scales will determine the physical dimensions of the disturbance under steady drifts.

The curves in Figure 2.6 show the electron temperature as a function of altitude for the fluxes and locations described in Table 2.1. Each curve gives the temperature for electrons along a single flux line, which were initially at the specified altitudes when the power beam was turned on. These curves give the temperature at $t = 200$ seconds which corresponds to the length of time the plasma remains in the beam; at this time the temperature has almost reached the steady state but the electron density would continue changing if the flux line could remain within the beam.

The heat is deposited near 300 km and most of it is conducted downward to altitudes near 200 km where the neutral particles are sufficiently numerous to cool the plasma. The energy loss processes used in the calculation include the excitation of rotational degrees of freedom in the diatomic gas and excitation of fine-structure transitions in atomic oxygen. The calculation does not include energy losses due to excitation of vibrational levels in N_2 which becomes progressively more important for $T_e > 2000^\circ K$. At the highest power fluxes, the vibrational losses may become noticeable, although the relatively low concentration of diatomic molecules in the F-region diminishes the importance of these losses, as discussed by Meltz and LeLevier[5].

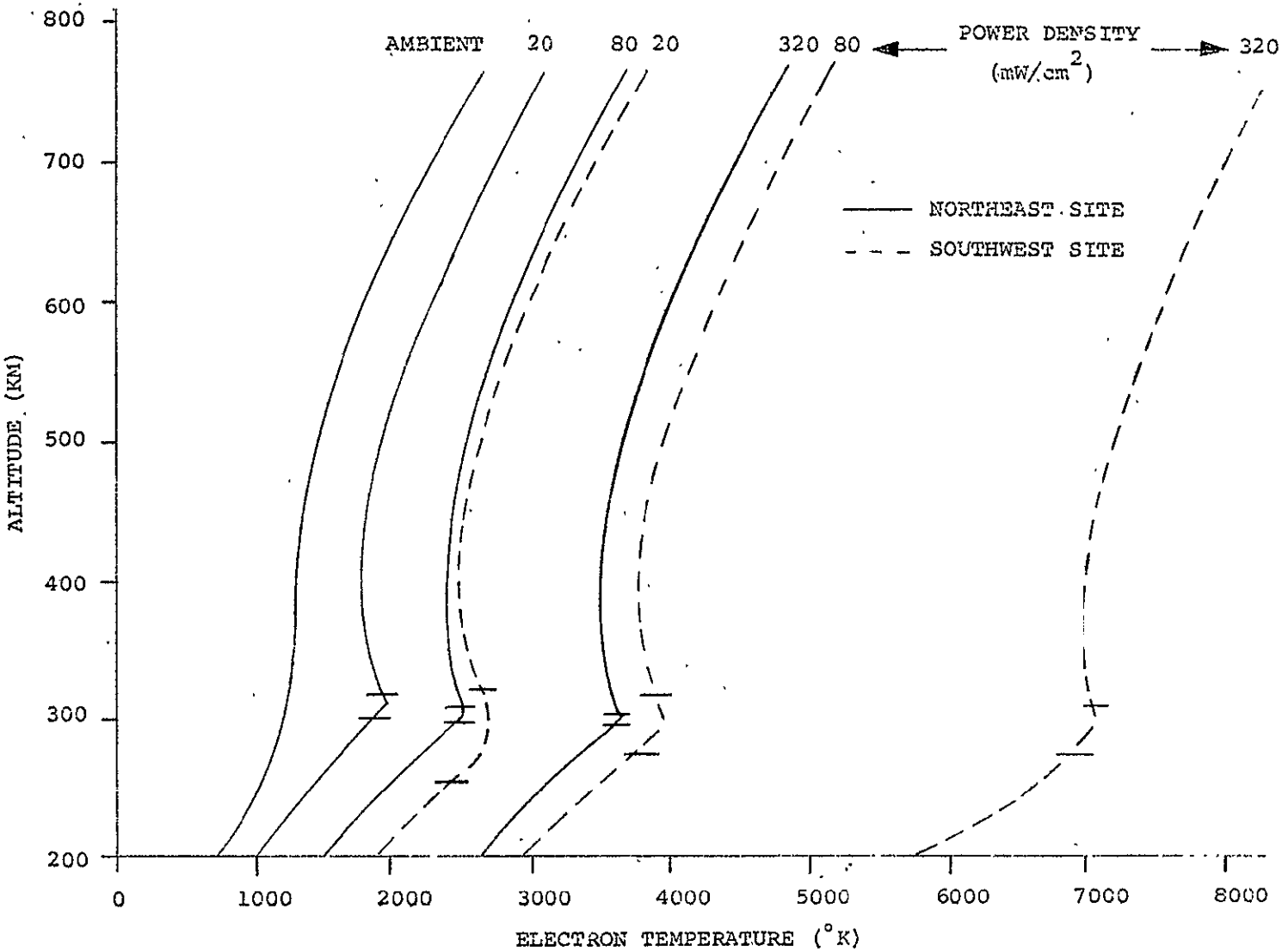

FIGURE 2.6 Steady-state temperature of the nighttime ionosphere as a function of altitude for the power levels and locations specified in Table 2.1. The slash marks on each curve specify limits for the altitude range, centered near 300 km, over which the flux line was heated.

The boundary conditions for the differential equations have been discussed earlier[5], but we generally try to move the boundary altitudes far enough away from the dissipation region so that the precise boundary conditions are not important. For example, the electron temperature in Figure 2.6 was assumed to remain at the ambient value at the bottom boundary at 170 km. This boundary condition is only approximate; yet it causes little error in the electron temperatures above 200 km because most of the thermal energy is absorbed by the neutral gas before it can be transported down to 170 km. The temperature rise in the neutral gas is insignificant because its concentration is so much greater than the electron concentration.

Contours of the fractional increase in electron temperature in the meridian plane containing the axis of the power beam are shown in Figure 2.7. The largest increases are about 50 percent for the 20 mW/cm^2 power beam, and occur in the immediate vicinity of the beam near the peak electron density. However, an increase of 25 percent occurs at points hundreds of kilometers above the beam. These high temperatures would only exist in a plane slab about 10 km thick and parallel to the meridian plane.

The electron temperature as a function of altitude during daytime operation of the solar-powered satellite is shown in Figure 2.8. A comparison with Figure 2.6 shows that the ambient daytime temperature is considerably higher, in part due to the productions of photoelectrons. However, the temperature increase caused by the microwave heating is considerably smaller because the increased electron density and higher temperatures increase the thermal conductivity and effectively reduce the thermal resistance between the dissipation region and the lower ionosphere.

The fractional decrease in electron density caused by 200 seconds of microwave irradiation at the peak of the F-layer is shown in Figure 2.9, for both daytime and night-time irradiation at the Northeast site.

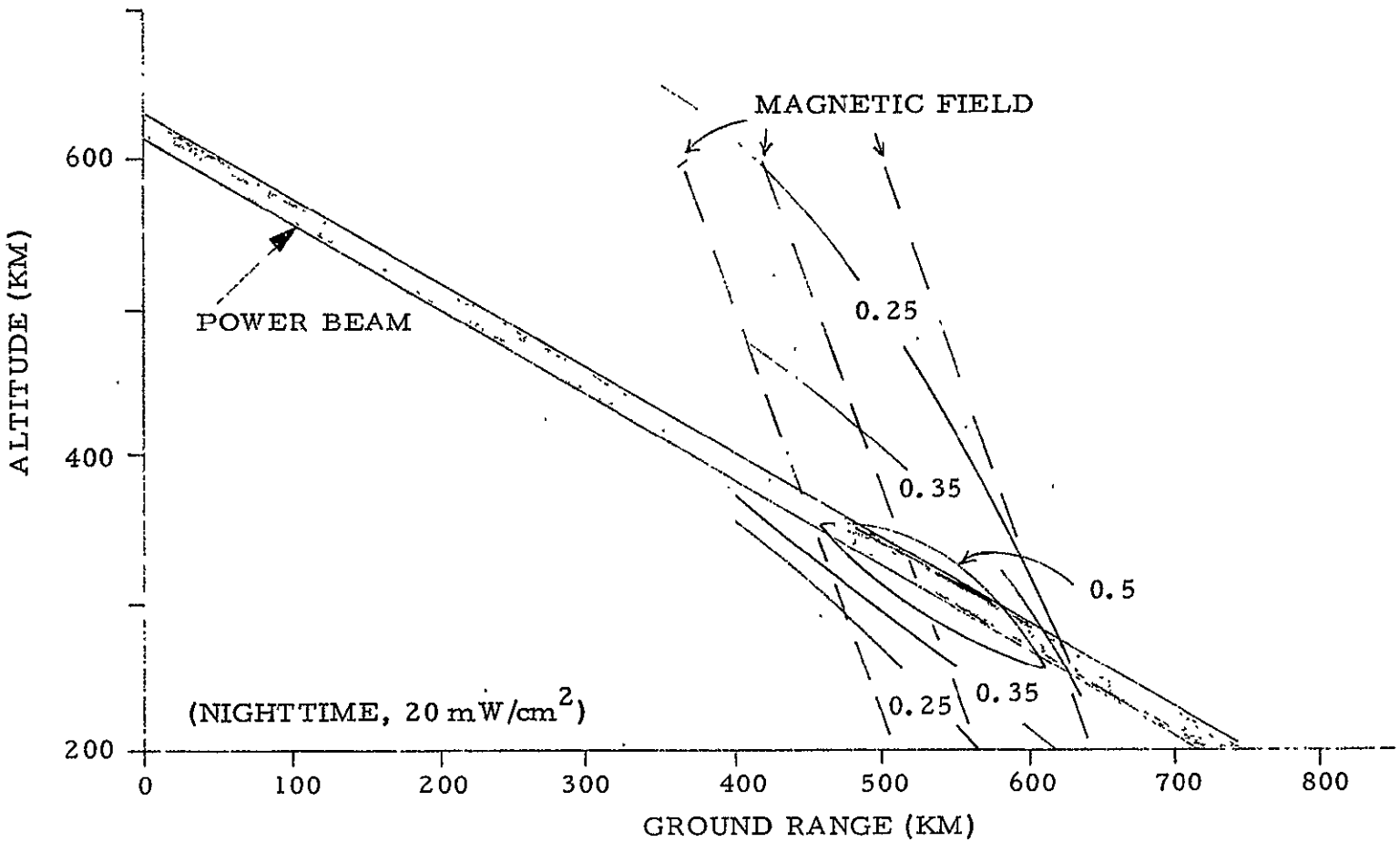

FIGURE 2.7 Contours showing the fractional increase in temperature of the electrons in the meridian plane through the axis of the beam, for a nighttime profile at the Northeast site. The curve labeled 20 mW/cm^2 in Figure 2.6 gave absolute values of temperature along a particular magnetic field line which is shown intersecting the power beam at 310 km altitude in this figure. The largest temperature rise is about 50 percent above ambient and occurs in the vicinity of the beam near the peak of the F-Region where $n\nu$ (and therefore Ω) is largest.

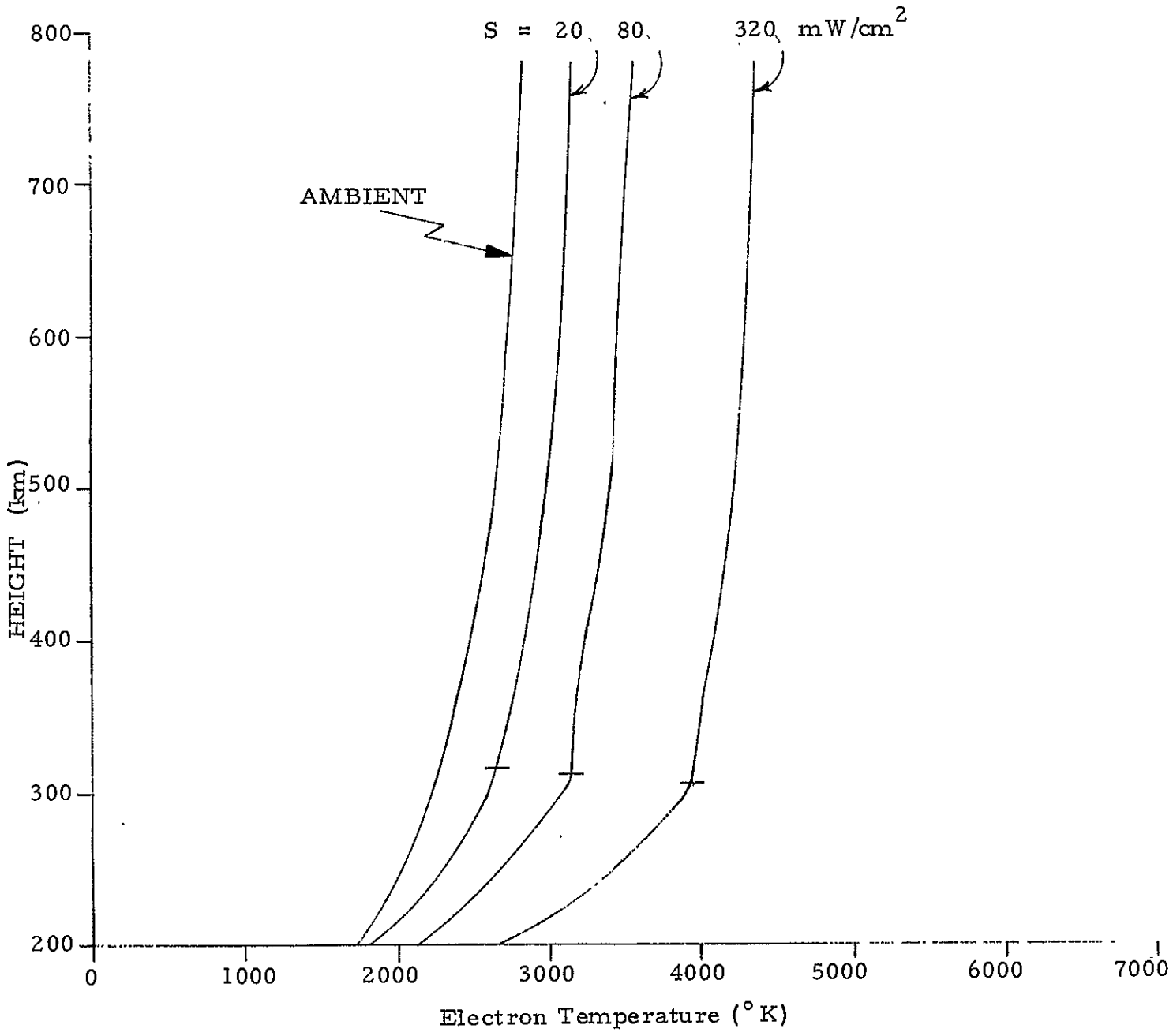

FIGURE 2.8 Electron temperatures at the Northeast site during the daytime for three different power densities.

with n_2 the sum of N_2 and O_2 densities in cm^{-3}. Here we give the equations in the form appropriate for 2450 MHz. At higher frequencies, the ohmic heating decreases as $1/f^2$. The precise form for arbitrary frequency has been described in References 6-8, with the most detailed exposition in Reference 7.

The U_1 represent various energy loss processes. Although U_2 and U_4 are included in our numerical results, they are relatively unimportant to our results. U_2, which involves the electron energy lost to exciting fine-structure transitions in atomic oxygen, becomes significant above 90 km where the relative concentration of atomic oxygen is large. U_4 is the elastic loss which is small compared to inelastic losses. Then U_1, the loss rate due to rotational excitation in the neutral gas, is

$$U_1 = 3.15 \times 10^{-10} \; n_2 \; \delta T_e / \sqrt{T_e} \qquad (6)$$

where we used Dalgarno's formula[11] expressed in our units. Here $\delta T_e = T_e - T_N$ is the change in electron temperature from its ambient value, which equals the neutral temperature.

For low-power fluxes, where the ambient electron temperature is changed by less than 50 percent, U_3 can also be ignored. However, it becomes important for large electron temperatures and for lack of a more accurate formula, we find that Dalgarno's tabulated loss rates[11] can be fitted to the equation.

$$U_3 = 1.25 \times 10^{-21} \; n_2 \left(T_e^4 - T_N^4 \right) \quad . \qquad (7)$$

With this form U_3 will be greater than U_1 for electron temperatures exceeding 1800° K.

For weak fields, say about one mW/cm^2, the electron temperature increase will be less than 10° K with U_3 much smaller than U_1. However, U_3 increases rapidly with temperature and becomes very important for power densities exceeding $10 mW/cm^2$. In fact, the critical power S_c was defined[6] as

a power level above which the loss terms due to U_1 and U_2, by themselves, are not sufficient to keep the temperature stable, without including the losses due to U_3 and U_4. For 2450 MHz at 60 km, the critical power is $15 mW/cm^2$. Figure 2.10 plots the rate of change of temperature as a function of temperature for several values of S/S_c. The rapid drop in this curve at large temperatures is due to U_3. Without the term U_3, the curve for $S = 1.25 S_c$ would remain positive for all T_e, and Equation (4) would require the temperature to continually increase.

The electron temperature, after it has reached a steady state in the presence of the power beam, has the magnitude shown in Figure 2.11, as a function of the power flux. The temperature increases shown in this figure are several thousand degrees Kelvin for the fluxes typical of the power beam, but they are restricted to the volume indicated by the beam. The temperatures at 100 and 110 km are reduced by U_2, the energy loss to fine structure transitions in atomic oxygen, because the relative concentration of atomic oxygen becomes larger with altitude. The critical power density S_c is also increased due to the atomic oxygen concentration. The plot was not extended beyond $50 mW/cm^2$ to avoid going to temperatures higher than the data points to which the curve for U_3 had been fitted.

The altitude dependence of the electron temperature is shown in Figure 2.12 for several power fluxes. The atomic oxygen concentration tends to reduce the temperatures above about 90 km.

The electron density in the D-region is a function of many complicated chemical reactions which are not well understood, but we can expect the density to be drastically changed by the large jump in electron temperature. A first approximation to the electron density might be given by a recombination equation

$$\frac{\partial n}{\partial t} = q - \alpha(T_e) n^2 \quad . \tag{8}$$

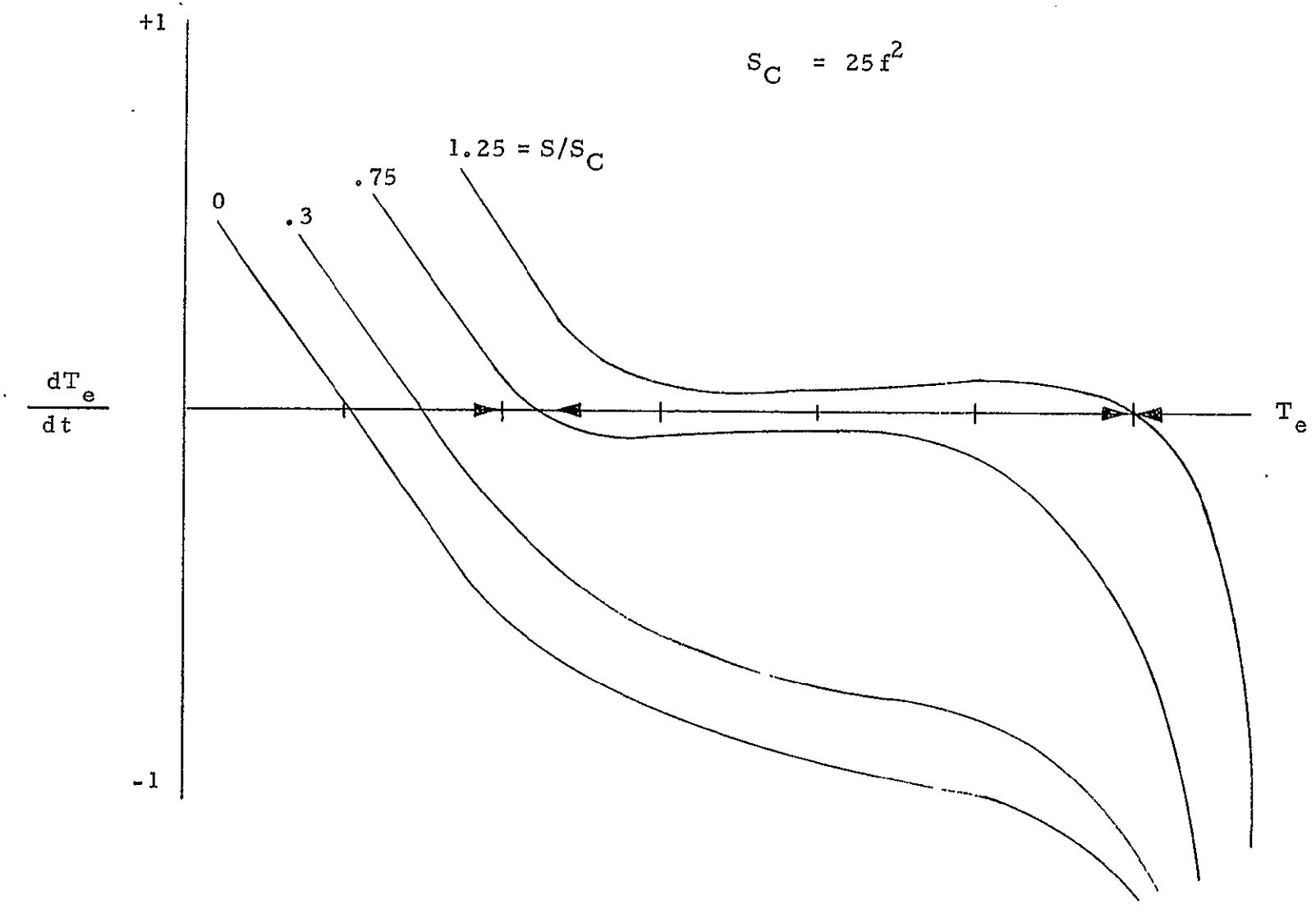

FIGURE 2.10 Plot of the rate of change of electron temperature at 60 km altitude in arbitrary units as a function of temperature for several incident fluxes. Temperatures relax to the equilibrium temperature where the derivative is zero, at which point the temperature is stable.

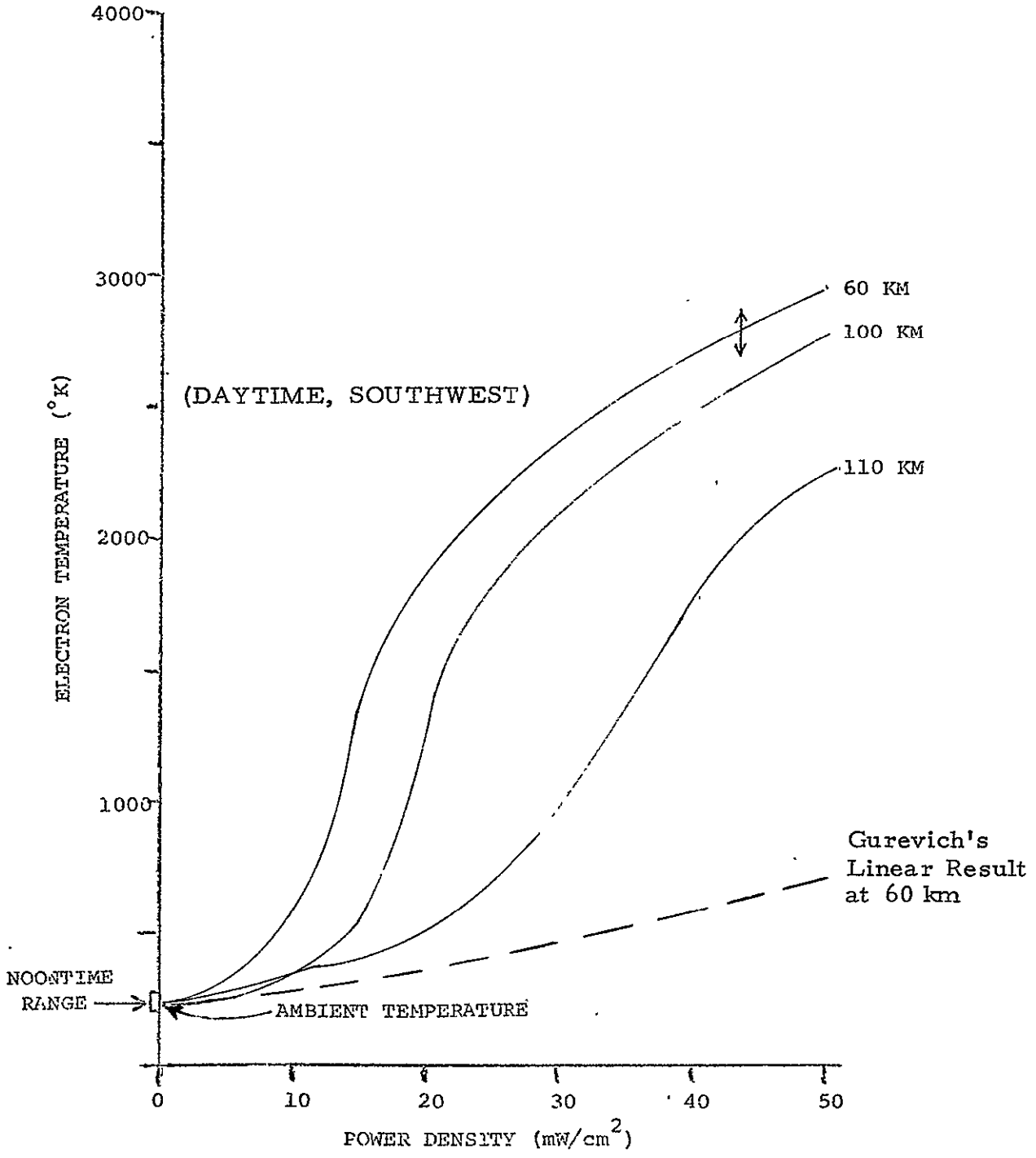

FIGURE 2.11 Electron temperature at 60, 100 and 110 km altitude as a function of incident power flux. The dashed straight line is the result which would have been obtained if Gurevich's parameter G , which is the fractional energy loss per collision, had been assumed to be independent of electron temperature, as is correct for weak power fluxes.

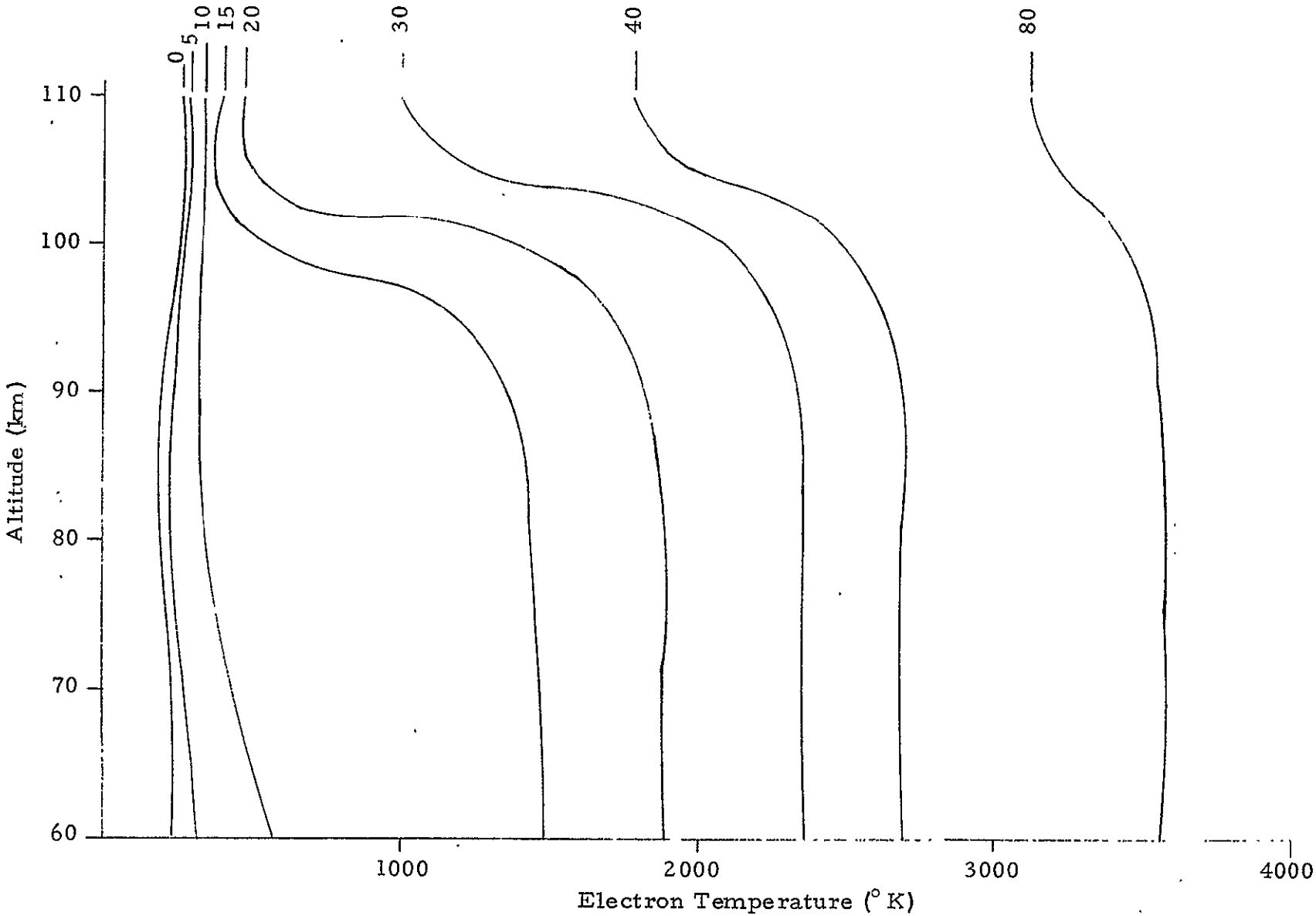

FIGURE 2.12 Electron temperature as a function of altitude for power fluxes from 0 to 80 mW/cm^2. Intermediate fluxes like 20 mW/cm^2, may exceed the critical flux at lower altitudes but be below the critical flux at 110 km, since the critical flux increases as the relative concentration of atomic oxygen becomes larger.

where q is a source term due to photoionization. If n_o is the equilibrium density and T_o is the equilibrium temperature in the absence of the power beam

$$q = \alpha\left(T_o\right) n^2 \quad . \tag{9}$$

The electron temperature increases from T_o to its steady-state temperature T_e on a millisecond time scale, so that on the time scale of Equation (8) it can be considered to jump instantaneously from T_o to T_e. (In the HF case, S and therefore T_e are gradually changing as a function of time, and Equation (8) must be solved numerically.) In the present case, Equation (8) has an analytic solution which is

$$n(t) = n_o \sqrt{\frac{\alpha\left(T_o\right)}{\alpha\left(T_e\right)}} \quad \frac{1 - A\, e^{-t/t_o}}{1 + A\, e^{-t/t_o}} \tag{10}$$

where

$$t_o = \left\{ 2 \left[\alpha\left(T_o\right) \alpha\left(T_e\right)\right]^{1/2} n_o \right\}^{-1} \tag{11}$$

and

$$A = \frac{\sqrt{\alpha\left(T_o\right)} - \sqrt{\alpha\left(T_e\right)}}{\sqrt{\alpha\left(T_o\right)} + \sqrt{\alpha\left(T_e\right)}} \quad . \tag{12}$$

Equation (10) shows that the equilibrium electron density is

$$n_{eq} = n_o \sqrt{\frac{\alpha\left(T_o\right)}{\alpha\left(T_e\right)}} \tag{13}$$

and that equilibrium is reached over a time t_o inversely proportional to the electron density.

The dissociative recombination coefficient was taken to be

$$\alpha = 5 \times 10^{-6} \left(180/T_e\right) \qquad (14)$$

which is consistent with published recombination rates involving water-cluster ions,[12] and would lead to an increase in electron density occurring over times on the order of 10 minutes. These times are consistent with the absorption history observed during HF heating,[13] where the ionospheric absorption increased for about 10 minutes after the heating radiation was applied and decays over the same period of time when the heater is turned off.

Table 2.3 shows typical times, t_o, based on Equations (11) and (14), which gives the minutes required to reach steady state.

TABLE 2.3 Scale Time t_o (Minutes)

n_o \ S	10 mW/cm^2	20 mW/cm^2
1000	3.4	6.2
100	34	62

The electron density at 60, 70 and 80 km is plotted as a function of time in Figure 2.13 for 20 mW/cm^2 in the power beam, using Equation (14) for the recombination coefficient. Few water cluster ions are found above 80 km and near this altitude α should change from Equation (14) to the NO^+ coefficient $\alpha = 5 \times 10^{-7} \left(300/T_e\right)^{1.2}$.

The absorption coefficient in dB/km is shown in Figure 2.14 as a function of altitude for a 10 MHz ordinary wave passing through the ambient ionosphere, through an ionosphere which has been heated by the 20 mW/cm^2 beams for one second which is long enough for a steady-state temperature to be reached, and through an ionosphere which has been heated for 20 minutes.

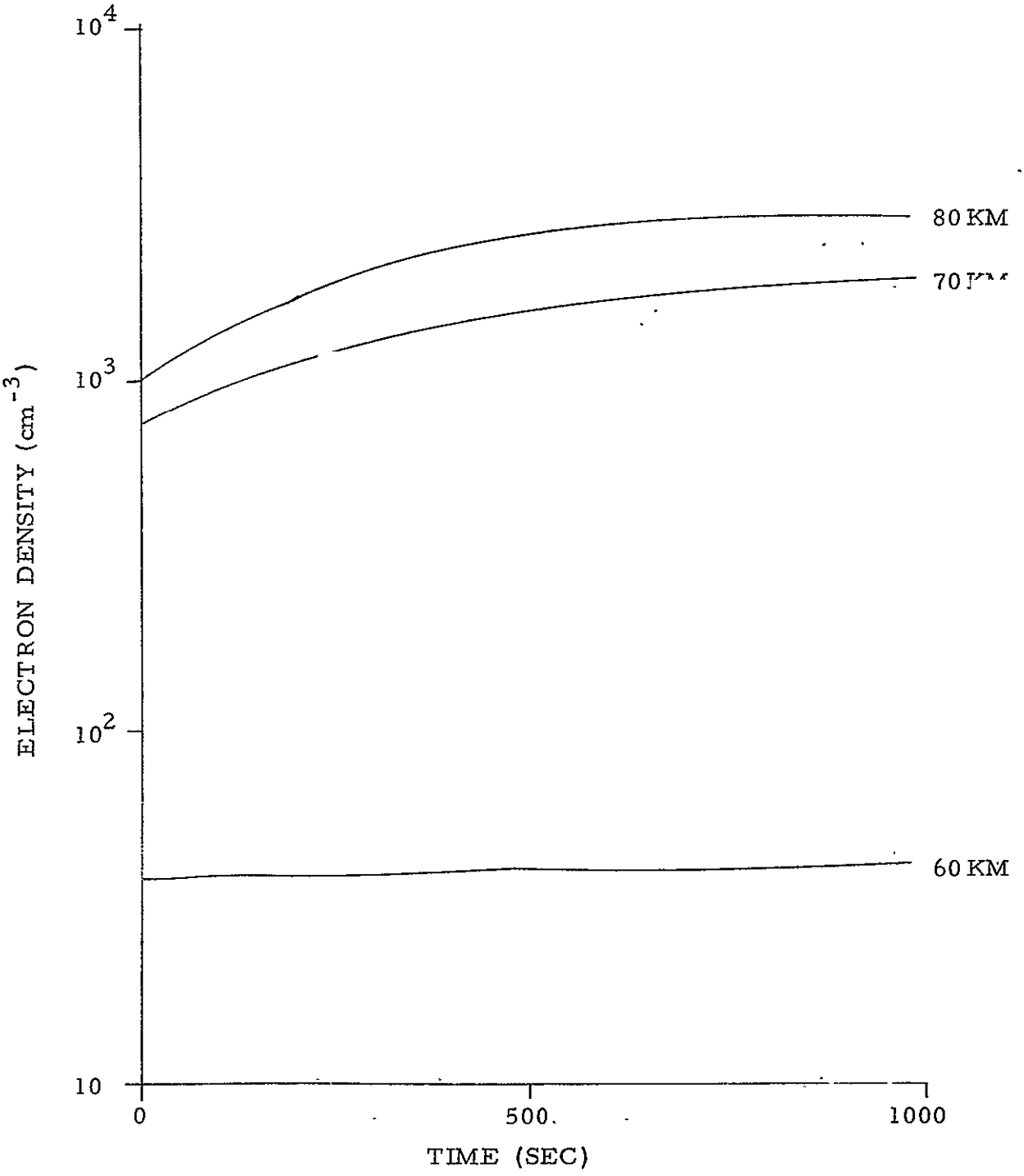

FIGURE 2.13 Electron density as a function of time for 60, 70 and 80 km with a 2450 MHz power density of 20 mW/cm^2.

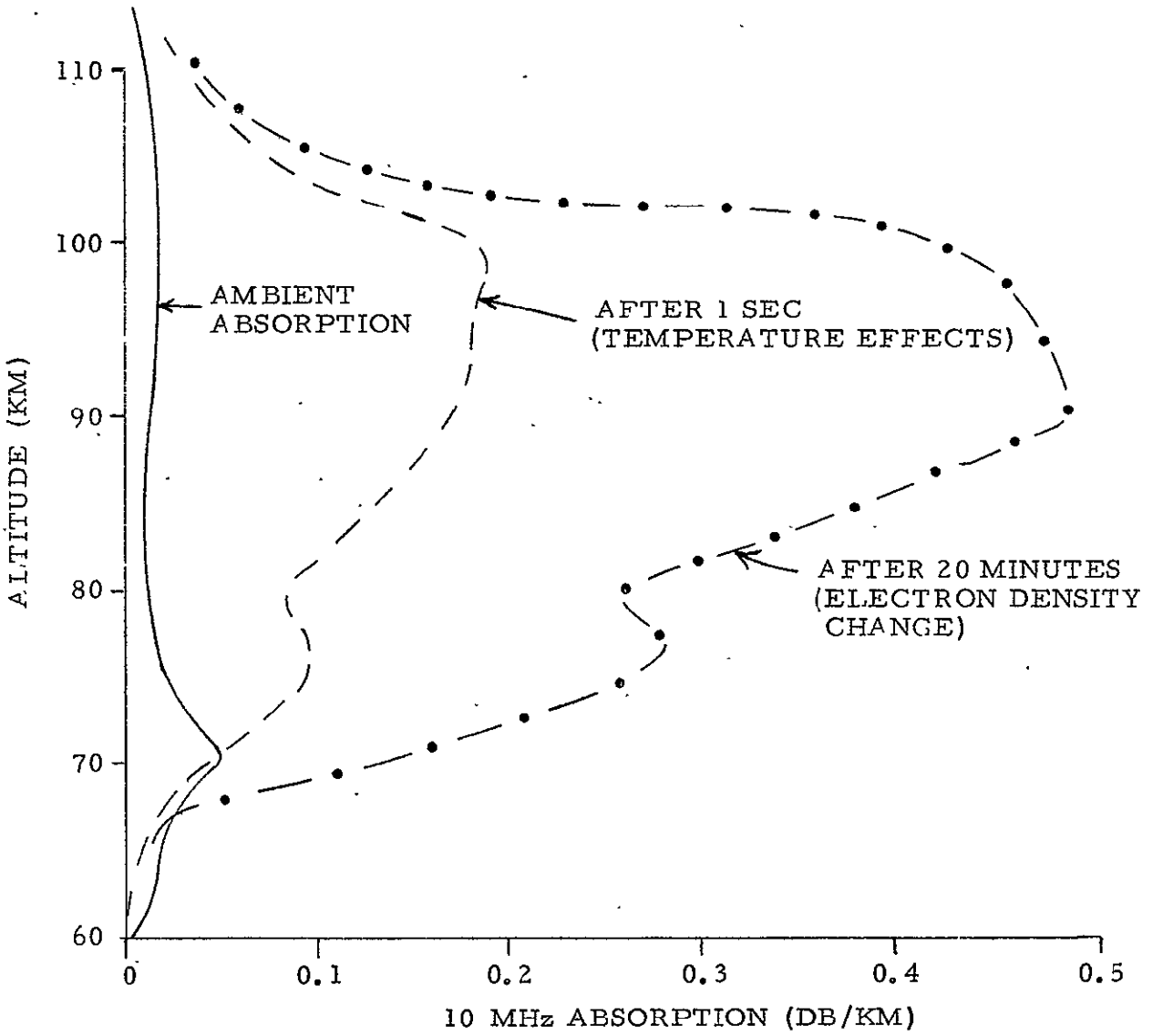

FIGURE 2.14 Absorption coefficient per km for the power in a 10 MHz ordinary wave passing through the heated portion of the D-Region. NOTE: The integrated absorption is in excess of 10 dB for a 10 MHz wave.

An interesting aspect of Figure 2.14 is that heating the ionosphere below 70 km reduces the absorption coefficient instead of increasing it. The reason for this is that the absorption coefficient is proportional to

$$\frac{\nu_{eff}}{\omega'^2 + \nu_{eff}^2} \tag{15}$$

where $\omega' = \omega \pm \cos\theta\, \omega_\beta$ where ω_β is the angular electron cyclotron frequency, θ is the angle between the propagation direction and the magnetic field, and $\pm$ sign is + for the ordinary wave and - for the extraordinary wave. In the high frequency approximation, Equation (15) becomes ν_{eff}/ω^2 which increases in proportion to T_e as T_e increases. However, if ω' is much less than ν_{eff}, then Equation (15) is proportional to $1/\nu_{eff}$ which is inversely proportional to the electron temperature so that the absorption decreases. Since ω' is smallest for the extraordinary wave, heating the ionosphere is likely to decrease the absorption of extraordinary waves which propagate below 70 km. As a matter of fact, Utlaut[13], in the ionospheric heating experiment, has observed that an extraordinary probe signal has relatively less increased attenuation during the heating of the D-region than does the ordinary wave; although this result has not been explained to date, it is consistent with the term in Equation (15). However, calculations which would confirm this hypothesis[7] have not been definitive inasmuch as they require an accurate knowledge of the ionospheric profile at the precise time of the experimental measurement and measurement of the attenuation of the o and x modes, preferably at several different frequencies.

The changes in electron density which occur after 20 minutes of irradiation are responsible for the large increase in absorption that is shown for the dot-dash curve in Figure 2.14 in comparison with the dashed curve which is drawn for times shortly after the beam is turned on, so that only the electron temperature has had time to adjust. The electron density changes were calculated on the basis of the recombination coefficient for water cluster ions given in Equation (14).

This recombination model is oversimplified and, in particular, should be modified above 80 km where a recombination coefficient appropriate to diss dissociative recombination of NO^+ ions would be more appropriate.

In the D-region, horizontal winds of varying velocity will cause fluid elements to drift across the beam with speeds on the order of 50 M/sec. These winds will move fluid across the beam in about 200 seconds, which is long compared with the relaxation time of the temperature, but short compared to the time required for the recombination processes determining the electron density to come to a steady-state. Therefore, the electron density disturbance will produce a wake extending outside the beam, although the temperature disturbance will be confined to the volume of the power beam.

The gradients in electron density in the D-region will tend to cause "blooming" of the beam, in the sense that a laser beam causes blooming in the atmosphere and also to cause the beam to be refracted into the direction of the wind. However, this will be a weak effect due to the high frequency of the microwaves compared to the plasma frequency. For the same reason, this effect will also be weak in the F-region but its tendency will be reversed because the microwave beam acts to decrease the electron density and therefore to cause self-focusing instead of "blooming" and to cause the beam to be refracted downwind, instead of upwind.

2.2.3.2 Interactions of Lower-Frequency Propagation with the D-Region

The changes in electron density will cause the electron density contours to bulge downward as shown in Figure 2.15. These contours neglect wind drift which would reduce the electron density in the upwind direction and cause a small "wake" in the downwind direction. The contours correspond to electron densities which will reflect frequencies ranging from 63 to 900 kHz.

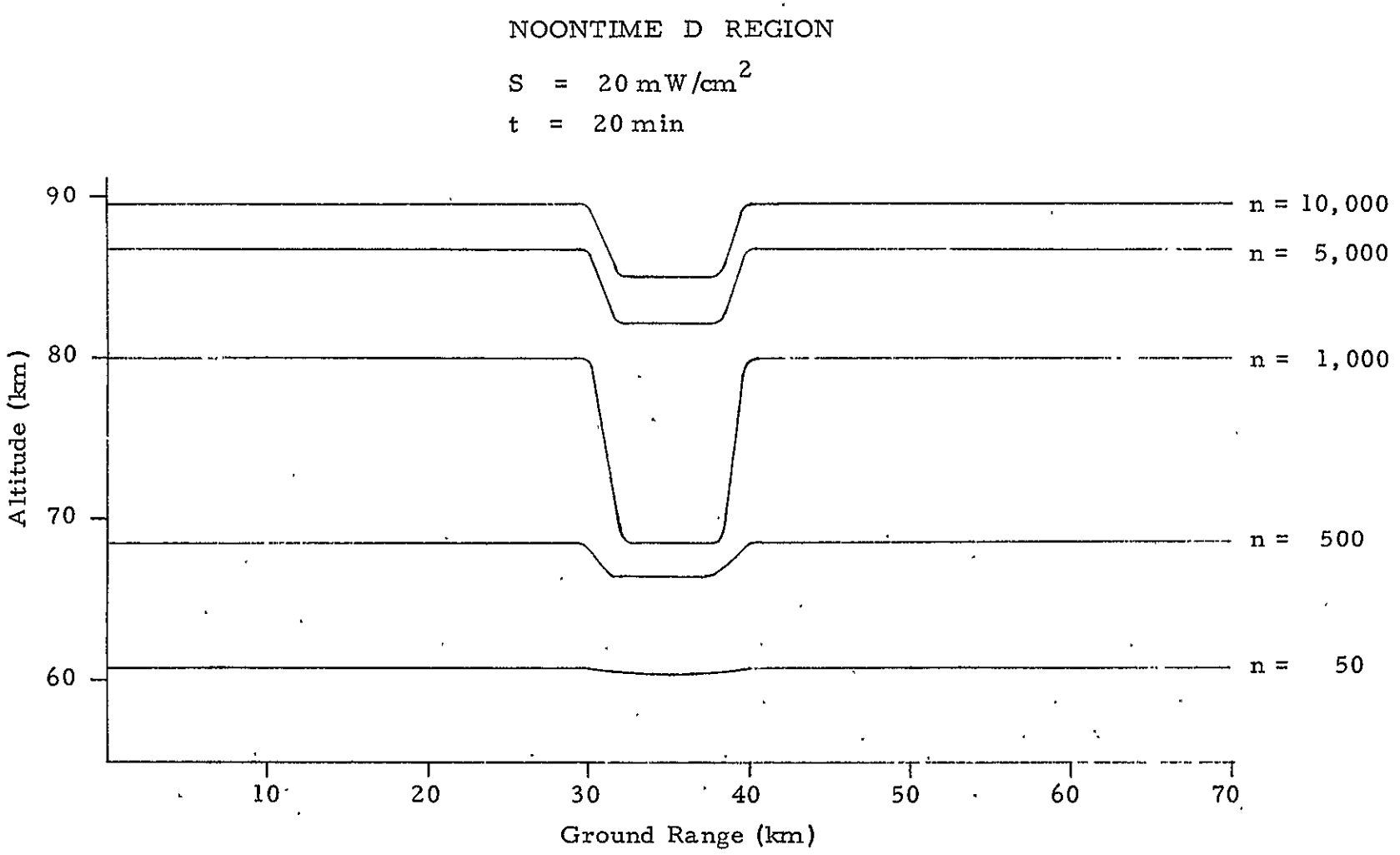

FIGURE 2.15 Electron density contours in the vicinity of a vertical power beam for 20 mW/cm^2 at 2450 MHz. The beam is assumed to have been turned on for 20 minutes and the effect of wind drift is neglected.

The absorption coefficients in Figure 2.14 make it clear that signals propagating through the disturbed region will suffer severe attenuation. The beam dimensions are small enough so that little signal energy will propagate directly through a single beam; however, this problem will become more severe if large systems with many beams are ultimately designed.

The effect of the disturbance will depend on the size of the Fresnel zone relative to D, the diameter of the power beam and of the disturbance. If the Fresnel zone is small compared to D, the reflection from the contours will be a geometrical reflection from the reflecting contour, so that most propagation paths will be unaffected although certain locations may be shadowed and others may receive multipath signals. On the other hand, if the Fresnel zone is much larger than the disturbance, no path will be shadowed although there may be a small amount of fading in the received signal.

The geometry for a Fresnel zone in which energy is reflected from a horizontal plane is shown in Figure 2.16a. The reflection occurs from a point O on the surface such that TOR is the shortest distance for a path reflected from the medium where

$$\overline{TOR} = 2h/\sin\theta \quad . \tag{16}$$

Consider a point A which is located at (x, y) on the reflecting plane where x is the distance to be measured along the intersection of the reflecting plane and the plane TOR, while y is measured perpendicular to TOR. Then

$$TAR = \sqrt{h^2 + y^2 + (h\cot\theta + x)^2} + \sqrt{h^2 + y^2 + (h\cot\theta - x)^2}$$

$$\cong \frac{2h}{\sin\theta} + \frac{1}{h}\left(x^2 \sin^3\theta + y^2 \sin\theta\right) \quad , \tag{17}$$

where terms of order x^3 and y^3 are neglected.

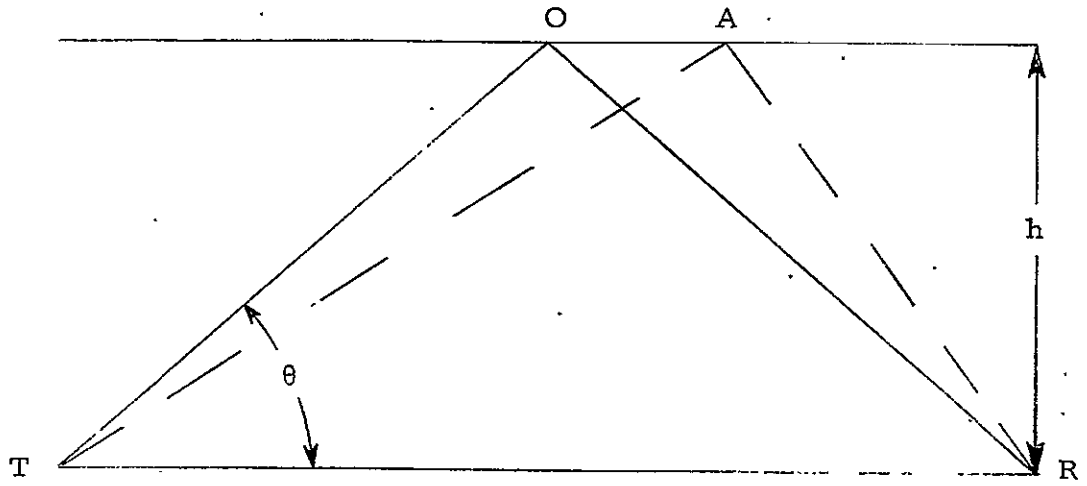

(a) $\overline{TAR} - \overline{TOR} = \lambda/2$

FIGURE 2.16-a Geometry of propagation path reflecting from a plane at a height h above the transmitter T and receiver R.

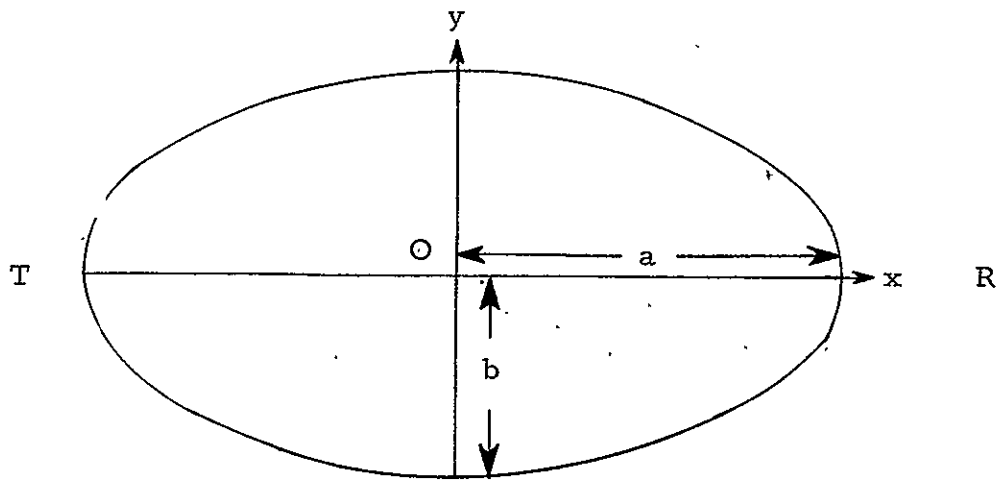

(b) ELLIPTIC FRESNEL ZONE

FIGURE 2.16-b Ellipse corresponding to the Fresnel zone in the reflection plane.

Therefore, the Fresnel zone is bounded by the locus

$$x^2 \sin^2 \theta + y^2 = \frac{\lambda h}{2 \sin \theta} \tag{18}$$

which describes an ellipse with a semi-major axis a, which lies in the plane TOR as shown in Figure 2.16b. Here

$$a = \left(\frac{h\lambda}{2 \sin \theta}\right)^{1/2} / \sin \theta \tag{19}$$

and the semi-minor axis is

$$b = \left(\frac{h\lambda}{2 \sin \theta}\right)^{1/2} \tag{20}$$

The results are shown in Table 2.4 as a function of frequency and elevation angle θ, where the reflection height is taken to be 70 km.

TABLE 2.4 Dimensions of Fresnel Ellipse

Angle	Frequency (MHz)	a (km)	b (km)
90°	5	1.5	1.5
90°	1	3.2	3.2
90°	0.5	4.6	4.6
90°	0.1	10.2	10.2
45°	5	2.4	1.7
45°	.1	5.5	3.9
45°	0.5	7.7	5.5
45°	0.1	17.2	12.2
5°	5	56.3	4.9
5°	1	126	11.0
5°	0.5	178	15.5
5°	0.1	398	34.7

Roughly speaking, the Fresnel zone can be considered to exceed the size of the disturbed region for frequencies below 1 MHz. Since the reflection frequency for the highest contour shown in Figure 2.15 is 900 kHz, the frequencies which are reflected in the D-region cannot be treated by geometrical optics alone.

2.2.4 RECOMMENDED THEORETICAL STUDIES

The great bulk of theoretical work on the HF ionospheric-modification program[1] was devoted to understanding the plasma instabilities which were generated by HF heating. To date, only a small amount of effort has been devoted to understanding the instabilities which might be produced by the high-power microwave transmissions (although Appendix B of Reference 14 was devoted to a study of the field-aligned structure which might be caused by the self-focusing instability[15]).

The development of the plasma instability theory for the HF ionospheric modification experiments provides a great deal of background knowledge which will be useful in studying the high-power microwave phenomena. However, the HF experiments uncovered many effects which were not anticipated in the theory and the same situation may be encountered when a solar power station produces an unprecedented combination of high power and high frequency microwaves. In these circumstances, one requires a careful analysis of the possible effects that may occur under these conditions.

In one respect, the microwave interaction is simpler to study since there is no reflection height and the effects, such as the parametric decay instability, which depend on the radiowave frequency being close to the plasma frequency will be less important. However, the heating calculations given in this paper indicate that a great deal of thermal energy is available to drive instabilities in the plasma. Some instabilities, such as the drift-resistive instability which is driven by large plasma gradients, should be re-examined under the more intense disturbances which may now occur. Other instabilities, such as field-aligned diffusion modes and self-focusing instabilities, and effects such as enhanced airglow within the heated volume in the F-region need to be considered.

The high microwave frequency makes it more difficult to affect the power beam than it is to affect the propagation characteristics of lower frequency radiation propagating through a modified ionosphere. An analysis of the self-focusing instability indicated that field-aligned instabilities would grow only if the wave-

length was on the order of 500 meters or larger, and such long wavelengths would not affect control of the power beams. However, even though no serious effects have been identified, it is instructive to recall that the field-aligned structures created by the HF modification experiment scattered radio waves with frequencies as high as UHF and VHF, when the propagation direction had the proper orientation relative to the magnetic field. This suggests that great care must be taken before concluding that scintillations will not be produced that affect satellite communications.

In addition to analyzing possible effects due to instabilities, several improvements could be mentioned that might be made in analyzing the fluid dynamics of ohmic heating. Although it was possible to estimate the effects of wind drifts in the D-region and electrodynamic drifts in the F-region, these drifts were not specifically included in the analysis given in this report. The electron energy loss due to vibrational excitation of N_2, which proved to be vitally important in the D-region calculations, was not included in the F-region, partly because of the scarcity of N_2 at these altitudes and partly because it was a high temperature effect which became important above 2000° C. The high temperature obtained with the 320 320 mW/cm^2 power beam might be modified by this effect. Since the microwave disturbance is not only hotter, but also is more limited in lateral extent than the HF experiment, it may be important to reconsider the methods by which particles can leak to adjacent lines of force. The heating is going to cause local changes in the conductivity in the E-region which may modify, at least locally, the dynamo currents near 120 km altitude. The effects of chemical recombination and photoproduction were ignored in the F-region although these effects will clearly modify electron density perturbations during the daytime. The aeronomy of the D-region is complex but a more accurate model of the chemistry is needed to determine the electron density changes accurately.*

Because of their possible importance to the MPTS, the tasks described above, along with the additional analysis required to relate these physical results to the propagation of communication signals through the disturbed ionosphere and to the control of the power beam transmission should be carried out early in the development plan for a microwave power transmission system.

* Appendix B contains a preliminary investigation of the effects of Microwaves on ion chemistry.

2.2.5 RECOMMENDED EXPERIMENTAL STUDIES

The experience with HF heating of the ionosphere[1] suggests that it would be extremely overoptimistic to assume that our theoretical undertaking of ionospheric plasma instabilities is so complete that there will be no surprises when the operation of the MPTS is begun. Therefore, it is recommended that a series of experimental approaches be designed, beginning with the least expensive, which will give us a high degree of confidence in our understanding of the microwave-ionospheric interactions before a solar satellite is actually deployed.

Fortunately, one experiment has already been carried out, in a sense, namely the experimental work carried out in the HF ionospheric modification experiments.[1, 13] The relevance of the experiments is due to the fact that ohmic heating scales as the power flux divided by f^2, although the critical fields for the onset of plasma instabilities do not always have the same scaling factor.

The ohmic heating in the HF experiments differs from the microwave heating in several ways:

1. The HF frequency is close to the plasma resonance frequency which makes an analysis of the instabilities difficult and introduces refractive effects, deviative absorption and plasma turbulence near the reflection height.

2. The Platteville HF experiment heats over an area 100 km in diameter while the microwave beam is less than 10 km in diameter.

3. The Platteville heater delivers a flux which, after scaling, is comparable to an MPTS only near the reflection height, where the Airy swelling factor is important.[2] Thus a vertical height range of only 2 - 3 km is heated while the MPTS more typically heats a given flux line over an altitude range of, say, 20 km.

A more realistic experiment can be designed by going to a frequency above the plasma resonance at f_{max}, say 20 MHz. With a large enough antenna, the radio waves could be focused in the F-region over an area comparable to the power beam area and with power fluxes which scale to the 20 mW/cm^2 level contemplated for the microwave transmissions. Some analysis is underway elsewhere[16, 17] to evaluate the possibility of obtaining useful information from the

Aerecibo facility in Puerto Rico. If one MW were transmitted at 20 MHz from an antenna aperture of 400 meters, a power density of 1.27×10^{-3} mW/cm^2 could be obtained for a 10 km beam at an altitude of 300 km. This power density would scale to 19 mW/cm^2 at 2450 MHz.

2.3 MPTS IONOSPHERIC INTERACTIONS

2.3.1 INTRODUCTORY REMARKS

This section addresses the impact of the ionospheric changes brought about by the power beam on other users as well as on the power beam and phase control system. The basic assumption underlying this study is that the ionospheric perturbations brought about by the heating are no different than those which occur naturally. For example, ionospheric irregularities occur in equatorial and polar regions which produce amplitude variations known as scintillations. Irregularities of this type could occur as a result of plasma instabilities associated with the MPTS. However, the power beam effects might be different from naturally occurring phenomena in the following two ways:

a. Power beam will increase occurrence of these effects in mid-latitude regions (CONUS) where heretofore they did not occur with as great a frequency as in the equatorial or polar regions.

b. Local effects of the power beam could be more severe than naturally occurring phenomena and thus provide a more severe effect on signals which traverse the ionosphere in these localized regions.

To study the impact on other users, we have investigated and identified various systems and the extent to which they might be affected. The systems are classified as to applications; namely, navigation systems, communication systems and DoD radars. They have been selected to span the frequency range from 10 kH to 6000 MHz. The possible effects of the power beam on each system are discussed as well as our recommendations for further investigation (theoretical and experimental). It was clearly impossible under the current effort to make an exhaustive study to identify and discuss more than a representative set of systems However, we have identified those systems which we believe have a particularly important role in the future and also span a large frequency range. Since the ionospheric effects are strongly related to frequency of transmission, the results of this study can be extrapolated to affects on systems not discussed which utilize a specific frequency.

Clearly, as an experimental program is brought to fruition, classes of users will be identified in further detail. Experimental measurements will, in the future, be defined which will either use the actual system or experiments which simulate effects on systems when geographical location of a specific system (such as large DoD radars) make it impractical to run coordinated experiments.

Table 2-5 summarizes the ionospheric effects and some general classes of systems that could be affected. Several effects are listed in Table 2-5 which were outside the scope of the present study and for which we would recommend further study; generation of traveling ionospheric disturbances, harmonic generation of RFI, and chemistry changes due to excessive heating from the power beam.

The effects described in Table 2-5, even if they occur in a region localized with respect to the power beam, can potentially effect users at ranges upward or 2000 km from the interaction region. Another way of viewing this is that a user is affected by the power beam in an area defined by the intersection of his local horizon and the ionosphere. Figure 2-17 schematically illustrates this point by showing the area of potential interaction for the F-layer and D-layer with respect to a user. Any power beam passing through the potential area of interaction could affect the operation of the user. For example, a user located in the middle of the of the U. S. would be affected by every power beam that is contained in the U. S. For one power beam the probability of interaction might be small; however, for over 100 power beams, all located within the area of interaction, the potential for user interaction will significantly increase. The size of this increase depends on the orientation of the power beam with respect to the user and the size of the geographical disturbance caused by the power beam. The area of interaction shown is defined by the line-of-sight propagation from the user. However, for VLF systems like Omega, which propagate via the earth ionosphere waveguide over distances large compared to the interaction region, the effects of the power beams will be observed over larger geographical areas than indicated.

Before discussing specific systems in detail, some examples of how ionospheric disturbances, both natural and man-made, affect the systems will be described. This will provide a graphical representation of the possible effects that can occur.

TABLE 2-5. SUMMARY OF IONOSPHERIC EFFECTS

PHENOMENOLOGY	POSSIBLE EFFECT	UNRESOLVED QUESTIONS	SYSTEMS EFFECTED
ABSORPTION (80 KM)	• SIGNAL LOSS FOR HF COMMUNICATIONS • MODIFY VLF SIGNALS USED FOR NAVIGATION	• GEOGRAPHICAL SIZE AND MAGNITUDE • LOCATION QF EFFECT WITH RESPECT TO XMTR LOCATIONS	• HF COMMUNICATIONS • OMEGA • LORAN
IONOSPHERIC DEPLETION (HORIZONTAL GRADIENTS)	• LIMIT FREQUENCY WINDOW FOR HF COMMUNICATIONS • DISPLACEMENT OF POWER BEAM	• GEOGRAPHICAL SIZE AND MAGNITUDE • EFFECT OF CONTINUOUS HEATING	• POWER BEAM • HF COMMUNICATIONS
IONOSPHERIC IRREGULARITIES	• SCATTERS ENERGY PROPAGATING THROUGH REGION (SCINTILLATIONS & ASPECT SENSITIVE SCATTER)	• NON-LINEAR EFFECTS - DOES IT OCCUR AT 2.45 GHZ - FUNCTION OF POWER DENSITY • LIFETIME AND GEOGRAPHICAL DISTRIBUTION	• PILOT BEAM • COMMUNICATIONS (HF/SATELLITE) • NAVIGATION (GPS) • DOD RADARS (SPACETRAK, SURVEILLANCE)
TRAVELING WAVES	• SCATTERS ENERGY • VARIATIONS IN RADAR TARGET LOCATION	• OVER WHAT DISTANCES DO THEY TRAVEL	
RFI HARMONIC GENERATION	• INCREASED INTERFERENCE FOR OTHER USERS	• DOES IT OCCUR?	
CHEMISTRY CHANGES			

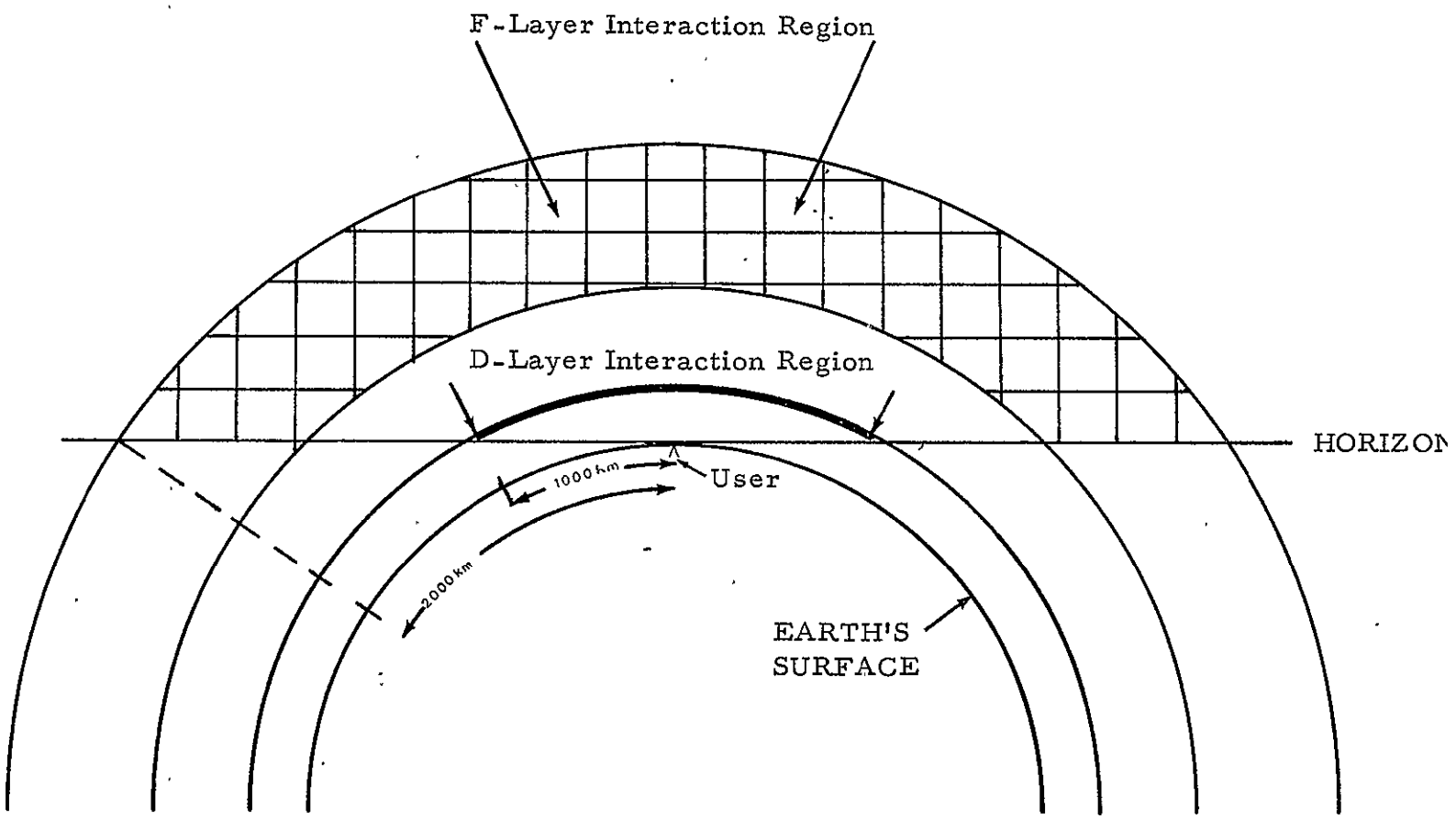

FIGURE 2.17 F-LAYER AND D-LAYER INTERACTION REGION

2.3.2 IONOSPHERIC EFFECTS FOR SELECTED RADIO WAVE PROPAGATION EXAMPLES

2.3.2.1 Examples to be Described

Three examples of ionospheric effects on radio wave propagation will be described: (1) effects of magnetically disturbed ionosphere on 16 kHz transmissions, (2) effects of ionospheric irregularities on 254 MHz transionospheric propagation, and (3) effects of Platteville heating on HF propagation. The first example will illustrate the possible effects of changes in the F-layer as predicted by ohmic heating. The last two examples will illustrate results of plasma instabilities which could be induced by a microwave power beam.

2.3.2.2 Effects of Disturbed Ionosphere on 16 kHz Transmissions

In Section 2.2.2, the effects of ohmic heating on the F-layer are described. F-layer electron densities decrease by from 5 to 40% depending on the magnitude of the horizontal motion of electrons in the F-layer. This decrease is comparable in size to the effects of magnetic storms, which produce a 10 to 20% decrease in mid-latitude F-layer electron densities for weak storms and a 30 to 40% decrease for strong magnetic storms. Although the magnitude of the MPTS induced ionospheric modifications is comparable to the natural occurring phenomena, the geographical distribution of the power beam induced modification has not yet been predicted. This prediction would require further improvements to the theoretical model to include horizontal motions across the earth's magnetic field. This modification is recommended for continued theoretical studies to further understanding of the effects of the MPTS on the ionosphere.

However, it is well known that magnetic storms produce ionospheric disturbances which seriously disrupt HF communications as well as VLF propagation. Figure 2.18 shows the effects of a magnetic storm on 16 kHz propagation for a 1500 km path.[19] The two cycles of phase advance at 16 kHz correspond to a 37.5 km change in phase path which will result in a significant range error for systems such as Omega, which operates at 10.2 kHz.

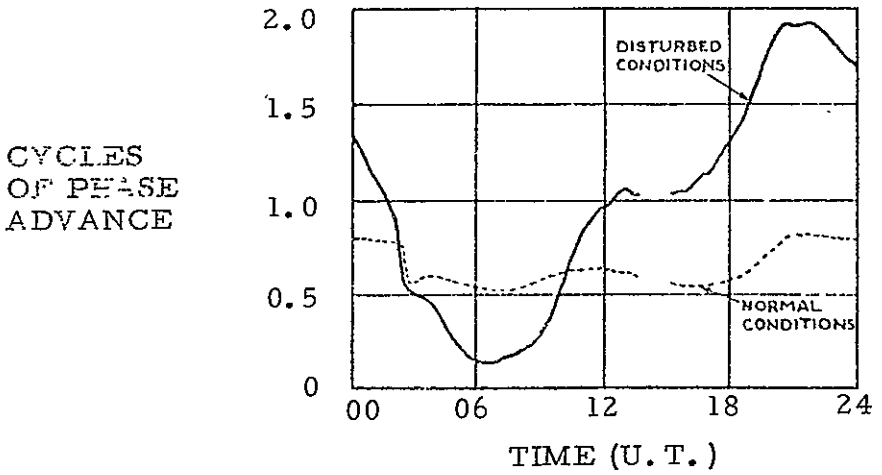

FIGURE 2.18 Effects of magnetic storm on 16 kHz propagation from Rugby, England to Rome.

This illustrates the potential effect that power beam heating could have on Omega navigation systems. Of course, the geographical size of the man-made disturbance, as well as the cumulative effects of over 100 power beams of which several might affect a specific propagation path, still has to be considered. Finally, the analysis presented here is by analogy (i.e., comparing power beam effects with naturally occurring phenomena) and will require experimental verification before the quantitative effects of the MPTS on other users can be established.

2.3.2.3 Effects of Ionospheric Irregularities

Ionospheric irregularities (also called spread-F) could be caused by plasma instabilities generated from the effects of ohmic heating. For example, the self-focusing plasma instability (see Appendix B in Reference 14) is predicted to produce instabilities in the 70 - 100 meter wavelength range at power densities which vary from 70 mW/cm^2 (for 100 meter wavelength) to 200 mW/cm^2 (for 70 meter wavelength). Irregularities of this wavelength are what produce scintillation (rapid fading) of transionospheric signals in the UHF/VHF frequency range.

During the Platteville heating experiment[13] ionospheric irregularities were observed in the 100 meter wavelength regime. The results of the Platteville heating are not directly related to microwave power beam effects because the Platteville heating is done at a frequency near the plasma frequency of the ionosphere. This increases the effective heating by at least an order of magnitude. Also, the heating from the Platteville heating experiment occurs over a limited height range (approximately 1 km) near the plasma frequency, whereas the power beam provides a constant heat source over tens of kilometers. However, the results did indicate the occurrence of irregularities at power densities equivalent to 20 mW/cm^2 at 2.45 GHz. Further, the occurrence of these irregularities was unexpected. (i.e., not predicted) and it is risky at this stage of our understanding to predict the occurrence or non-occurrence of irregularities as a result of power

beam heating at 2.45 GHz. This factor is one of the main reasons that an experimental program is required to determine if and to what extent ionospheric irregularities are produced.

However, it appears likely that at power densities above 20 mW/cm^2 there is a possibility of causing irregularities, and at power densities above 50 to 70 mW/cm^2 there is a strong likelihood of producing significant ionospheric perturbations. Further, if these plasma instabilities occur and ionospheric irregularities are generated with sufficient intensity, they could have a significant impact on the performance of many systems that propagate through or under the ionosphere. Because of the high potential for producing deleterious effects, further study and experimental verification is highly recommended to determine the magnitude of the effects, assess the impact on other users, and determine the impact on the power beam as well as the phase control system of the MPTS.

For example, Figure 2.19 shows an example of scintillations at 254 MHz[21] at Natal, Brazil from LES-6 satellite transmissions. Upwards of 20 - 30 dB fading is observed as a result of ionospheric irregularities. This demonstrates the effects on signals which propagate through an irregularity region.

A further example of the effects of ionospheric irregularities was obtained from the Platteville heating experiment, where Raytheon had the responsibility for investigating HF backscatter from the heating region by building, operating and analyzing HF backscatter from a ring array. The ring array is a circularly phased array which maps out backscattered energy from the ionosphere as a function of range and azimuth. Figure 2.20 illustrates the results of the Platteville heater on HF backscatter. With the heater off, the return observed is from normal ionospheric reflections and is confined in range and azimuth. Also, its Doppler spectra is highly coherent. After the heater is turned on for only several seconds, the effects of the modified ionosphere is exhibited as a multiple of returns in range and azimuth concordant with a decrease in the Doppler purity of the returned

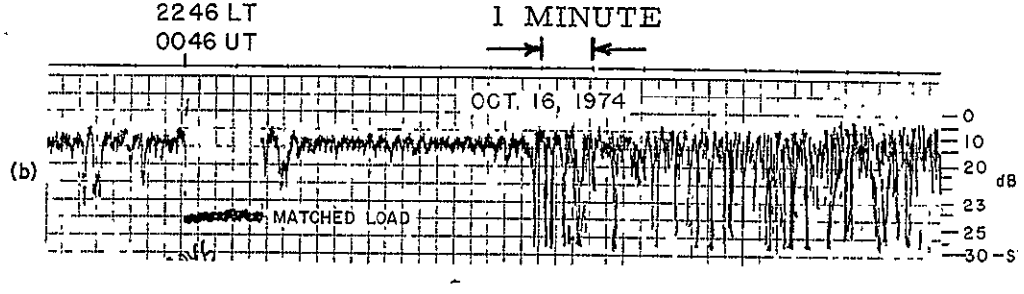

FIGURE 2.19 EXAMPLE OF SCINTILLATIONS AT 254 MHz FROM LES-6 SATELLITE TRANSMISSIONS

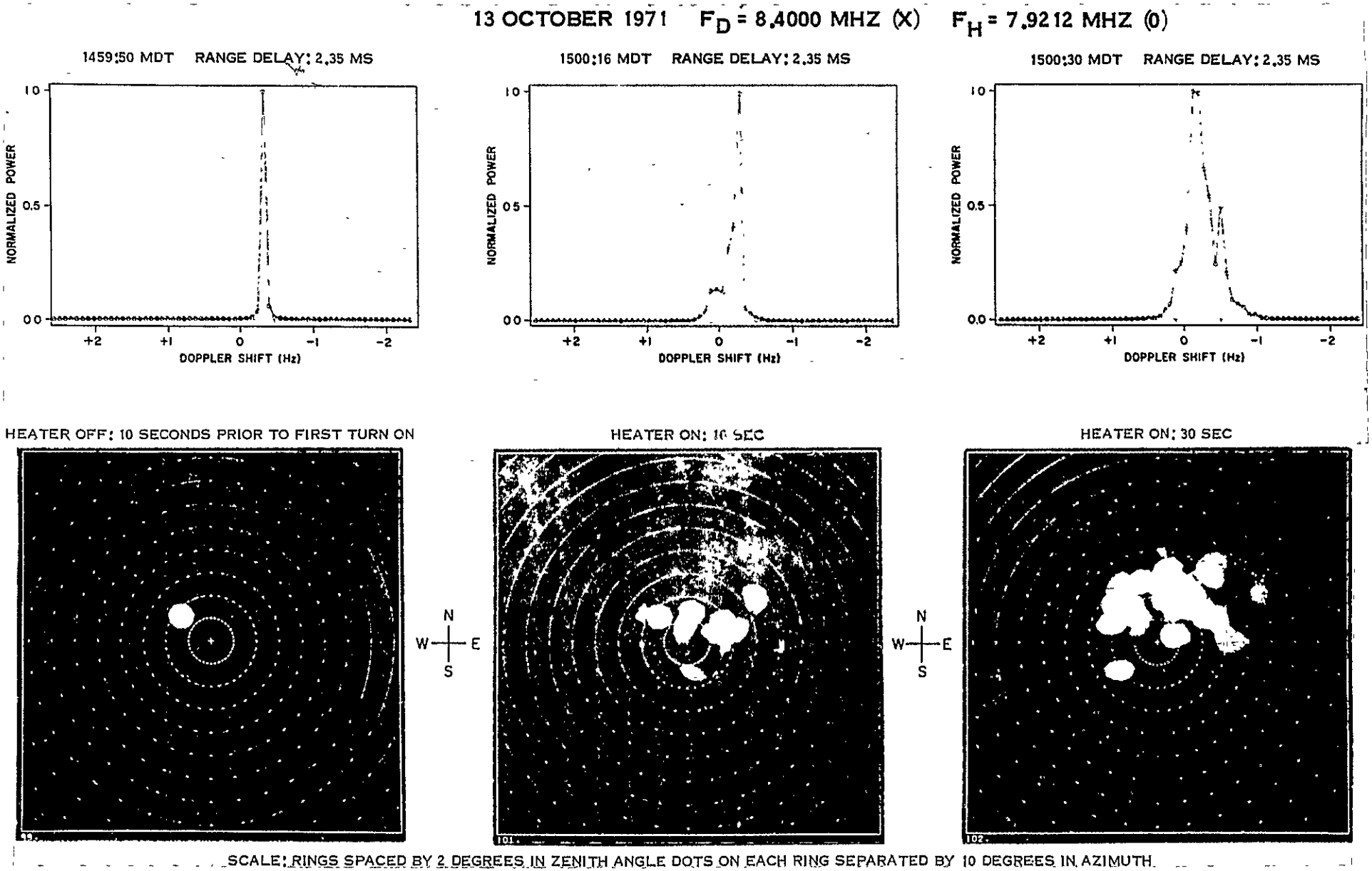

FIGURE 2.20 IONOSPHERIC EFFECTS ON HF BACKSCATTER INDUCED BY PLATTEVILLE HEATER

signals. This illustrates the creation of ionospheric irregularities as a result of the Platteville heating experiment. It also illustrates one type of diagnostic measurement facility that will be required during an experimental verification program. This facility will map out the region over which irregularities occur as well as demonstrate the effects that the irregularities will have on HF systems.

2.3.3 OTHER USERS

Tables 2-6, 2-7 and 2-8 list other user systems for navigation, communication and DoD radars, respectively. Each table shows the principle system characteristics, identifies potential power beam ionospheric effects and makes recommendations. It is important to remember that only a limited number of examples have been selected. However, the systems have been selected to span the RF domain from 10 kHz to 6 GHz and thus indicates potential impact on most users. It is clear that if an experimental program for evaluating ionospheric effects is undertaken, a critical element will be the design and implementation of experiments which will quantitatively determine the risk that the MPTS ionospheric effects pose to other users.

The experimental program will have to answer the following questions:

1. Will the power beam effects be more intense and occur more frequently when compared to naturally occurring ionospheric disturbances?
2. Will the effects be limited to the power beam or will the perturbations occur over larger geographical areas?

2.3.4 POWER BEAM AND PHASE CONTROL SYSTEM

A phase control system is required to keep the power beam focused on the ground rectenna. A pilot beam system is being considered which transmits from the ground (actually located in the middle of the rectenna) and, by comparing

TABLE 2-6 OTHER USERS: NAVIGATION SYSTEMS

SYSTEM	SYSTEM CHARACTERISTICS	POWER BEAM EFFECTS	RECOMMENDATIONS
OMEGA	• 10.2 KHZ, CW • 8 STATIONS, TDMA • SINGLE FREQUENCY HYPERBOLIC SYSTEM (PHASE COMPARISONS)	• IONOSPHERIC EFFECT COULD CAUSE SUDDEN PHASE ANOMALIC • PHASE ANOMALIES COULD INCREASE LOCATION ERROR BY A FACTOR OF 5 (1 TO 5 MILES).	• THEORETICAL CALCULATIONS OF POWER BEAM EFFECTS AND COMPARE WITH OBSERVED SPAs. • ESTABLISH SEVERAL OMEGA LINKS WHICH PASS THROUGH HEATED VOLUME.
LORAN C	• 100 KHZ, PULSE • GROUND WAVE (2000 KM) AND SKY WAVE (8000 KM) • HYPERBOLIC SYSTEM	• NONE ON GROUND WAVE • FOR SKY WAVE USERS POWER BEAM COULD DEGRADE PERFORMANCE ALTHOUGH SKY WAVE USERS FAR REMOVED FROM DISTURBED REGIONS.	• LIKELY NOT TO BE SIGNIFICANTLY EFFECTED. • SINCE LORAN C EQUIPMENT READILY AVAILABLE, PARALLEL EXPERIMENTS WITH OMEGA SHOULD BE CONSIDERED.
NAVSTAR GPS (GLOBAL POSITIONING SATELLITE) 1st SATELLITE IN MAY 1977	• THREE-D LOCATION USING 4 SATELLITES • 1200 AND 1600 MHZ (TWO FREQUENCIES ELIMINATE RANGE ERROR OF IONOSPHERE) • USE OF IONOSPHERIC MODEL FOR SINGLE FREQUENCY USER • DESIGNED FOR LOW GAIN OMNI-RECEIVE ANTENNA	• ELECTRON DENSITY CHANGES WILL NOT EFFECT TWO-FREQUENCY USERS. • ELECTRON DENSITY CHANGES INCREASE ERROR BUDGET FOR SINGLE-FREQUENCY USERS. • IRREGULARITIES COULD CAUSE SCINTILLATIONS WHICH COULD PREVENT SYNC ACQ BY UNSOPHISTICATED USER.	• POSITIONING SYSTEM OF THE 1980s AND ITS IMPORTANCE MAKES IT MANDATORY TO EXPERIMENTALLY DETERMINE EFFECTS OF HEATING. • MONITOR PERFORMANCE OF GPS, PARTICULARLY OVER EQUATORIAL REGION.

TABLE 2-7 OTHER USERS: COMMUNICATION SYSTEMS

SYSTEM	SYSTEM CHARACTERISTICS	POWER BEAM EFFECTS	RECOMMENDATIONS
HF	• 3-30 MHZ • USES IONOSPHERE AS REFLECTOR TO PROPAGATE AT RANGES FROM 400-800 KM	• PROPAGATION OUTAGES • LOSS OF COMM LINKS • MANY USERS EFFECTED - HAM - MILITARY - CIVILIAN	• ESTABLISH SEVERAL HF LINKS WHICH PASS THROUGH AND NEAR HEATING REGIONS DURING EXPERIMENT.
AFSATCOM	• ~ 260 MHZ ~ 340 MHZ • SATELLITE-TO-AIRCRAFT COMMUNICATION SYSTEM	• FADING DUE TO SCINTILLATIONS • ASPECT SCATTER COULD CAUSE MULTI-PATH DEGRADATION	• SIMULATE WITH GROUND-BASED COMMUNICATION SYSTEMS. • FLY AIRCRAFT WITH COMM. SYSTEMS NEAR HEATING REGION. • MEASURE SCINTILLATIONS AT 400 MHZ CAUSED BY HEATING.
INTELSAT/ MARISAT	1200 MHZ 1600 MHZ 6000 MHZ } MARISAT 4000 MHZ	• FADING, IF SEVERE COULD BE SIGNIFICANT	• MEASURE SCINTILLATION DURING HEATING EXPERIMENT.

TABLE 2-8 OTHER USERS: DOD RADARS

SYSTEM	SYSTEM CHARACTERISTICS	POWER BEAM EFFECTS	RECOMMENDATIONS
OTH	• 5-30 MHZ • USES IONOSPHERE AS REFLECTOR TO ILLUMINATE LARGE AREAS • SURVEILLANCE FOR CONUS	• COVERAGE SECTOR MAINLY OCEANS, SO EFFECTS LIMITED TO SIDELOBES • ASPECT-SENSITIVE SCATTER FROM IRREGULARITIES AND GROUND BACKSCATTER DOPPLER SPREADING IN SIDELOBES MASK TARGETS	• DURING EXPERIMENT A SMALL-SCALE OTH RADAR SHOULD BE BUILT AND OPERATED (RADAR IS ALSO USED AS A DIAGNOSTIC TOOL FOR EVALUATION OF IONOSPHERIC EFFECTS).
SURVEILLANCE AND SPACETRAK RADARS	• VHF-UHF • DETECT SLBMs AND SPACETRAK	• IF IN MAINLOBE CAUSE - SEVERE TARGET FADING - RANGE ERRORS	• GROUND BASED BACKSCATTER OBSERVATIONS DURING HEATING EXPERIMENT

measured phase at sections or subarrays of the transmitter array with a centrally located reference phase, the power beam is kept in focus on the ground. The possibility was investigated under previous studies[13] that ionospheric perturbations could impair performance of the pilot beam phase control system. Also studied at this time was the possible effect that the ambient ionosphere, as well as the modified ionosphere, would have on displacement or dispersion of the power beam.

Further investigation under this effort tends to confirm the conclusions of our previous MPTS study (for power densities below 100 mW/cm^2) that:

1. Negligible displacement or dispersion of the high power beam by ionospheric effects will occur.

2. The ground-based pilot phase front at the transmitting antenna will not be significantly affected by ionospheric perturbations.

However, we believe that as the pilot beam and phase control system is a critical element of the MPTS system, significant risk could still be incurred if the above conclusions were not experimentally verified to some degree. Section 4.4 of this report describes in further detail the objectives and implementation of the currently recommended phase control orbital experiments. In short, it is recommended that in addition to further simulation of the pilot beam control system, a 100 m and possibly a 1 km linear array be placed at GEO orbit and that the phase control system using the ground based pilot beam be verified. The ground based pilot beam would be located so that its path traverses the region being modified by a facility which simulates the heating effects of the power beam.

2.4 TECHNOLOGY AND DEMONSTRATION PROGRAM

2.4.1 PROGRAM PLAN

The overall elements in the currently proposed MPTS ionospheric effects technology program are described in Table 2-9. A detailed breakdown of each major element is described in Tables 2-10a and 2-10b. The three basic elements of the program are the theoretical studies, ionospheric modification facility (including associated ground experiments), and the orbital experiments. This section will specifically address the requirements for the ionospheric modification facility and the orbital experiments. The reason for this is that these items form the major cost elements of the technology program and, in addition, recommendations for continued theoretical studies and other user experiments (ground based experiments) have been described in Sections 2.2.4 and 2.3.3, respectively.

2.4.2 REQUIREMENTS FOR IONOSPHERIC MODIFICATION FACILITY

As discussed previously in this report, it is recommended that an ionospheric modification facility be established to simulate the effects of the MPTS primarily on other users of the ionosphere. The requirements for the ionospheric modification facility are determined by specifying the likely operating range of the microwave power system. Table 2-11 lists the power beam parameters as a function of DC power out from the rectenna. (Details of the microwave power system specification can be found in Appendix A.) This table shows that a peak power density (P_D) in the ionosphere of 14 mW/cm^2 with a 3 dB spot size in the ionosphere of 6 km is the appropriate specification for a 4GW system. Also shown on this table is the diameter of the ground based rectenna for receiving 95% of the transmitted power, as well as the power density at the first sidelobe, assuming a 24 dB down sidelobe level. An arrow in Table 2-11 shows the power output for what is considered the baseline system.

TABLE 2.9 MPTS IONOSPHERIC EFFECTS PROGRAM - SUMMARY

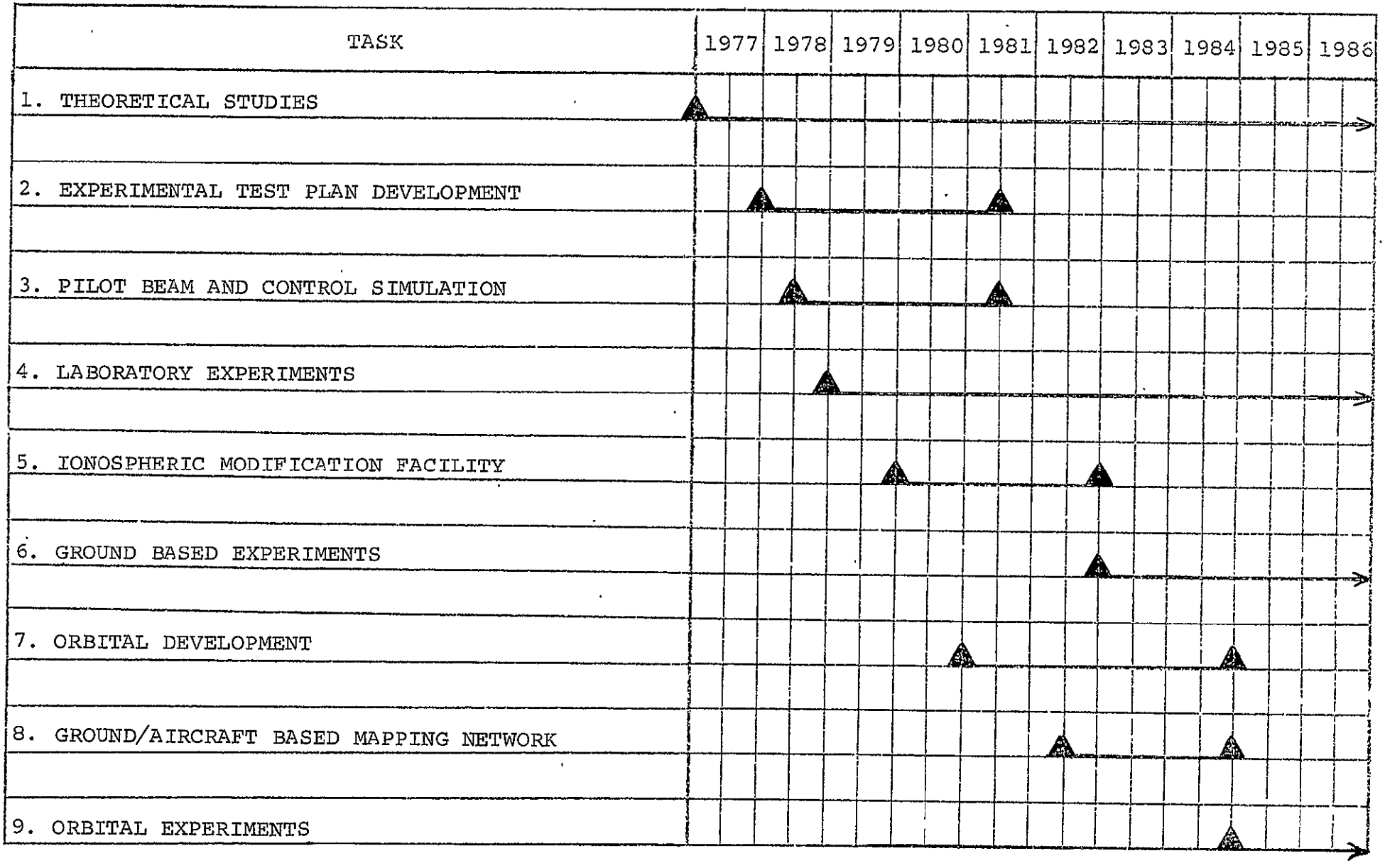

TABLE 2-10a MPTS IONOSPHERIC EFFECTS PROGRAM

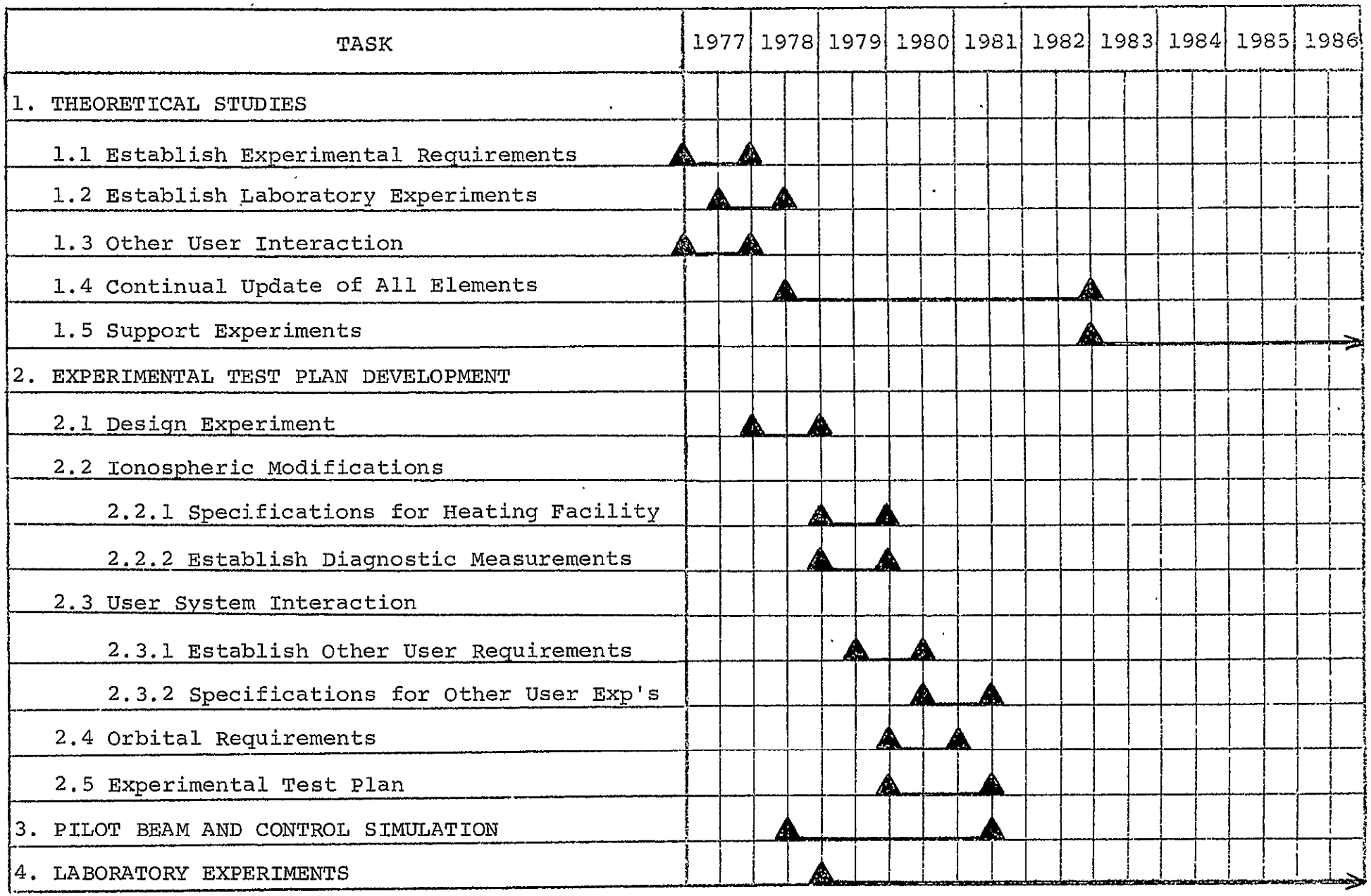

TABLE 2.10b MPTS IONOSPHERIC EFFECTS PROGRAM - Continued

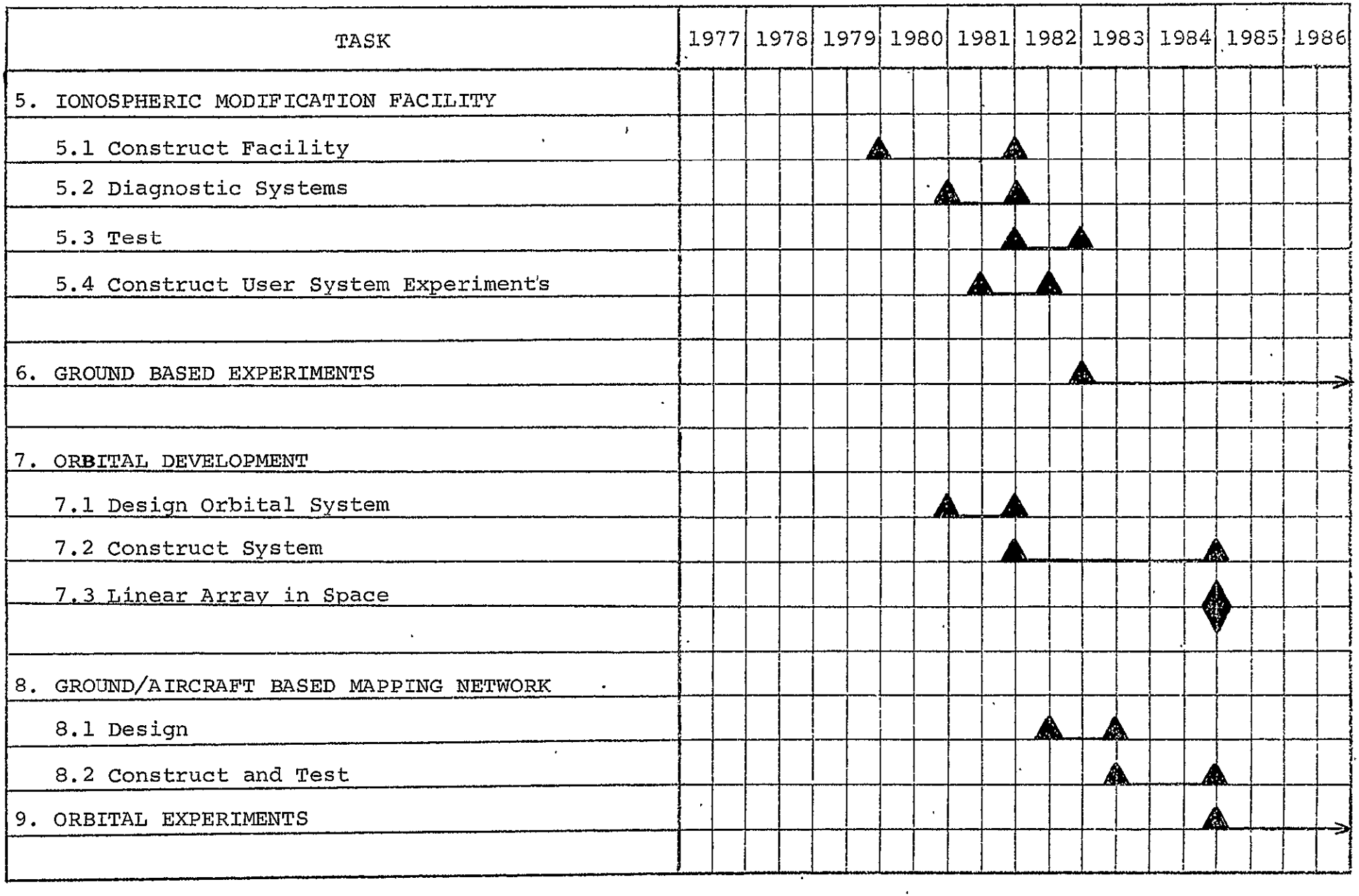

TABLE 2-11 POWER BEAM PARAMETERS AS A FUNCTION OF DC POWER FROM RECTENNA (P_G)

P_G (GW)	Max P (mW/cm^2)	3 dB Spot Size, D_S (km)	95% Power Diameter (km)	P_D at Sidelobes (mW/cm^2)
4	14	6.0	10.9	0.06
5	22	5.4	10.3	0.09
5.258	24	5.2	10.0	0.10
6	31	4.9	8.9	0.12
7	43	4.5	8.2	0.17
8	56	4.2	7.7	0.22
9	70	4.0	7.3	0.28
10	87	3.8	6.9	0.34

NOMINAL MPTS SYSTEM

Figure 2.21 relating the probability of being constrained to operate at below a specific power density to peak power density at the ground was constructed to define the region of interest for MPTS power density. The figure has two curves: one for ionospheric constraints and the second for biological/ecological constraints. Considerable judgement was involved in their formulation, however, the following specifics apply. Below 15 to 20 mW/cm^2 power densities, the MPTS has a high probability of being allowed to operate because studies indicated that adverse ionospheric effects are not likely to occur until these power densities are exceeded. As the power density increases the likelihood of adverse ionospheric effects increases and the the likelihood of being allowed to operate decreases. Because of the large effects which are likely to occur at power densities above 50 mW/cm^2 and because of the increased likelihood of plasma instabilities, it is unlikely that future systems will operate above these power densities. In addition, because current theories are suspect above these power densities, a rationale for operational acceptability would be unfounded. The uncertainty in further extrapolation decreases the likelihood that systems operating above this power density will be built. Also from the biological considerations point of view, it is unlikely that international agreement would be readily obtained for sidelobes much in excess of 0.2 mW/cm^2 which corresponds to a mainlobe density of approximately 50 mW/cm^2. It would appear that systems below 4 GW would have essentially no risk with respect to either ionospheric or biological constraints. However, cost analyses indicate that there is a decreasing economy of scale below 4 GW of power output. Based on these considerations, the likely range of operation is from 4 - 7 GW. Even for this operating range, it is shown that there is a significant program risk because of ionospheric effects on other users. As such, we have recommended an experimental program which will address power densities of the appropriate 3 dB spot size in accordance with Table 2-11 for systems between 4 and 7 GW.

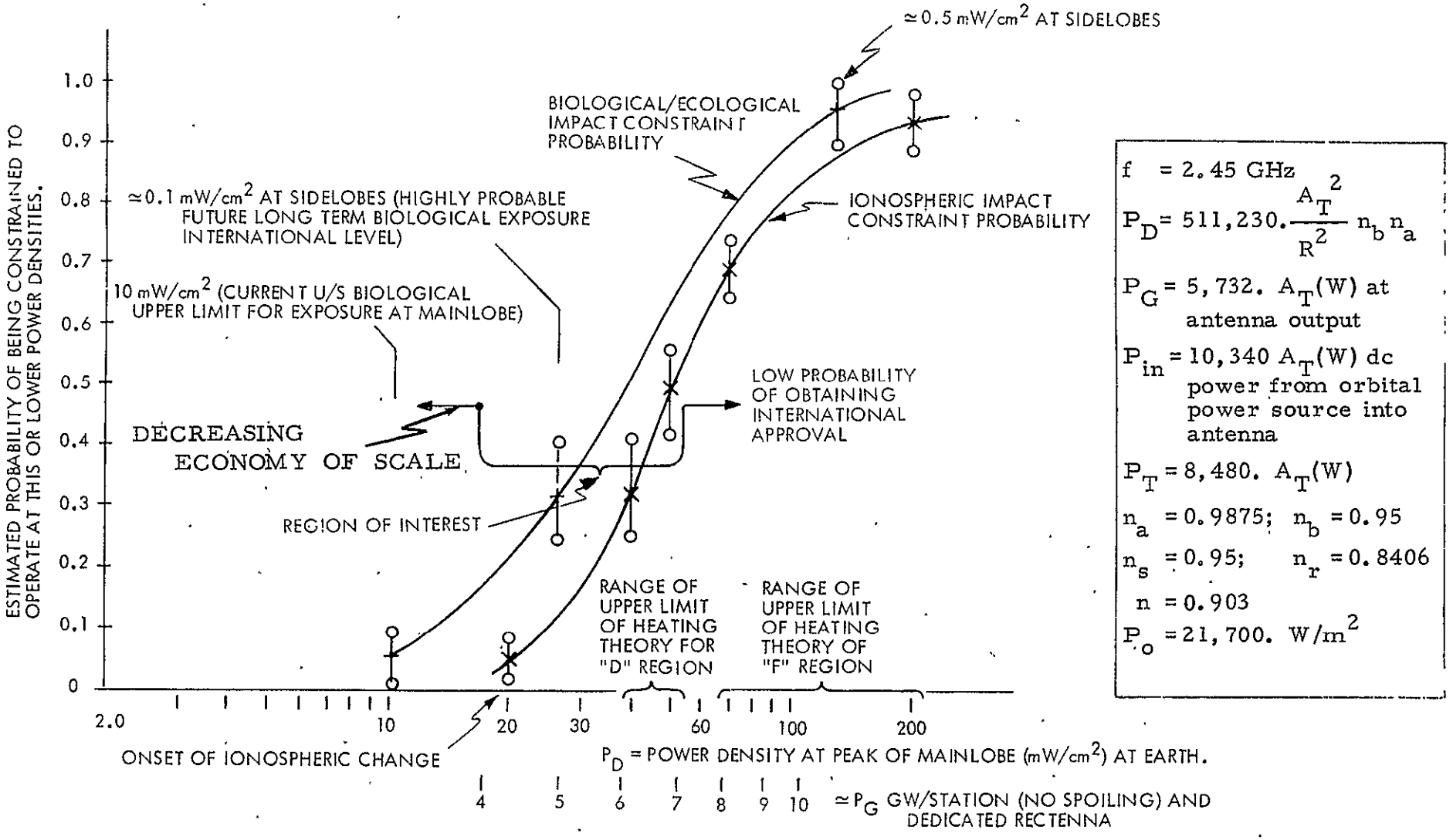

FIGURE 2.21 PROBABILITY OF BIOLOGICAL & IONOSPHERIC POWER DENSITY CONSTRAINT

2.4.3 OPTIONS FOR IONOSPHERIC MODIFICATION FACILITY

Table 2-12 lists the options for simulating the ionospheric effects of the MPTS. It should be understood that the primary purpose of the ionospheric modification facility is to evaluate the impact of the MPTS power beam on other users. It is then assumed to be available for inclusion in integrated tests with orbital test equipment associated with MPTS evaluation. Two classes of systems were considered: a heating facility from space and a heating facility from the ground. Clearly, a heating facility from space at GEO which provides the proper power densities and spot size over a long time period requires a full scale system, the first of which is assumed to be the prototype, to be built in the 1995 time frame. The ionospheric effects considerations should be specified much before prototype commitment probably in the middle 1980's and therefore an early alternate approach is required. A possibility that has been considered is to build a heating facility at LEO; however, the large and rapid horizontal motion of this heating facility would not allow steady state heating conditions to be approached because the time allowed by the satellite motion to heat a specific area in the ionosphere is too short. It is therefore not recommended for further study.

The remaining alternative for the near term is to provide a ground based heating facility. Four options were considered of which the first two uses existing facilities or upgrades existing facilities and are under investigation by Prof. Gordon of Rice University. Under the present effort we have specified the required heating facility at 20 - 60 MHz and 2.45 GHz. The advantage of the 20 - 60 MHz system, as will be shown, is that it requires modest power aperture products but assumes that the results can be scaled from 20 - 60 MHz to 2.45 GHz. The inclusion of a 60 MHz system is to allow some insight as to whether the results can be scaled in frequency over this limited frequency range, which would provide a level of confidence in scaling results to 2.45 GHz. This may be supplemented with a minimal 2.45 GHz test to specifically verify the extrapolation. The alternative is to provide a ground based heating facility at 2.45 GHz which simulates the effects of an operational facility but requires a very large power aperture product.

TABLE 2-12 OPTIONS FOR SIMULATING MPTS INDUCED IONOSPHERIC MODIFICATIONS

APPROACH	ADVANTAGES	DISADVANTAGES	COMMENT
Heat From Space			
A. GEO	Simulates operational system	Requires full scale system Earliest test in 1990's	Recommended for operational configuration
B. LEO	Possibly lower cost	Horizontal motion does not allow steady conditions to be approached	Not recommended
Heat from Ground			
A. Use Existing Facilities	Immediate results	Can only simulate D-Region effects in a limited manner	Under investigation by Prof. Gordon of Rice University
B. Upgrade Existing Facilities	Early results	To be determined	Under investigation by Prof. Gordon of Rice University
C. Conceived New Facilities at 20 - 60 MHz	Simulates power beam heating using relatively modest transmit powers	Assumes frequency scaling is valid Heats from ground up	Subject of this study
D. Conceived New Facilities at 2.450 GHz	Simulate effects at MPTS operating frequency	Requires large power aperture product	Subject of this study

2.4.4 GROUND BASED HEATING FACILITY

2.4.4.1 Specifications

The amount of ohmic heating produced by radio waves is inversely proportional to the square of the frequency of transmissions. Thus, for a given power density at a specified frequency the value of $P_D \lambda^2$ (P_D is peak power density, λ is wavelength of transmission) is proportional to the ohmic heating and if this product remains a constant while increasing λ^2, a proportional decrease in power density would result in the same ohmic heating. For the operational frequency of 2.45 GHz and a ground based simulation facility at 20 MHz, the required P_D to simulate effects of the power beam as a function of DC power output from the rectenna is listed in Table 2-13. Also shown is the value of $P_D \lambda^2$. This clearly illustrates the advantages of building a ground based heating facility at 20 MHz. One could further envision going to frequencies below 20 MHz, but remembering that there is a significant difference if heating is done near the plasma frequency of the ionosphere (as for the Platteville experiments), it is necessary (if there is any hope of scaling results to 2.45 GHz) to be at a frequency above the nominal plasma frequencies that are likely to occur.

Specifications for the ground based heater include the diameter of the heating array on the ground (D_H) and the power input required by the ground based heater. The diameter of the ground based heater is determined by:

$$D_H = 0.886 \times \lambda_H \times \frac{R_H}{D_S}$$

where λ_H is the wavelength of transmissions, R_H is the slant range to the heated region, D_S is the 3 dB spot size to be heated at range R_H. In the F-layer R_H is 350 km, while for the D-region R_H is 80 km. The equation for D_H assumes uniform weighting and shows, depending on the region in the ionosphere to be heated, different diameters of the ground based heating facility will be required.

TABLE 2-13 P_D REQUIRED AT 2.45 GHz, 20 MHz AND 60 MHz TO SIMULATE IONOSPHERIC EFFECTS OF POWER BEAM AS A FUNCTION OF POWER OUTPUT, P_G

(GW)	P_D at 2.45 GH_z (mW/cm^2)	P_D at 60 MH_z (mW/cm^2)	P_D at 20 MH_z (mW/cm^2)	$P_D \lambda^2 = K$ (W)
4	14	8.37×10^{-3}	0.93×10^{-3}	2.1
5	22	13.14×10^{-3}	1.46×10^{-3}	3.3
5.258	24	14.31×10^{-3}	1.59×10^{-3}	3.6
6	31	18.54×10^{-3}	2.06×10^{-3}	4.6
7	43	25.74×10^{-3}	2.86×10^{-3}	6.4

The required power input is determined by:

$$P_T = P_D \frac{R_H^2 \lambda_H^2}{A_H} \times \frac{1}{\eta}$$

where P_D is the maximum power density at the heated region, A_H is the area of the array on the ground ($A_H = \pi D_H^2/4$) and η is the efficiency of the transmitter subsystem specified at 60% for the purposes of this study. As shown above, $P_D \lambda^2$ is a constant K and, using the definition of A_H, the equation for P_T becomes:

$$\text{Input Power: } P_T = 2.70 \frac{K D_S^2}{\lambda^2} \quad \text{(watts)}$$

where the efficiency of the heater (rf/dc) is 60%. The values of K as a function of power output of the MPTS is shown in Table 2-13 and the 3 dB spot size as a function of power output is shown in Table 2-11.

The equation for P_T assumes that the distance to the heated volume is far enough so that the heated volume is in the far field of the transmissions. The near field/far field criteria is that the distance R_H be greater than $2D_H^2/\lambda_H$. If $2D_H^2/\lambda_H$ is greater than R_H, the equation for P_T is replaced by $P_T = P_D \times A_S$, where A_S is the area of the ionosphere to be heated. Since in the near field regime the energy propagates in a cylinder with no $1/R^2$ spreading, the area of the heater array on the ground, A_S, is equal to A_H (i.e., the diameter of the array on the ground, D_H, is equal to the diameter of the 3 dB spot to be heated, D_S).

2.4.4.2 Ground Based Heating Facility at 20 and 60 MHz

Since ohmic heating implies that $P_D \lambda^2$ is a constant, we can clearly see the benefit of establishing a heating facility at 20 MHz. The wavelength at 20 MHz is 122.5 times the wavelength at 2.45 GHz, which translates into a decrease in required power density of 1.5×10^4. Table 2-14 shows the specification for a ground based heater at 20 MHz for F-layer experiments. The near field/far field criteria for F-layer effects is that the diameter of the array be less than 1224m (this assumes that the height of the F-layer is greater than 200 km), which is not exceeded even for the 7 GW system. Two values of the required power input are shown in Table 2-14. The first column does not include self-induced D-layer effects of the HF heater, while the second column compensates for increased D-layer absorption due to the effects of the 20 MHz heater at D-layer heights. This factor would not apply at the operational frequencies because absorption, even for a modified D-layer at microwave frequencies, (2.45 GHz), is negligible.

In the operational system the width of the heating tube is essentially independent of slant range through the ionosphere because of the small variation in slant range (i.e., 36,650 km for F-layer heating and 36,920 for D-layer heating). However, for heating from a ground based facility the variation in the slant range to the D-layer (80 km) and the F-layer (350 km) is significant. Table 2-15 provides the specification for the HF heater at 20 MHz for D-layer experiments. The transmitter power is half that required for the F-layer experiment, because we do not have to include increased absorption in the D-layer due to transmissions. In fact, that is one of the D-layer effects we want to observe. The aperture of the heater is reduced for the D-layer experiments because to provide a fixed spot size at a shorter slant range requires a smaller aperture. By appropriate use of the ground based phased array, a heater facility designed for F-layer experiments can be used for D-layer experiments as well as for other regions in the ionosphere.

TABLE 2-14 SPECIFICATIONS FOR HF HEATER AT 20 MHz FOR F-LAYER EXPERIMENTS

P_G (GW)	Diameter of HF Heater, D_H (m)	P_T ① (MW)	P_T ② (MW)
4	776	0.91	1.80
5	861	1.04	2.08
5.258	895	1.16	2.31
6	949	1.34	2.68
7	1034 ③	1.57	3.13

① Power input exclusive of increased absorption in D-Layer due to HF heater.

② Power input including increased absorption in D-Layer due to HF he ater

③ Far field criteria is valid for F-Layer if $D_H < 1224$ m.

TABLE 2-15 SPECIFICATION FOR HF HEATER AT 20 MHz FOR D-LAYER EXPERIMENT

(GW)	D_H (m)	P_T (MW)
4	177	0.91
5	197	1.04
5.258	205	1.16
6	217	1.34
7	236	1.57

The HF facility proposed has approximately the same transmitted power as the Platteville heater (2 MW average power), but the Platteville array had a diameter of 110 meters[13] (and a spot size of approximately 85 km at 7.5 MHz), whereas the array proposed for the 20 MHz facility is 1000 meters. The HF facility at Arecibo[13] has a 305 meter array but only a 200 kW power output. The effective power output from Arecibo is only 3 dB below Platteville but heats an area approximately 1/4 the size of the Platteville heater (i.e., a spot size in the ionosphere approximately 42 km in diameter). The above information is included to show that the power aperture product that we propose for the 20 MHz facility is not unreasonable. It also suggests that modification of the existing facilities is not unreasonable or that an entirely new facility could be built using existing technology.

Finally, the specifications for a ground based heater at 60 MHz is provided in Table 2-16. The added absorption in the D-layer due to the 60 MHz transmissions is much smaller than for the 20 MHz system because D-layer absorption is inversely proportional to frequency squared. The advantage of building such a system (even for one power level) is that it can be used to increase our confidence in the frequency scaling law used to extrapolate results to 2.45 GHz.

TABLE 2-16 SPECIFICATION FOR 60 MHz HEATER FOR F-LAYER EXPERIMENT

P_G (GW)	D_H (m)	P_T ① (MW)	P_T ② (MW)
4	310	8.2	8.8
5	345	10.4	11.2
5.258	358	10.5	11.3
6	380	11.9	12.8
7	413	14.0	15.0

① Power input exclusive of increased absorption in D-Layer due to heater.

② Power input including increased absorption in D-Layer due to heater.

2.4.4.3 Ground Based Heater Facility at 2.45 GHz

The required input power (assuming 60% efficiency) for a ground based heater facility at 2.45 GHz which will simulate the effects of a 5.25 GW system at F-layer heights is calculated to be 8.9 GW (far field system) and 7.85 GW for a near field system. The far field system requires an aperture of 10 meters in diameter while the near field system requires an array aperture 5 km in diameter. Clearly either system requires excessive power.

An alternative is to build a scaled down system at 2.45 GHz. If only a 0.5 km spot size is required, the transmitted power required is 78.5 MW with an array diameter of 0.5 km. This facility cannot fully simulate the effects of the power beam because of its reduced spot size. However, under appropriate conditions (ionospheric horizontal drift velocities small enough to allow steady-state conditions to be reached) the operation of this facility could be used to validate extrapolation of results obtained from the 20 MHz heating facility. It may also be sufficient to obtain the operational effects on the MPTS pilot beam. Before a recommendation of this option can be formulated, further study is required to determine if the cost and scientific results of establishing a heating facility at 2.45 GHz is warranted. Particularly the possibilities of using existing facilities at Arecibo should be further explored. In addition, the possibility exists that a new facility could be built and used in conjunction with other intended applications of large scale microwave power transmissions.

2.4.5 ORBITAL EXPERIMENTS

2.4.5.1 Objectives - As parts of the Progressive MPTS Development Milestones with Objectives Relating to Ionospheric Interaction.

The objectives of these orbital experiments are to:

1. Conduct early tests of the MPTS prototypical hardware in the GEO environment at operational voltages, voltage gradient, current densities and thermal densities. Continue tests through the 11-year solar cycle.
2. Test the retrodirective (Pilot Beam) Phase Control System in the natural and simulated operational environments and determine requirements for ground based command systems to compensate for pointing drift and defocussing.
3. Determine the ambient ionospheric effects on the phase control system.
4. Determine the simulated induced ionospheric effects on the phase control system.
5. Determine the effect of the ambient ionosphere on the power beam.
6. Determine the effects of the ionosphere as modified by the ground based heater on the sensitive regions of the power beam.

To accomplish these objectives, an orbital experimental program consisting of two pre-prototype major steps is currently recommended: (1) The first step is to place a 100 meter linear array at GEO powered by prototypical rf generators currently assumed to be amplitrons with an input power requirement of approximately 150 kW. This test article is recommended to be in orbit in the early to middle 1980s. well in advance of the solar cycle peak in 1992. (2) The second

step is to place a 1 km linear array at GEO. This array is to be at least one waveguide wide and 1 km long with an input power requirement of about 2 MW This is in addition to full scale subarray testing at about the same power level. The 1 km linear array test article should be available, if required, for experiments about 1986.

The commitment to the prototype should be possible based on early test results from the 100 m test article. However, it would be prudent to include the 1 km test article in the program as a reasonable progressive step in terms of power and dimension toward the full scale prototype. Furthermore, as a continuation of the progressive MPTS development program, the prototype itself should be configured and tested in three major steps:

1. A 1 km linear array at least one subarray wide at GEO built on the prototype structure. This would utilize 50 to 500 MW of input power. It may be available in the early 1990's (assume 1992).

2. Building on and coherent with the above, a 1 km linear array at right angles to the one above. This totally would utilize 100 to 1000 MW and be available about one year after the above (assume 1993).

3. Building on the above, progressively fill in the gradrants to utilize the full input power of 6.5 to 12.0 GW to a single antenna. It may be available by the mid 1990's (assume 1995).

As this report is mainly concerned with ionospheric effects and developing a technology program which addresses ionospheric effects, the remaining discussion of the orbital experiments will pertain to information gained with respect

to the ionosphere. Of course the reader will bear in mind that there are other possibly more pressing reasons for the orbital experiments such as testing the hardware in space to implement the first objective above.

2.4.5.2 100 Meter Linear Array at GEO

Figure 2.22 schematically shows the 100 meter array at GEO. Also show is the area in the ionosphere being heated by the ground based heater facility and the path of the pilot beam from the ground through the ionospheric region modified by the ground based heater to the 100 meter array. This figure and Figure 2.23 (which is an exploded view of the ionospheric interaction region) illustrates that the pilot beam is only effected by a limited portion of the ionosphere. For exampl well within the 3 dB width of the heater, the primary segment of the pilot beam in the ionosphere, propagated to (subtended by) the 100 meter array at GEO is approximately 1 meter. Similarly for the 1 km array at GEO, the segment in the ionosphere would be approximately 10 meters. It is likely that significant, however small, phase perturbations would be produced in the pilot beam phase front over this region of the ionosphere. However, if the ambient or induced environment in the ionosphere produces significant defocusing or movement of the power beam, the pilot beam system could not automatically cause the power beam to refocus or re-point to the rectenna in the presence of these significant ionospheric effects. That is the pilot beam does not propagate the ionospheric perturbations across a significant portion of the power beam directly to the array at GEO because the pilot beam propagates primarily through a very limited region in the ionosphere as seen by the array at GEO. If the ambient ionosphere perturbes the power beam or modifications of power beam by ground based heater effects are significant, a ground based mapping network and ground based command control system in addition to the pilot beam control system would be required for compensation and it could be effective for long period perturbations compared to the ground to GEO transmit time.

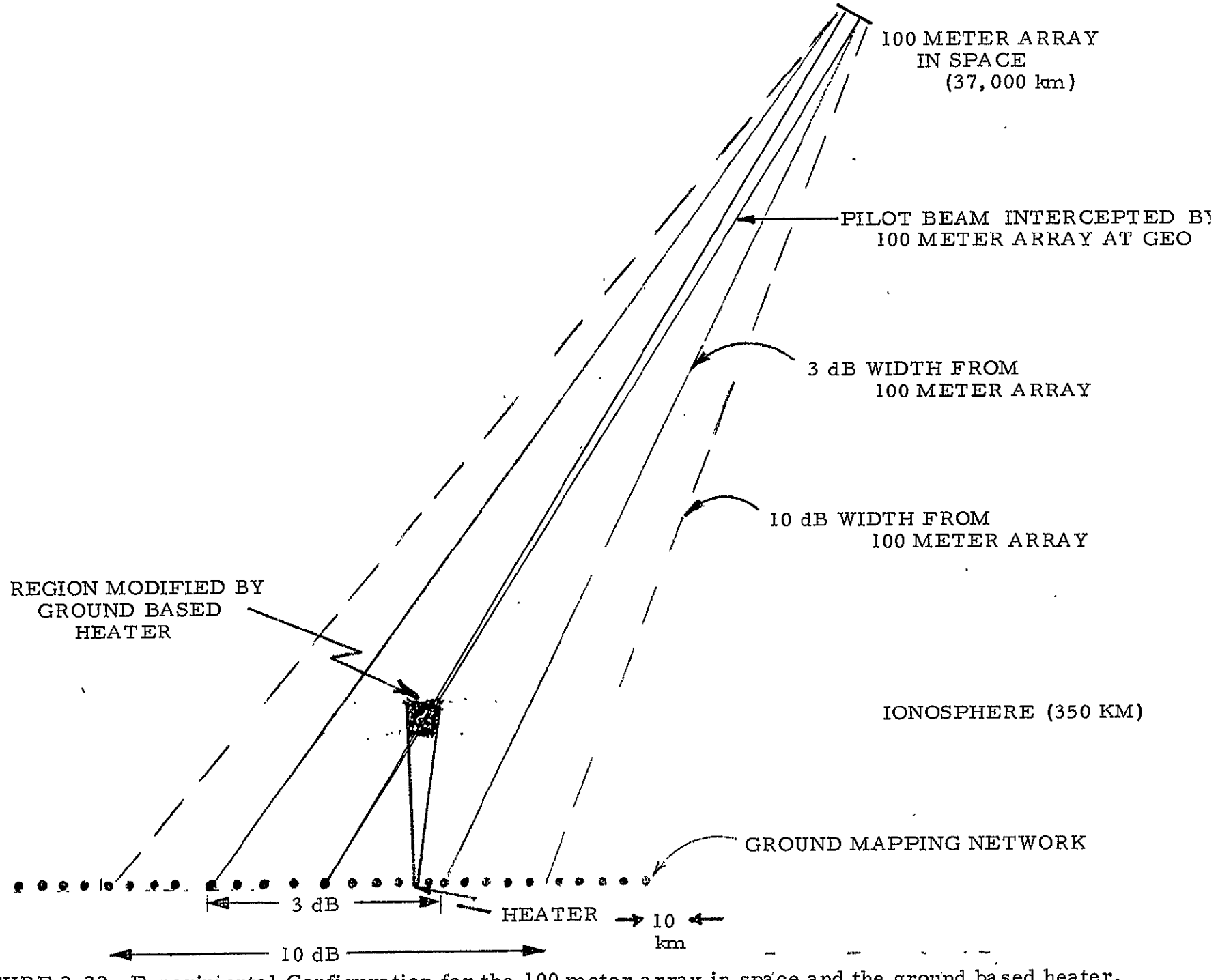

FIGURE 2.22 Experimental Configuration for the 100 meter array in space and the ground based heater.

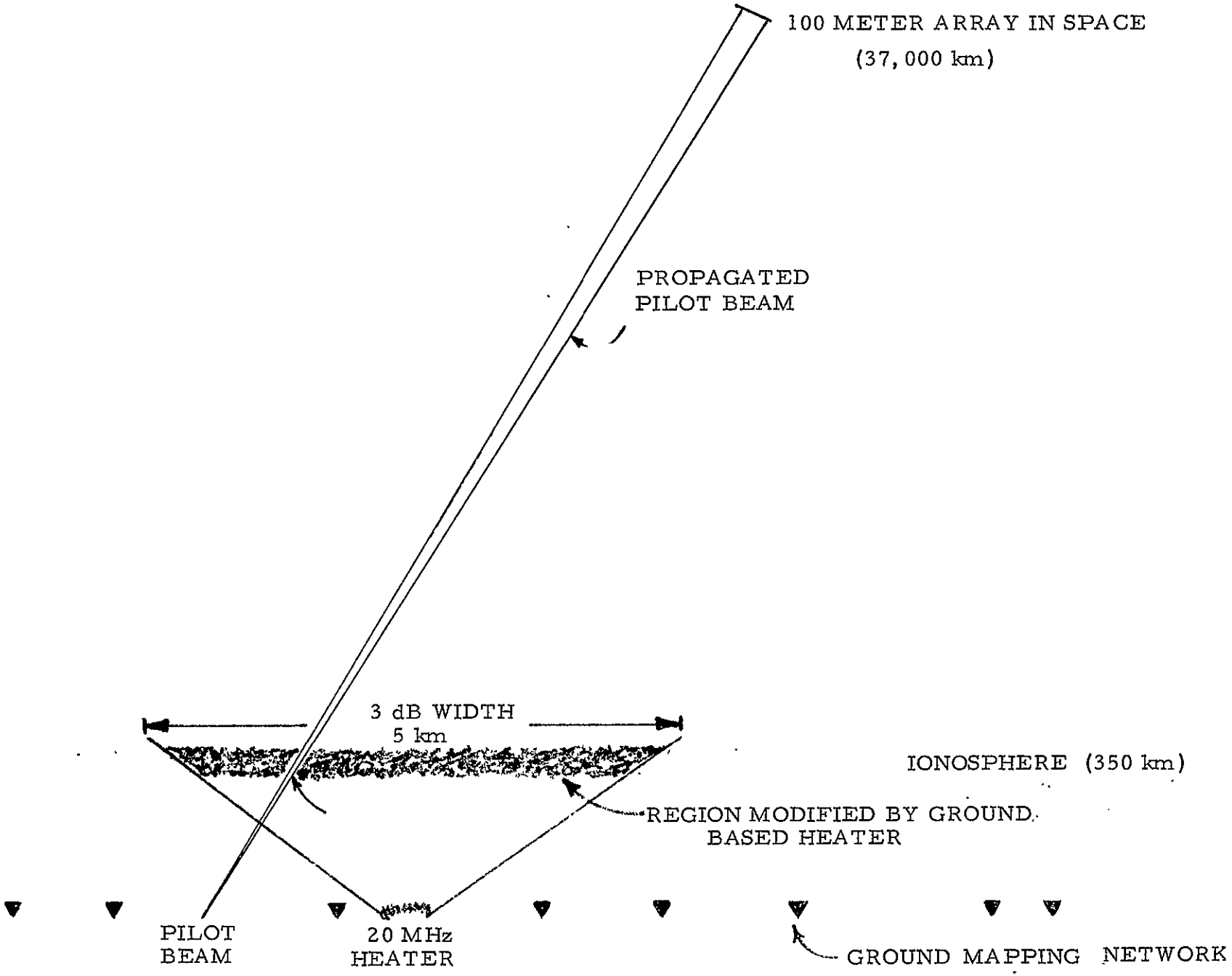

FIGURE 2.23 EXPLODED VIEW OF IONOSPHERE INTERACTION REGION

The objective of the 100 meter orbital experiment (in the light of the limitations discussed above) would be to:

1. Verify performance of the pilot beam control system in the absence of significant ionospheric interactions in removing the effects of orbital motions of the array at GEO.

2. Determine if the ionosphere will perturb the pilot beam phase front significantly and hence the retrodirective control system. NOTE: Although we do not believe that this is likely, the risk to successful operation of the system is too great to be accepted without experimental verification. It would also be prudent to include the compensating ground command system in the prototype at least.

3. Determine if the ambient ionosphere effects the power beam significantly. NOTE: Even though the power beam diameter is ten times the projected operational beamwidth, insight as to possible effects of the ionosphere on the power beam could lead to modifications of the phase control system which would greatly enhance the probability of successful operation of the prototype. Specifically the requirements for a ground based monitoring and control system should be established. In fact a combined retrodirective pilot beam and ground based monitoring and command system might be required. The pilot beam would remove effects of orbital perturbations and the ground based monitoring and command system would remove ionospheric effects.

2.4.5.3 1 km Linear Array at GEO

The major drawback for consideration of ionospheric interactions of the 100 meter array is the large beamwidth of the 100 meter power beam with respect to the beamwidth of the operational system. For this reason (again from an ionospheric viewpoint and realizing that a 1 km linear array would be a logical step in simulating the prototype) it is currently recommended that the next orbital experiment be a 1 km linear array. This in addition to providing a realistic test of the hardware in its operational environs would provide a power beam of the proper dimensions in one axis. The pilot beam now has an effective beamwidth in the ionosphere of approximately 10 meters which propagates directly to the 1 km array.

The objective of the 1 km array in GEO would be to evaluate the:

1. Effectiveness of the pilot beam in focusing the power beam in the presence of ambient ionospheric effects as well as in the presence of ionospheric modifications from ground based ohmic heating.
2. Perturbation on the power beam due to the ambient ionosphere as well as due to ionospheric modification from ground based ohmic heating.
3. Evaluate the pilot beam phase control system and upgrade the phase control system to include a ground based monitoring and command control system if required.

After prototype commitment the several steps in build up of the full scale prototype system will be evaluated to progressively confirm the concepts and their implementation as well as to finally certify operational readiness of the SSPS system. In this prototype stage, it will be possible to, very early, compare the long term data base of ionospheric effects of ground based heater with ionospheric effects of MPTS. It is believed that by following this step-by-step pro-

cedure the adverse effects of the ionosphere will not be a significant factor in the overall success of the MPTS and hence the SSPS system.

2.4.6 ROUGH ORDER OF MAGNITUDE (ROM) COST FOR MPTS IONOSPHERIC EFFECTS TECHNOLOGY AND DEMONSTRATION

The following will provide a ROM cost for the technology program from 1977 through 1986. As such, the estimate does not include the build-up of the prototype array in space nor does it include O & M costs and technical support beyond 1986. The cost elements will follow the program steps outlined in Table 2-9.

Table 2-17 lists the ROM costs for the MPTS Ionosphere Effects Technology and Demonstration Program; and, Table 2-18 lists the ROM costs for the Ground Based Ionospheric Modification Facility (both a 20 and 60 MHz system as shown).

TABLE 2-17 ROM COSTS FOR MPTS IONOSPHERIC EFFECTS TECHNOLOGY AND DEMONSTRATION PROGRAM

		ROM COSTS, $M
1.	Theoretical Studies	3.6 ± 25%
2.	Experimental Test Plan	1.3 ± 25%
3.	Pilot Beam Control Simulation	0.8 ± 50%
4.	Laboratory Experiments	0.4 ± 50%
5.	Ionospheric Modification Facility	80.0 ± 60%
	20 MHz	34.0 ± 60%
	60 MHz	126.0 ± 60%
6.	Ground Based Experiments	8.0 ± 60%
7.	Orbital Development	
	100 M Antenna Payload	47.0 ± 25%
	Subarray Antenna Payload	436.0 ± 25%
	1000 M Antenna Payload	47.0
8.	Ground Based Mapping Network	7.0 ± 60%
9.	Orbital Experiments	
	100 M Antenna Payload	29.0 ± 30%
	Subarray Antenna Payload	227.0 ± 60%
	1000 M Antenna Payload	193.0 ± 30%
	Sum Excluding 7 and 9	
	20 MHz Facility	$ 55.M ± 50%
	60 MHz Facility (Contingency)	$ 147.M ± 50%

TABLE 2-18 ROM COSTS FOR IONOSPHERIC MODIFICATION FACILITY

5 (B) IONOSPHERIC MODIFICATION FACILITY	20 MHz	60 MHz
GROUND HEATER		
Antenna	$ 1.0 M	$ 5.0 M
Cables	3.1	9.3
Building	1.4	1.4
Transmitters	4.2	21.0
Power Dividers	1.7	8.5
Computer System	1.0	1.0
Power Grid	5.0	15.0
Sub Station	0.8	1.5
Sub Station (5 Year Carrying)	1.6	3.1
Energy	4.5	25.0
	24.3	90.8
Management	3.0	10.0
	27.3	100.8
G & A + Fee	7.0	25.0
	$34.0 M	126.0M

(THIS PAGE INTENTIONALLY LEFT BLANK)

3.0 ANALYSIS OF CRITICAL INTERFACES BETWEEN THE SATELLITE AND THE MPTS

3.1 INTRODUCTION

The following critical interface problems which may affect the ultimate design of the microwave power transmitting system have been studied:

1. The effect of usage of a power transmission system operating at 40 kV on the overall weight and cost of the microwave power transmission system.
2. The effect of the overall structure of the satellite; i.e., the mast, the flex joint and the subarray structure on the amplitron thermal blockage or passive radiation of waste heat.
3. The effect of the dielectric carry-through structure on the microwave antenna.
4. The effect of material sublimation on the operation of the open cavities of the Amplitron.

Based on the results of this study, recommendations for specific approaches, further study or experimentation, and redesign of critical items are made. Section 3.1 describes the general nature of each of the critical interfaces and provides a summary of the key results. Section 3.2 through 3.5 describes in detail each of the critical interfaces listed above. Finally the recommended program plan based on the results of this study is presented in Section 3.6.

3.1.1 HIGH-VOLTAGE POWER DISTRIBUTION SYSTEM

From a system point of view, the transmission of power from the solar panels to the antenna would be more efficient in terms of the cabling weight, size and costs if the Amplitron were to operate at a high-voltage level. Cable sizes are based on the required current to be carried, and for a constant power

system, this varies inversely with the operating voltage. Further savings with a high-voltage system may be achieved due to the reduction in the number of crowbar units required to protect against arcing, and the reduced number of switch gear units to distribute a lower required total current flow inherent in a high-voltage system.

In order to quantify these potential savings, a 40 kV power distribution system was studied (Section 3.2). The approach to this study was to investigate both a system with Amplitrons operating at 40 kV and a system with Amplitrons operating at 20 kV but connected in series. The effect of the two different 40 kV systems on the cost and weight of the microwave power distribution system is presented.

3.1.2 THERMAL BLOCKAGE EFFECTS

A previous study[14] assumed that there was a 5% uniform solid angle structural blockage of the heat radiation to space from the rear of the Amplitrons with the blockage structures at a temperature of 120° C instead of the deep space temperature of -269° C. That study did not include the specific effects of the satellite mast, flex joint, and antenna subarray structure. In the current study an estimate of the effect of blockage by the various structures on the back of the MPTS antenna has been made and is described in Section 3.3.

The importance of this level of detail is that if the actual thermal blockage found, exceeds the assumed 5% figure, the installation and structural approaches will have to be modified or the overall antenna will have to increase in size in direct proportion to the increase in size of each Amplitron waste heat radiator.

3.1.3 DIELECTRIC CARRY-THROUGH STRUCTURE

In the baseline design of the satellite there is a structure on either side of the MPTS antenna which is made of a dielectric material connecting the two solar panels. This structure is identified as the 'dielectric carry-through' structure and its location is sketched in Figure 3.1. The MPTS antenna beam propagates through this structure twice every 24 hours (once every 24 hours per

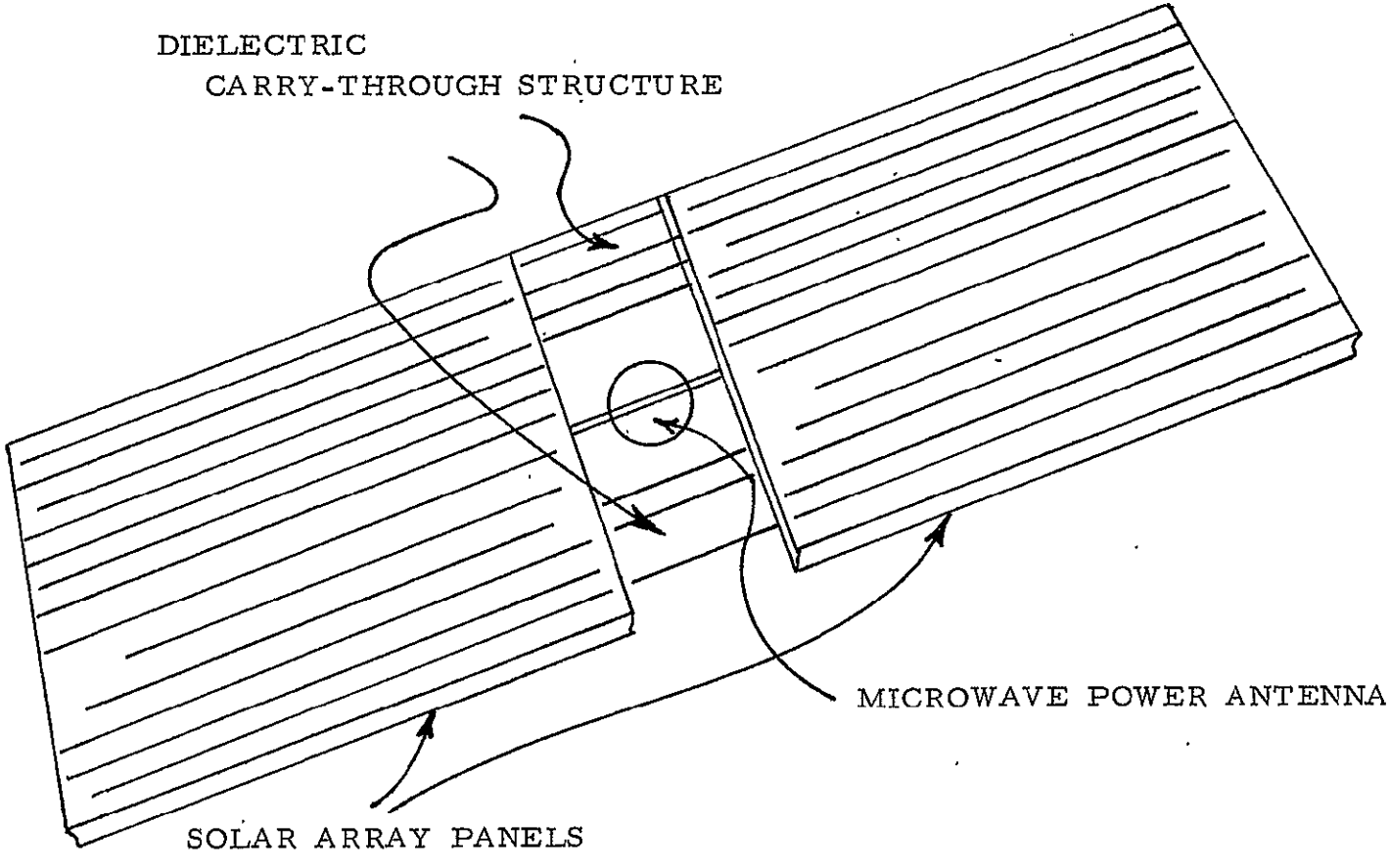

FIGURE 3.1 SATELLITE CONFIGURATION

each set of dielectric carry-through structure). It is necessary to determine what effects these structures will have on the microwave propagation or vice versa. The effects which have been analized (Section 3.4) are:

(a) The phase changes resulting from transmitting through a dielectric material will result in main beam power loss and higher sidelobes due to out-of-phase addition of the radiating elements on the antenna.

(b) The reflections from the carry-through structure will result in a heat flux on the antenna.

(c) Coupling absorption of the microwave energy may cause unwanted heating of the carry-through structure.

(d) Reflected RF energy may cause problems with sensitive RF circuitry.

It should be pointed out here that the radiated waste heat ($\simeq 3.3$ kW/cm^2) may overheat not only the local structure but the dielectric carry-through structure. Preliminary calculations indicate a maximum temperature of 169° C for the dielectric carry-through structure arising from the waste heat radiation.

3.1.4 MATERIAL SUBLIMATION EFFECT

This analysis (Section 3.5) has been performed in order to determine whether the sublimation products of the various materials which comprise the microwave power transmission system will cause the pressure immediately surrounding the Amplitron to cause the device to malfunction. Specifically will the sublimation process, increase the pressure surrounding the Amplitron from 10^{-13} TORR (ambient pressure at Geosynchronous Orbit) to 10^{-4} or 10^{-5} TORR which is the pressure at which the Amplitron will not operate?

3.1.5 RESULTS OF THE STUDY

The results of the present study are outlined in Table 3-1 in summary form. The description of the problems outlined above which were investigated in the present study along with the study results and conclusions are presented. As shown, the results are:

TABLE 3-1. INTERFACE STUDY SUMMARY & CONCLUSIONS

Subject	Problem Description	Results of Study	Recommendations
High/Low Voltage System	Microwave power transmission system operation at 40 kV, comparison with 20 kV baseline.	40 kV Amplitron not recommended. 20 kV Amplitrons in series a possible configuration.	Isolation problems associated with 20 kV Amplitrons in series require further
Thermal Considerations	Thermal blockage of Amplitrons by mast, flex joint, antenna structure.	Thermal blockage exceeds 5% figure previously assumed, requiring resizing of Amplitron and antenna or system reconfiguration to reduce blockage.	Design Amplitron with its waste heat radiation system to achieve low waste heat dissipation per unit area. Redesign overall antenna to minimize thermal blockage.
Dielectric Carry-Through Structure	Effect of Dielectric structure on: Beam forming Thermal Phase control	Phase change effect on far field beam pattern is minimal. RF thermal coupling negligible due to low electrical conductivity of carry-through material. Reflected energy may represent a major problem for phase control design. Waste heat radiation may overheat dielectric structure.	Antenna beam pattern test measurements with dielectric near field obstructions. Material tests to determine electrical properties of material. Carry-through structure redesign or elimination. Phase control system design.
Sublimation Problem	Pressure increase at Amplitron cathode due to trapped sublimation products.	None if aluminum waveguide is used. Organic compounds in immediate vicinity of Amplitron not advised.	Design Amplitron to ensure particle venting to free space.

- A 40 kV Amplitron at 5 kW output power represents a cost and weight penalty over the 20 kV, 5 kW tube.

- A 40 kV dc power distribution system operating with two 20 kV, 5 kW Amplitrons in series represents a weight and cost saving. However, there is a subarray isolation problem which must be analyzed further.

- The system requires further design effort to eliminate the need to enlarge the antenna due to a thermal blockage of Amplitrons located adjacent to the 108m bay structure and directly in the center of the antenna.

- The carry-through structure does not appear, from preliminary calculations, to be a problem both in terms of transmission losses, and structural heating. However, because of the complex nature of this problem, further experimental efforts are recommended particularly with respect to the phase control circuitry. This requirement, of course, depends on the final design configuration. It is recognized that a design configuration could be selected which will not include structures which interfere with the MPTS.

- Sublimation of materials adjacent to the Amplitron does not appear to have any significant effect on the successful operation of the Amplitron.

3.2 HIGH/LOW VOLTAGE MPTS STUDY

3.2.1 INTRODUCTION

This task deals with an extension of portions of work performed originally in the Microwave Power Transmission System Study[14]. In particular, the present study evaluates the specifics of a high voltage distribution system (40 kV) versus a low voltage distribution system (20 kV). Other effects of high voltage operation, such as safety and x-ray generation are also considered.

The task is limited to consider only the following:

a. Amplitron as the DC/RF converter

b. Microwave array impact only

c. High versus Low voltage limited to comparison of 20 kV and 40 kV systems

To operate an Amplitron at 40 kV results in major penalties in size and cost. To avoid this and to maintain a high voltage system, large groups of Amplitrons can be operated in series. Although this results in a reduction in the number of crowbar units and in the amount of conductor required, it adds complexity. High voltage insulation between subarrays is required. Not only is this isolation a mechanical problem, it also presents difficulties in control and power monitoring systems that will exist throughout the array. In addition and perhaps of more serious consequence is the safety impact on servicing operations.

The basic theory of Amplitron operation is a conversion of kinetic energy to RF energy. This is unlike a linear beam tube which converts potential energy to RF. The result is a lower electron velocity in the Amplitron and the resulting generation of lower energy x-rays. The average beam velocity in electron volts in an Amplitron is 20% of the cathode voltage.

3.2.2 40 kV AMPLITRON

The previous MPTS study[14] established the optimum design parameters for the Amplitron DC to RF converter. These basic parameters are as follows:

RF power added	-	5 kW
RF drive	-	1.25 kW
RF output	-	6.25 kW
RF gain	-	7 dB
DC/RF efficiency	-	85%
Voltage	-	20 kV
Current	-	0.3 amperes

For the present study involving a comparison of a 20 kV distribution system and a 40 kV distribution system, we also have to consider the feasibility of an Amplitron operating at 40 kV DC cathode potential. Operating an Amplitron at this potential is not recommended by Raytheon for the following reasons:

A. Maintaining the power added at 5 kW per Amplitron results in a tube current of 150 mA. At 40 kV, leakage current increases relative to true beam current and at the reduced beam current of 150 mA it can be an appreciable portion of the total current. This leakage current represents wasted power and results in reduced efficiency.

B. Increasing the power per tube would be a possible solution to the high leakage current. However, it has been shown that higher output power involves sacrifices in both grams/watt and dollars/watt. A graph indicating this tradeoff is given by Figure 3.2.

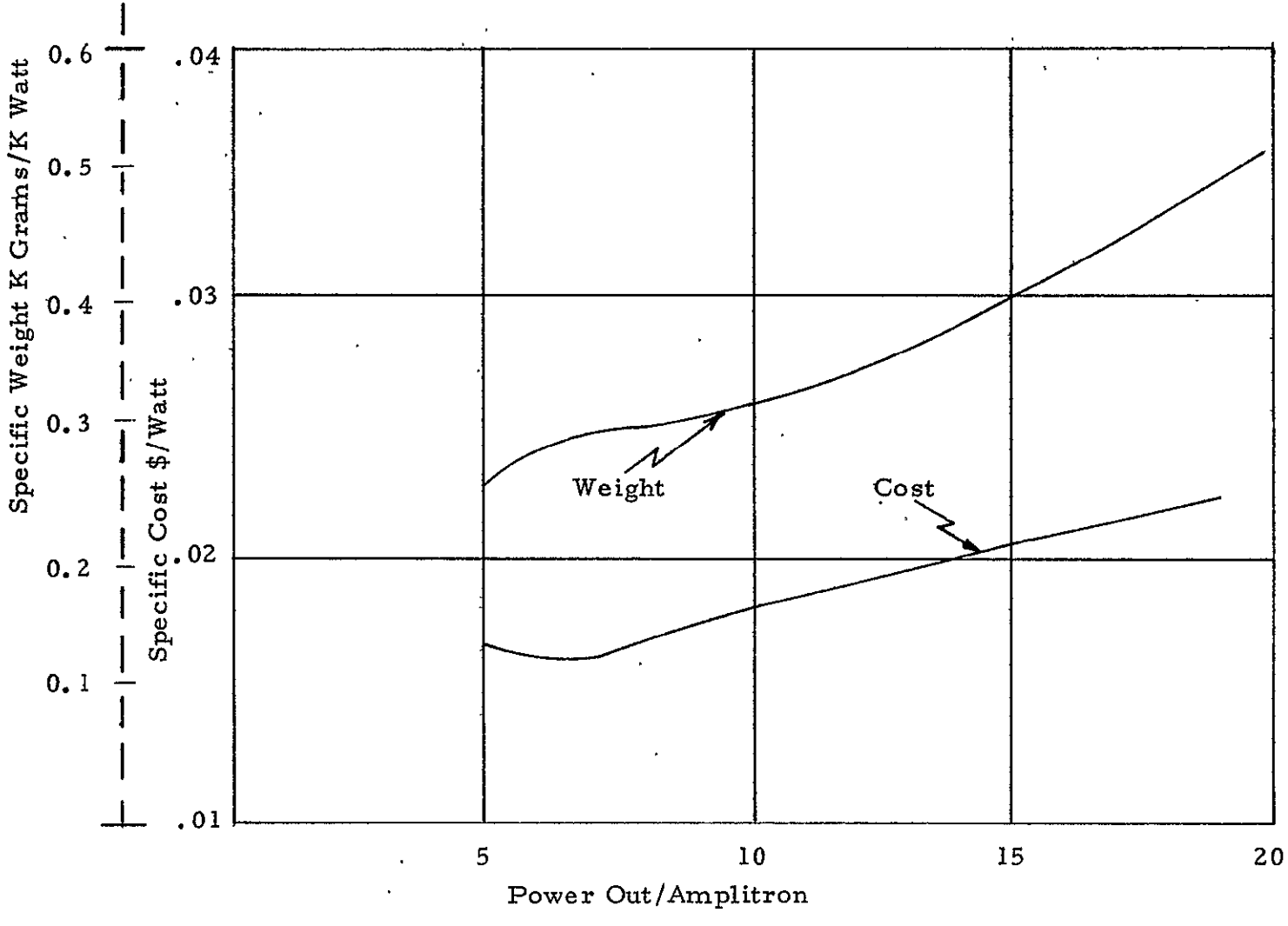

FIGURE 3.2 AMPLITRON COST & WEIGHT -VS- POWER PARAMETRIC STUDY

If we assume that it is desirable to maintain a constant ratio of leakage current to beam current, and that the leakage current is proportional to voltage, then the higher voltage Amplitron would operate at 40 kV and 0.6 amperes, and result in a 20 kilowatt RF power added device. From the data of Table 3-2, we obtain the following:

RF Power	Weight	Amplitron Cost
5 kW - 20 kV	0.32 gm/W	0.018 $/W
20 kW - 40 kV	0.6 gm/W	0.023 $/W
% increase	87.5%	35.3%

These estimated increases in both the Amplitron weight and cost make the use of a higher voltage Amplitron undesirable. If a higher voltage operating system is otherwise necessary, an alternative technique, such as operating Amplitrons in series, should be used. Table 3-2 is a tabulation of characteristics of both the 20 kV and 40 kV Amplitron.

3.2.3 POWER DISTRIBUTION SYSTEMS

In the power distribution system for the microwave array there are three specific requirements that must be considered. These are as follows:

A. Operating Voltage: It has been established that operating a CFA at high voltage is not optimum. Thus, to use a high voltage distribution system we must operate tubes in series.

B. Crowbar: The crowbar protective unit must present a momentary diversion of energy between the load and power source. In a series tube arrangement, the crowbar unit has to be located in series with the power feed from the prime power source, but not at an intermediate voltage point.

C. Reliability: In the proposed system for high voltage distribution we are faced with operating a large number of Amplitrons in a series parallel combination. By its nature of interrupting high voltages, a crowbar unit is basically current limited. By operating the CFA's in series, the number of tubes per crowbar unit can be doubled.

TABLE 3-2 COMPARISON OF 40 KV -VS- 20 KV AMPLITRON

CHARACTERISTIC	20 KV	40 KV
Voltage	20 kV	40 kV
Current	0.3 amp	0.6 amp
Power Added	5 kW	20 kW
Weight	0.32 grams/watt	0.6 grams/watt
Cost	0.018 $/watt	0.023 $/watt

COMMENTS

- To main efficiency, it is necessary to increase power per tube from 5 kW to 20 kW when voltage increases from 20 kV to 40 kV.
- Higher power per tube entails high cost and weight penalties.

Figure 3.3 is an illustration of the operation of CFA's in series. Two or more subarrays are grouped together with one crowbar unit. This group is then connected in series with a second similar group.

3.2.3.1 Subarray Distribution

The number of Amplitrons required and the power per subarray is independent of whether a 40 kV or 20 kV power distribution system is used. Thus, within any given subarray the distribution is the same for both high and low voltage distributions.

The MPTS report[14] developed the quantity and approximate locations of crowbar and switchgear units in the array. Figure 3.4 of this report repeats the general data of Figure 5-16 (Volume II) of the MPTS report. The total array is subdivided into 5 areas (selected to be of approximately equal power per area). The antenna for this configuration has a 10 dB Gaussian taper with a five step approximation to the Gaussian curve. Over the surface of the antenna, the number of crowbar units associated with each subarray varies from two crowbars per subarray to one crowbar per four subarrays at the perimeter of the microwave antennae.

Detail wiring interface between the crowbar unit and the Amplitrons was not examined as part of the MPTS report. In this report, a subarray/crowbar located in Area 4 plus a center unit have been examined.

Cabling from the subarrays in the fourth power area to the Amplitron tubes is represented physically by Figure 3.5. As is observed in this figure, the specific configuration outlined operates 18 Amplitrons in parallel from each feeder This same quantity of 18 Amplitrons on one feeder is used throughout the array. This feeder is estimated to run for a total length of 22 meters, and carries a normal current of 5.4 amperes.

Wire size for this feeder can be obtained by the calculations in Table 3-3. These indicate that a wire size of #20 aluminum wire is satisfactory. To be slightly more conservative, a wire size of #19 wire will be used. An average wire temperature of 150° C was assumed for this cable. Figures 3.6 and 3.7 represent the dense Amplitron packaging that occurs at the center of array and indicates the effect of distribution wiring shadowing the Amplitrons.

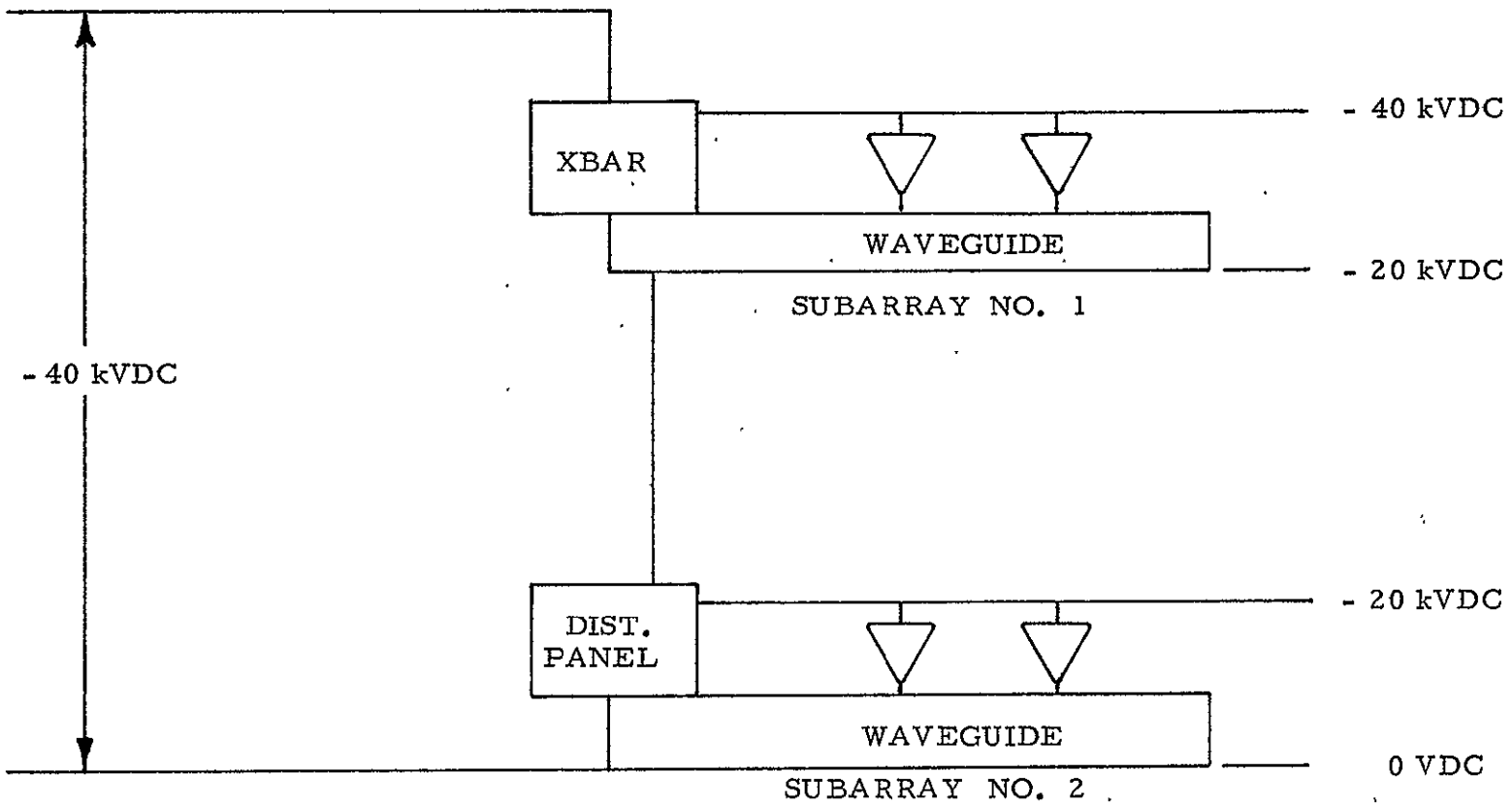

COMMENTS:

- Number CFA's out of service when XBAR fires is doubled.
- Subarray No. 1 must be insulated from support structure.
- All control and monitoring signals require isolation.
- Service and maintenance equipment must provide for isolation or equipment shutdown.

FIGURE 3.3 ILLUSTRATION OF SERIES OPERATION OF AMPLITRONS

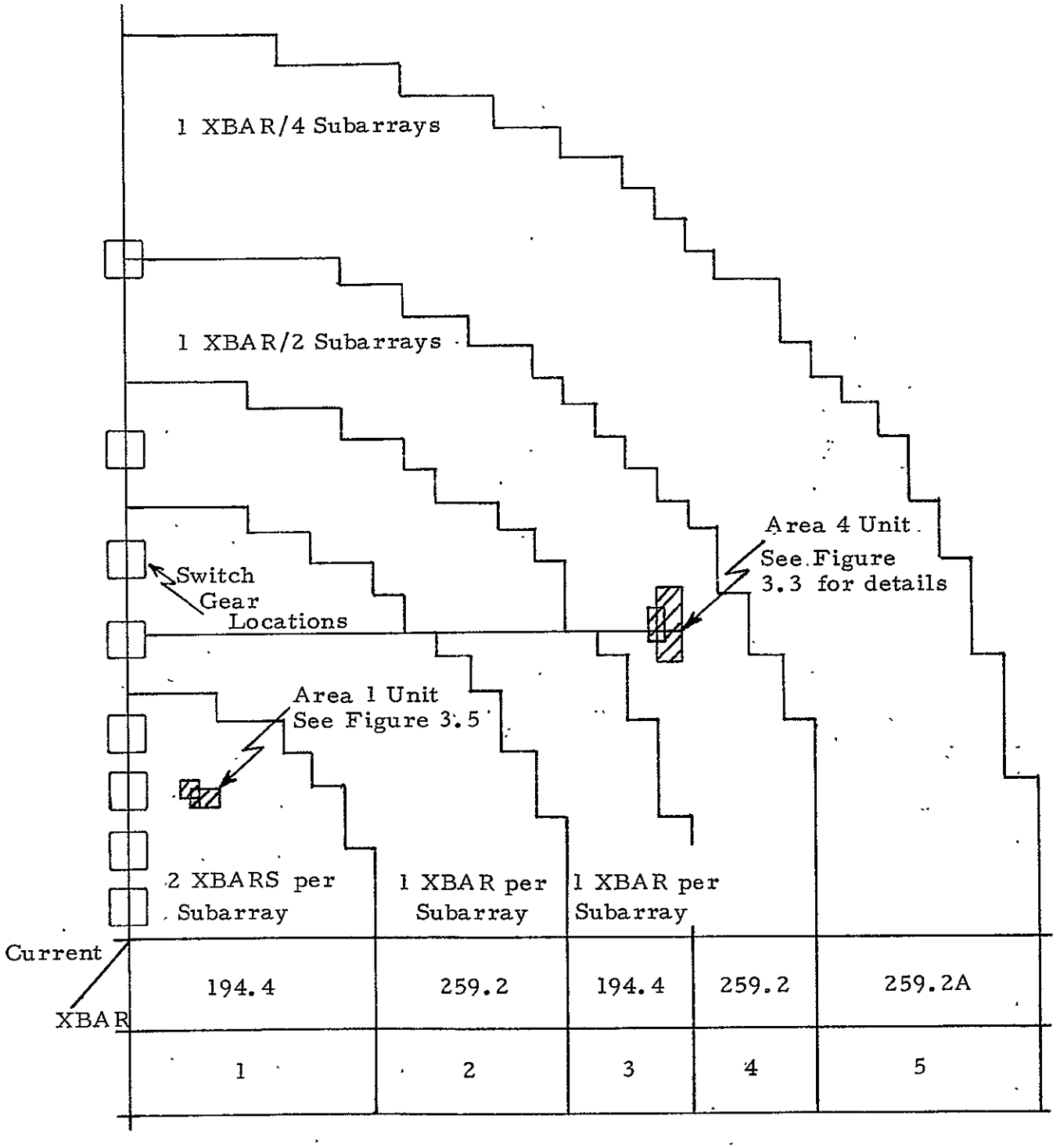

FIGURE 3.4 LOW VOLTAGE DISTRIBUTION CROWBAR AND SWITCHGEAR DISTRIBUTION

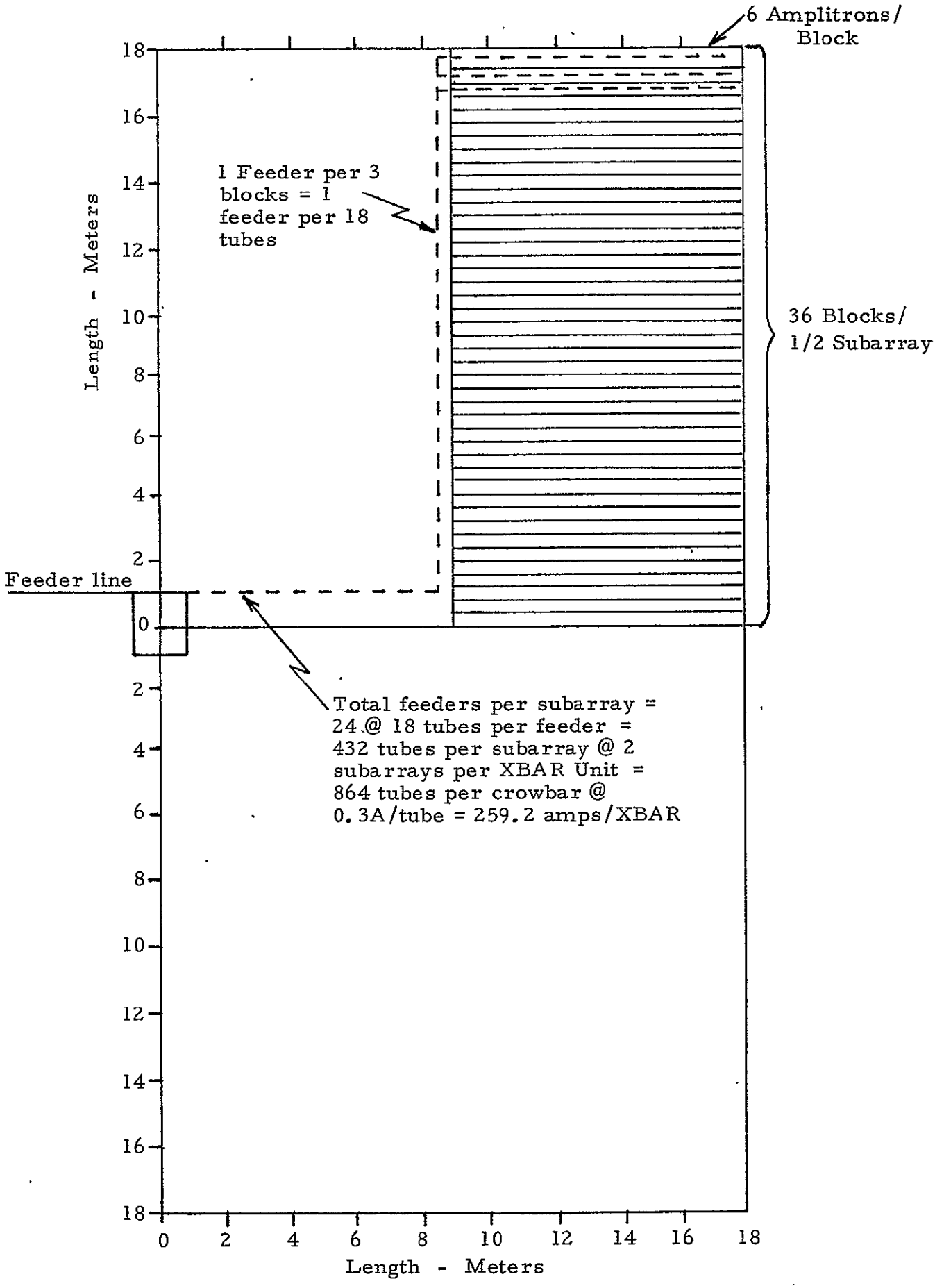

FIGURE 3.5 SUBARRAY CABLING CONFIGURATION

TABLE 3-3 SUBARRAY WIRE SIZE CALCULATIONS FOR 20 kV SYSTEM

Power loss = .01% = $(.0001 \times 5.4 \times 20 \times 10^3) = 10.8$ watts

Voltage drop = $\frac{10.8}{5.4A} = 2.0$ volts

$R = \rho \frac{\ell}{A}$

$\rho = 2.828$ μohms/cm^3 at 20°C

ssume operating temp = 150°C

$P_{T2} = 2.828 \times 10^{-6} \left[1 + .0049 \ (150^{\circ}C - 20^{\circ}C) \right]$

$= 2.828 \times 10^{-6} \left[1.637 \right] = 4.63 \times 10^{-6}$

$A = \frac{\rho \ell}{R} = \frac{(4.63) \times 22 \times 100}{2.0} = 5093 \text{ cm}^2 \times 10^{-6}$

$A = .005 \text{ cm}^2$

or round wire

radius = $\sqrt{\frac{.005}{\pi}} = .03989$ cm

Diameter = $\frac{2 \times .03989 \times 1"}{2.54 \text{ cm}} = .0314" = \underline{31.4 \text{ mills}}$

his corresponds to a #20 wire (dA = 31.96 mills)

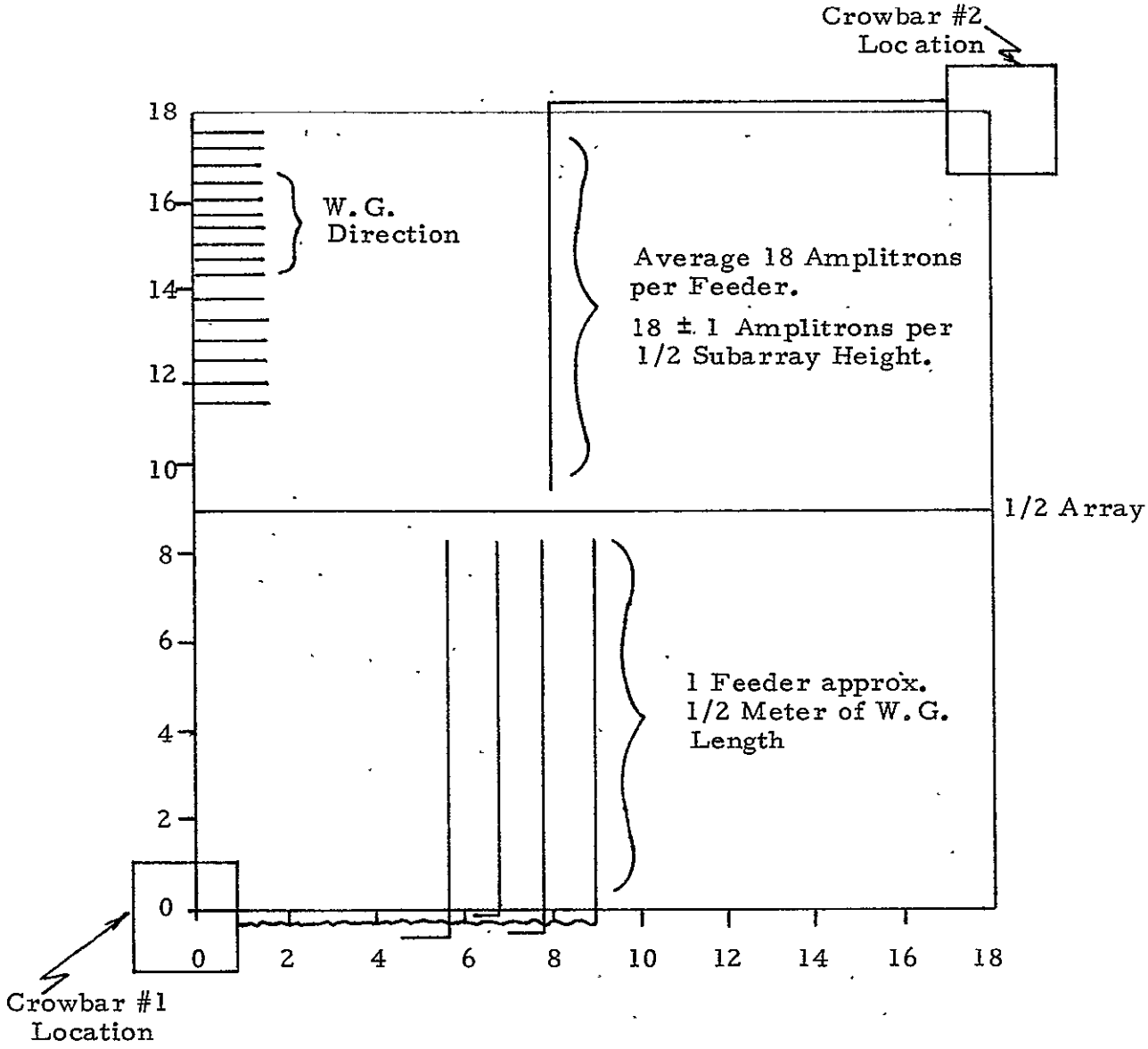

No Amplitrons/Subarray	=	1296
No Amplitrons/Feeder	=	18
No Feeders/Array	=	72
No Feeders/XBAR	=	36

FIGURE 3.6 CENTER AREA SUBARRAY

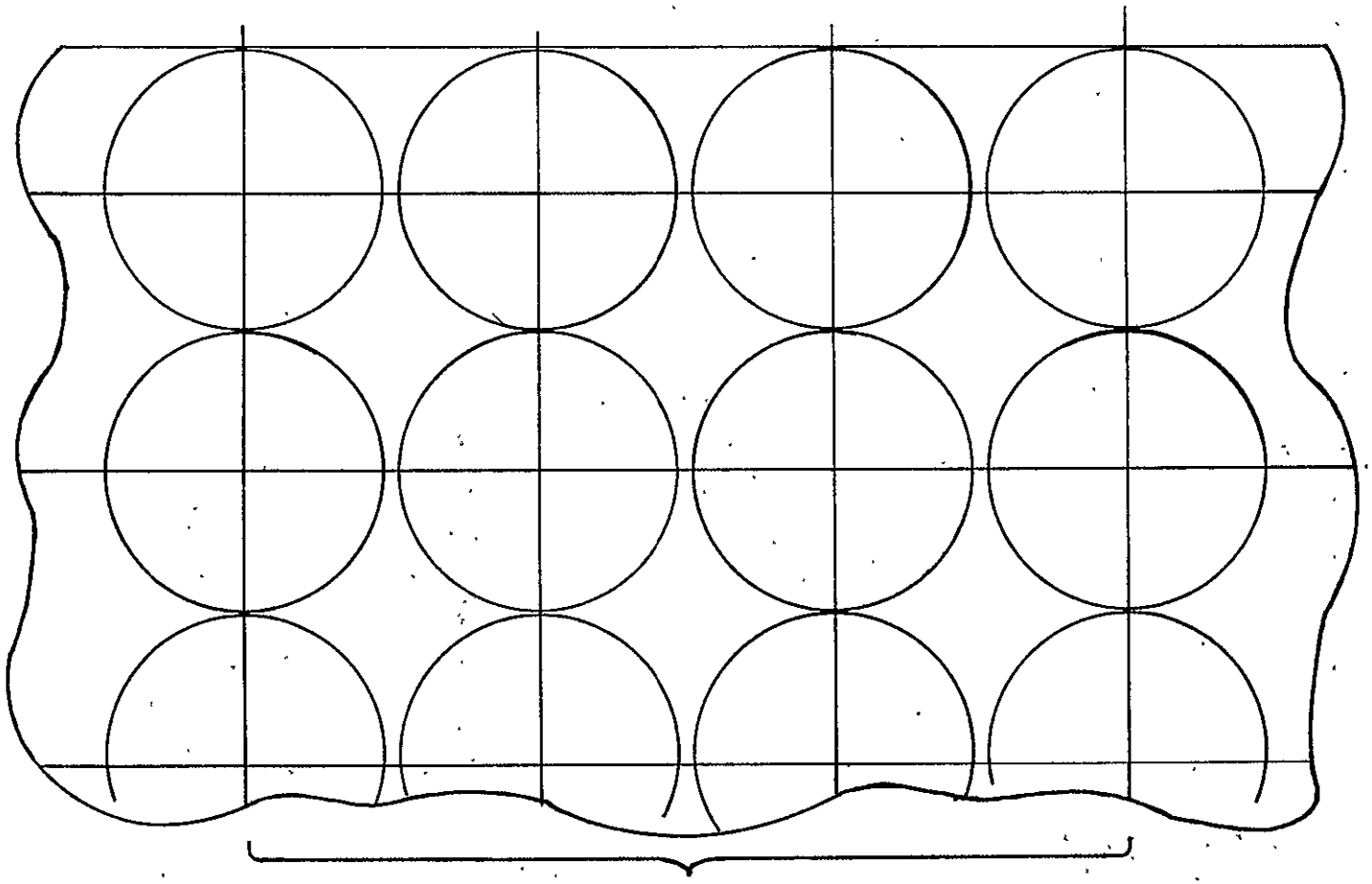

FIGURE 3.7 CENTER SECTION AMPLITRON LAYOUT USING SQUARE CONFIGURATION (MOST DENSE SUBARRAY CONFIGURATION)

3.2.3.2 Power Distribution Cost Summary

By using rough layouts of the subarrays, crowbar and switchgear locations, estimated cable sizes and lengths for all distribution feeders have been obtained. These parameters have been combined with other elements of the system to obtain overall parameters. Figure 3.8 is a simplified block diagram indicating the main elements of the distribution system. An estimate of the critical parameters of these elements are given in Table 3-4. A total summary of weight and cost are outlined by Table 3-5.

3.2.4 X-RAY GENERATION IN AMPLITRONS

People experienced in high voltage vacuum tubes as a source of x-rays, generally consider as a rule of thumb that x-rays do not exist below 20 kV. Actually, there is no such sharp dividing line. X-rays generated by low voltage devices, however, are soft x-rays, which are easily attenuated to extremely low levels. Experience has then indicated that below 20 kV any x-rays generated are so highly attenuated by surrounding media that exposure is not a problem.

Amplitrons used in the microwave array operate at 20 kV. Thus, x-rays would not be considered a significant problem at this voltage. However, because of the special nature of this application, a more detailed examination has been made.

In discussing x-ray generation in RF tubes, it is significant that a distinction be made between crossed field devices like the Amplitron and linear beam devices like the klystron. In a linear beam device, the DC to RF conversion is a conversion of potential energy to RF energy. Electrons in a linear beam device are accelerated to 100% of cathode voltage before entering the RF interaction area. In a crossed field amplifier, due to the action of the perpendicular magnetic field, the electrons rotate in nearly equipotential circles around the cathode with a relatively slow drift to the anode. In an Amplitron, the average electron velocity is twenty percent of the applied voltage. The insert below is a memo from Mr. G. MacMaster of the Engineering Department of Raytheon's Microwave and Power Tube Division reviewing these facts.

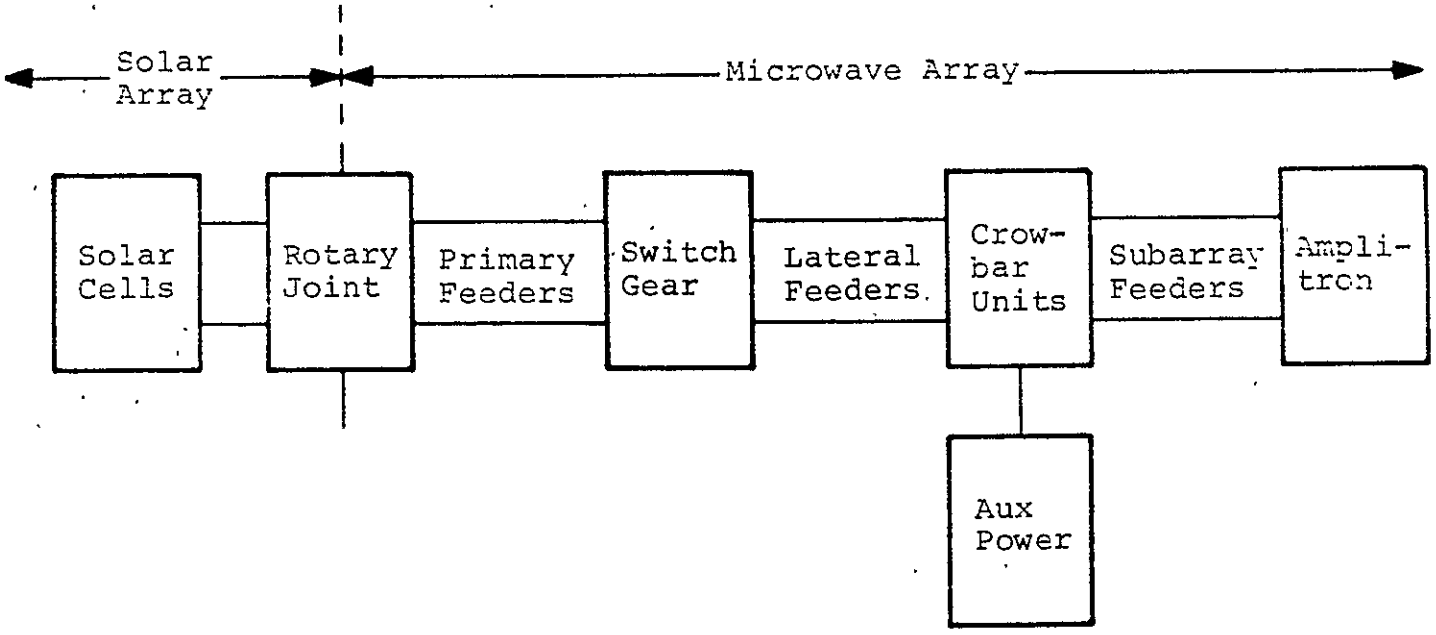

FIGURE 3.8 BLOCK DIAGRAM POWER DISTRIBUTION SYSTEM FOR AMPLITRONS

TABLE 3-4 COMPARISON HIGH -VS- LOW VOLTAGE DISTRIBUTION SYSTEM FOR AMPLITRONS

	Low	High
A. Primary Feeders		
Wire Size	Bundles #4/0 wire	Bundles #4/0 wire
Total Length	228×10^3 meters	161.4×10^3
Total Wgt	66×10^3 kg	46.7×10^3 kg
Cost	4.4 $/kg	4.4 $/kg
B. Switch Gear Unit		
Number	32	32
Total Wgt	55.2×10^3	40.0×10^3
Unit Cost	178×10^3	126.0×10^3
C. Lateral Feeders		
Wire Size	Approx. #3 AL	Approx. #3
Total Length	252.7×10^6 meters	179.8×10^6
Total Wgt	18.3×10^3	12.9×10^3
Cost	4.4 $/kg	4.4 $/kg
D. Crowbar Units		
Number	1769	885
Total Wgt	300×10^3 kg	195×10^3 kg
Unit Cost	$ 28×10^3	36×10^3
E. Subarray Feeders		
Wire Size	#19 AL	#19 AL
Total Length	3.42×10^6 meters	3.42×10^6 meters
Total Wgt	6100 kg	6100 kg
Cost	4.4 $/kg	4.4 $/kg
F. Auxiliary Power		
Number	1769	1769
Total Wgt	88.4×10^3 kg	88.4×10^3 kg
Cost	29.5×10^3 kg	29.5×10^3 kg

TABLE 3-5. SUMMARY COMPARISON HIGH -VS- LOW VOLTAGE DISTRIBUTION SYSTEM FOR AMPLITRONS

Distribution System	Wgts (x 10^5 kg)		Cost (x 10^5 $)	
	Low	High	Low	High
Primary Feeders	66	46.7	290.4	205.5
Switch Gear Units	55.2	40.0	5696.0	4032.0
Lateral Feeders	18.3	12.9	80.5	56.7
Crowbar Units	300	195	49532.0	31860.0
Subarray Feeders	6.1	6.1	25.0	25.0
Auxiliary Power	88.4	88.4	52185.0	52185.0
TOTAL	534	389	107808.9	88364.2

"The x-ray radiation from most Amplitrons is so low that no lead shielding is required.

The low x-ray radiation from the Amplitron stems primary from the energy conversion system in which the average velocity of the electrons does not exceed about twenty percent of the input voltage. Hence, in a tube which operates at an anode voltage of forty kilovolts, the average kinetic energy of the electrons does not exceed eight kilovolts, a level of voltage at which only very soft x-rays can be generated.

The energy conversion system is in sharp contrast to that in the klystron and conventional traveling wave tubes where all the electrons are first accelerated to the full anode potential so that any electrons which are not collimated in the beam will cause emission of x-rays when they strike the sides of the drift tubes or cavities. Furthermore, a large percentage of the electrons reach the collector with energies sufficiently large to excite hard x-rays, some of them reaching the collector at energies greater than the anode voltage of the tube.

Generally speaking, anode voltages for Amplitrons are about half of those for klystrons and traveling wave tubes of equivalent power level. This provides an additional advantage in favor of the Amplitron from the standpoint of x-ray radiation."

In an Amplitron operating at 20 kV, the average electron potential is only 4 kV. Table 3.6 shows an approximate calculation of the x-ray generated by 4 kV electrons at an average current of 300 milliamperes striking a copper anode. X-ray generation is 0.64 milliroentgens per hour. The large attenuation obtained from these soft x-rays is indicated by Table 3-7. When 4 kV x-rays pass through 0.25 cm of copper, they are attenuated by greater than 10^{-25}.

3.2.5 SUMMARY

The study of high voltage versus low voltage power distribution has indicated both a weight and cost advantage to the higher voltage system. However, because it is necessary to operate groups of Amplitrons in series to maintain the tube cost and weight optimum, several other problems appear. The details of how this voltage isolation can be accomplished between major portions of the

TABLE 3-6. X-RAY RADIATION IN AMPLITRONS: INTENSITY GENERATED

- Empirical formula for intensity emitted by an X-ray tube is:(A)

$$I = (1.1 \times 10^{-8}) \; Zi \left(\frac{V}{d}\right)^2$$

where:

I = Roentgens per minute

d = Distance inches

V = Kilovolts

i = Current in milliampere

Z = Atomic no. of target

- For a distance = 1 foot and for 4 KeV electrons

I = 0.64 milliroentgens per hour possible fron Amplitron with no shielding.

(A) VanName, Modern Physics, Prentice-Hall, 1962, p. 161

TABLE 3-7. X-RAY RADIATION IN AMPLITRONS: EFFECT OF ATTENUATION

- Although CFA is not shielded, there is no direct path for x-rays generated at anode to exit tube without passing through materials.
- Assume that all x-rays must pass through a min. of 0.25 cm of copper.
- Attenuation can be calculated

$I = Io\, e^{-\mu m dm}$

Io = Initial intensity

μm = Total mass absorption coefficient

dm = Mass thickness = pd

ρ = Mass density of absorber

- For copper at 4 keV $\mu m \approx 40$

$I = Io \times 1.76 \times 10^{-25}$

array, and the effect upon control signals, servicing procedures and handling equipment have not been explored. A final selection of a system considering the isolation problems presented should be held in abeyance until the isolation issue has been addressed in detail.

Power distribution within subarrays has been examined. Amplitrons in a group of 18 in parallel are fed from the crowbar unit with No. 19 aluminum wire. This wire size is based on an average temperature of 150° C and a power loss of .01%.

In an Amplitron, the conversion of DC to RF energy occurs as a result of a decrease in the kinetic energy of the electrons. The average electron kinetic energy is 20% of the applied beam potential. The resulting low electron velocity results in a relatively low amount of x-ray generation and, in addition, the x-rays that are generated are soft x-rays and easily attenuated. No problem from x-rays generated by the Amplitrons are anticipated.

3.3 THERMAL ANALYSIS - STRUCTURAL BLOCKAGE

3.3.1 INTRODUCTION

In order to radiate the large quantity of microwave power required from the MPTS antenna, a large average power density must be applied to limit antenna size, weight and cost. Furthermore, the power distribution must be tapered to limit sidelobe power density to be within potentially acceptable ecological limits at the ground. This results in a particularly high power density requirement over the central region of the antenna which is limited by the inefficiency of the RF generators and the ability to dissipate the associated waste heat generated over large areas in the same central region or pay the unreliability, complexity, weight and cost penalties of transporting the waste heat many meters to the power density regions remote from the central region. The baseline antenna is divided into ten regions of constant power density which are stepped to approximate the required distribution associated with a 10 dB Gaussian taper or other similar distributions to limit the sidelobe power densities to approximately $0.1\ mW/cm^2$. The central region of the baseline transmitting antenna therefore has high efficiency Amplitrons packed such that each associated waste heat radiator almost touches its neighbor in order to get the required maximum power density. Therefore, any increase in the size of the Amplitron due to an inefficiency in radiating waste heat serves to decrease the allowable thermal power density, decreasing the allowable RF power density thereby decreasing the allowable transmitted RF power or increasing the total antenna area.

The design of the Amplitron shown in Figure 3.9 was based on the following considerations:

(a) the maximum operating temperature of the cathode $\leq 650^\circ C$

(b) the maximum anode temperature $\leq 350^\circ C$ in order to limit the magnet temperature

(c) solar heat input $\sim 1395\ watt/m^2$

(d) waste heat dissipation of the Amplitrons = 882 watts. This represents an 85% efficiency factor for 5 kW added power.

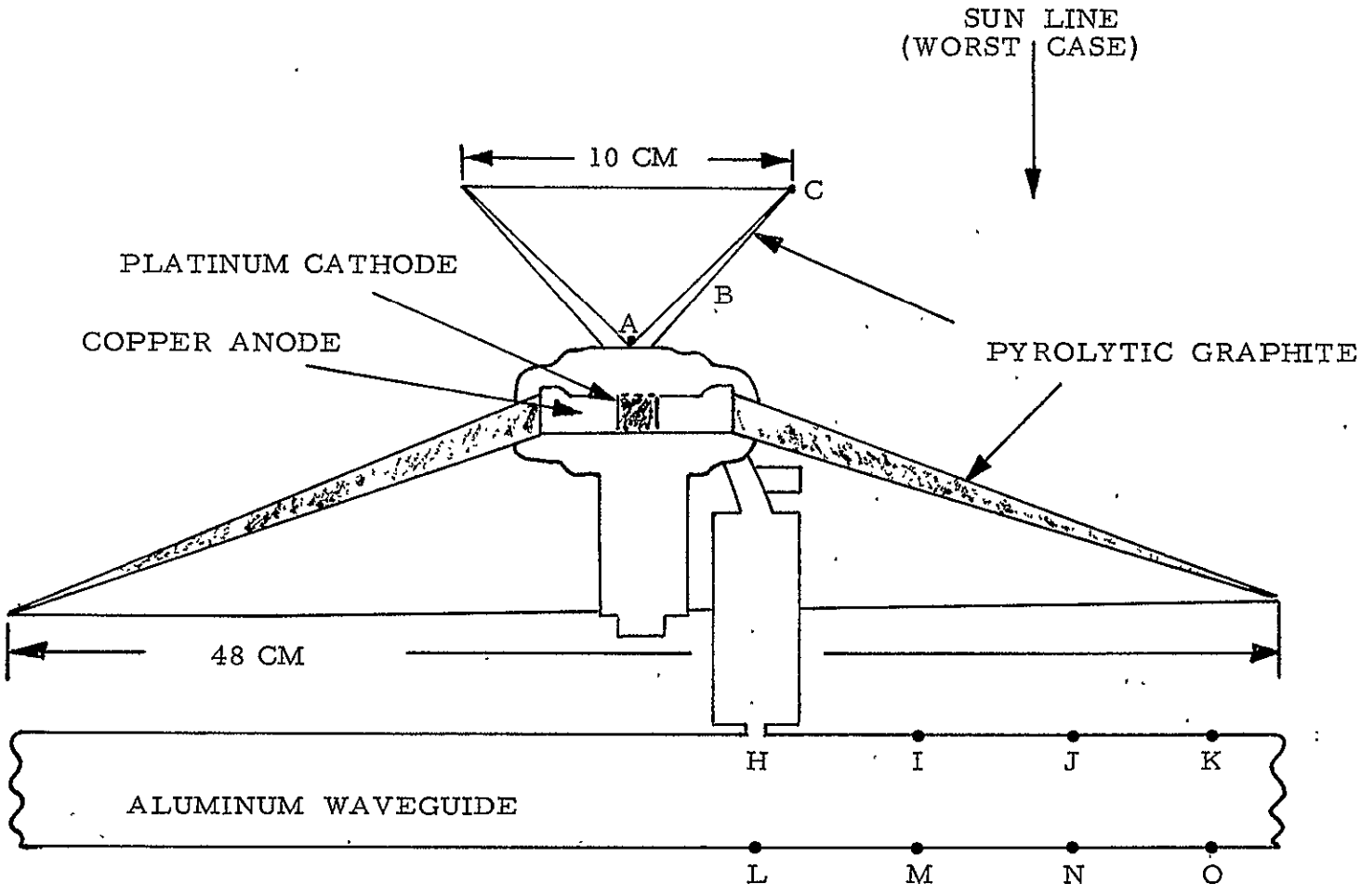

FIGURE 3.9 AMPLITRON CONFIGURATION

The Amplitron radiates waste heat into a solid angle which is not quite 2π steradians. It was assumed for the previous MPTS study[14] that there was approximately five percent of the radiating solid angle which contained structure at 120° C and which limits the waste heat radiation in that sector. The purpose of this task is to analyze the thermal obstructions of the Amplitron to determine a more precise estimate of the blockage for the baseline configuration.

If the blockage exceeds the five percent figure which resulted in the present Amplitron passive thermal radiator design, the configuration of the Amplitron radiator will change to reflect the increased radiated heat input of the obstructions. In order to maintain the same equilibrium temperature profiles previously determined, the radiation surface area of the Amplitrons will have to increase. Any increase in size of the Amplitron has a direct impact on the antenna size. This is so because the Gaussian weighting applied to the antenna beam must be maintained, and the present baseline configuration of the antenna has Amplitrons packed to maximum density. Consequently, in order to maintain the power distribution either the Amplitron radiators are increased in size, to radiate more heat, and thereby increase the overall antenna size or another more efficient method of cooling the Amplitrons must be found.

The relative effect of the structures which thermally block the Amplitrons is shown in Figure 3.10.

The mast, because of its distant location, has approximately the same blockage effect on Amplitrons located at any point on the antenna.

For the subarray support structure and electrical equipment, the blockage is different for different Amplitron locations on a subarray. For these conditions an Amplitron located at the center of a subarray and one located at the edge near the screw jacks is considered.

The flex joint is at present only a conceptual design. An estimate of its blockage effect will be made on this basis and on a requirement that it alone not exceed the five percent blockage margin.

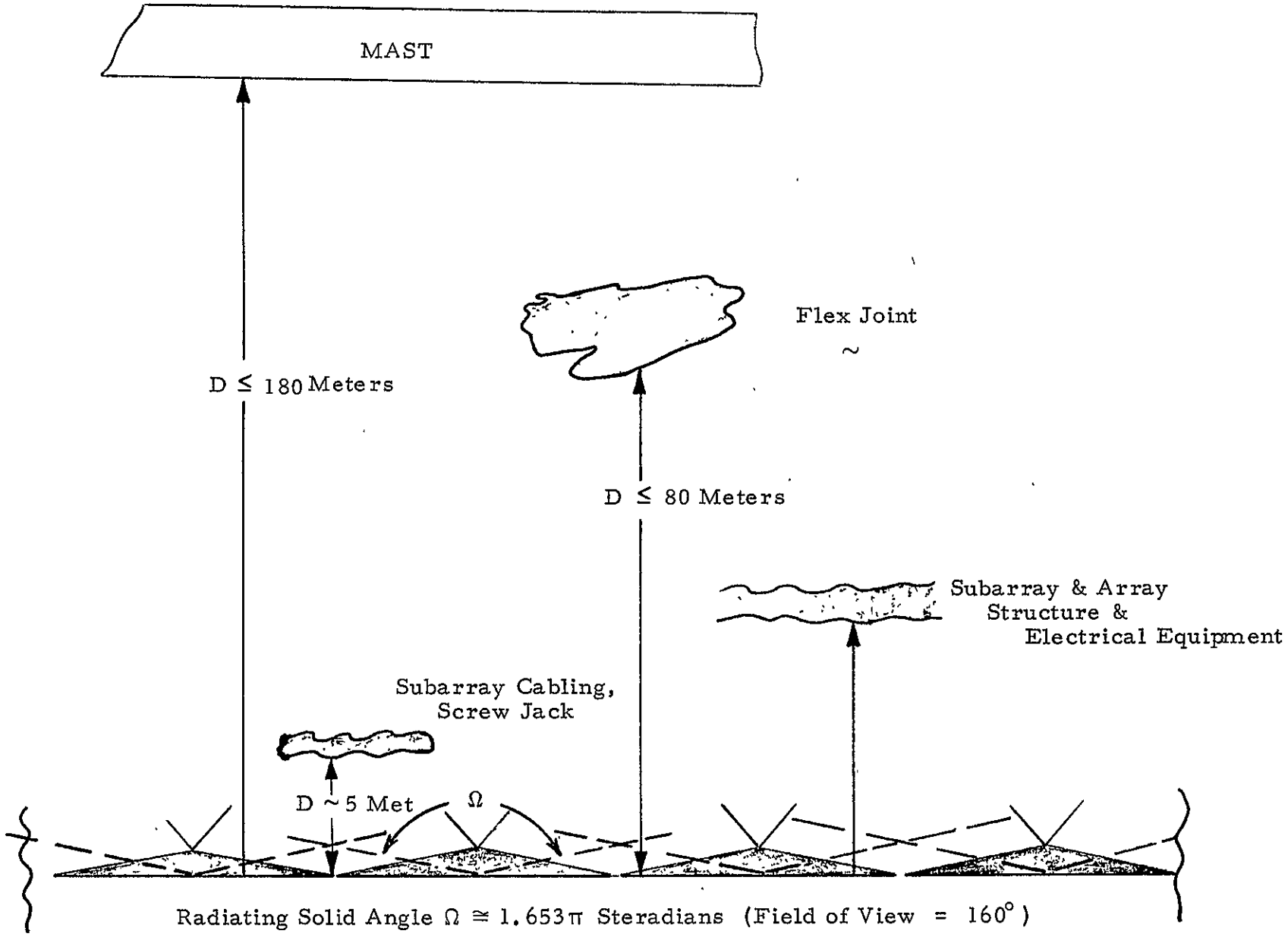

FIGURE 3.10 AMPLITRON THERMAL BLOCKAGE CONFIGURATION

The blockage contributions for the items shown schematically in Figure 3.10 will be made in the following sections along with an example as to the total blockage which an Amplitron located in the central antenna region will undergo.

Finally, conclusions will be drawn as to any increase in antenna size due to the blockage considered.

3.3.2 MAST

Figure 3.11 shows the mast structure as seen by the antenna. The structure carries 24 conductors each 0.83m in diameter. These conductors represent the primary longitudinal structural members for the mast. Approximately every 20 meters along the mast there is a grid of one meter triangle structural members each of which has three 6.6 cm cap members. A cross-section of the mast is shown in Figure 3.12.

Though the conductors appear to be aligned, as shown in this figure, a majority of the individual conductors may be distinguished from a point on the antenna surface. The total blockage contribution of the conductors is defined by the number of conductors distinguished by a point on the antenna, the diameter of a conductor, and its distance from the antenna surface. The solid angle represented by the mast, to an Amplitron in the center region of the antenna is shown by Figure 3.13. An average distance of 220 meters is assumed in order to compute the angles shown. This is the distance from the center line of the mast to the Amplitron location. The angle α is computed by taking the blockage due to 24 conductors to be:

$$\alpha = \frac{(24)\,(.83\text{m})}{220\text{m}}$$

$$\cong 5.2^\circ$$

The contribution to α from the lm triangle structural 6.6 cm wide caps is estimated to be approximately 20%. This increases α to;

$$\alpha \cong 6.24^\circ$$

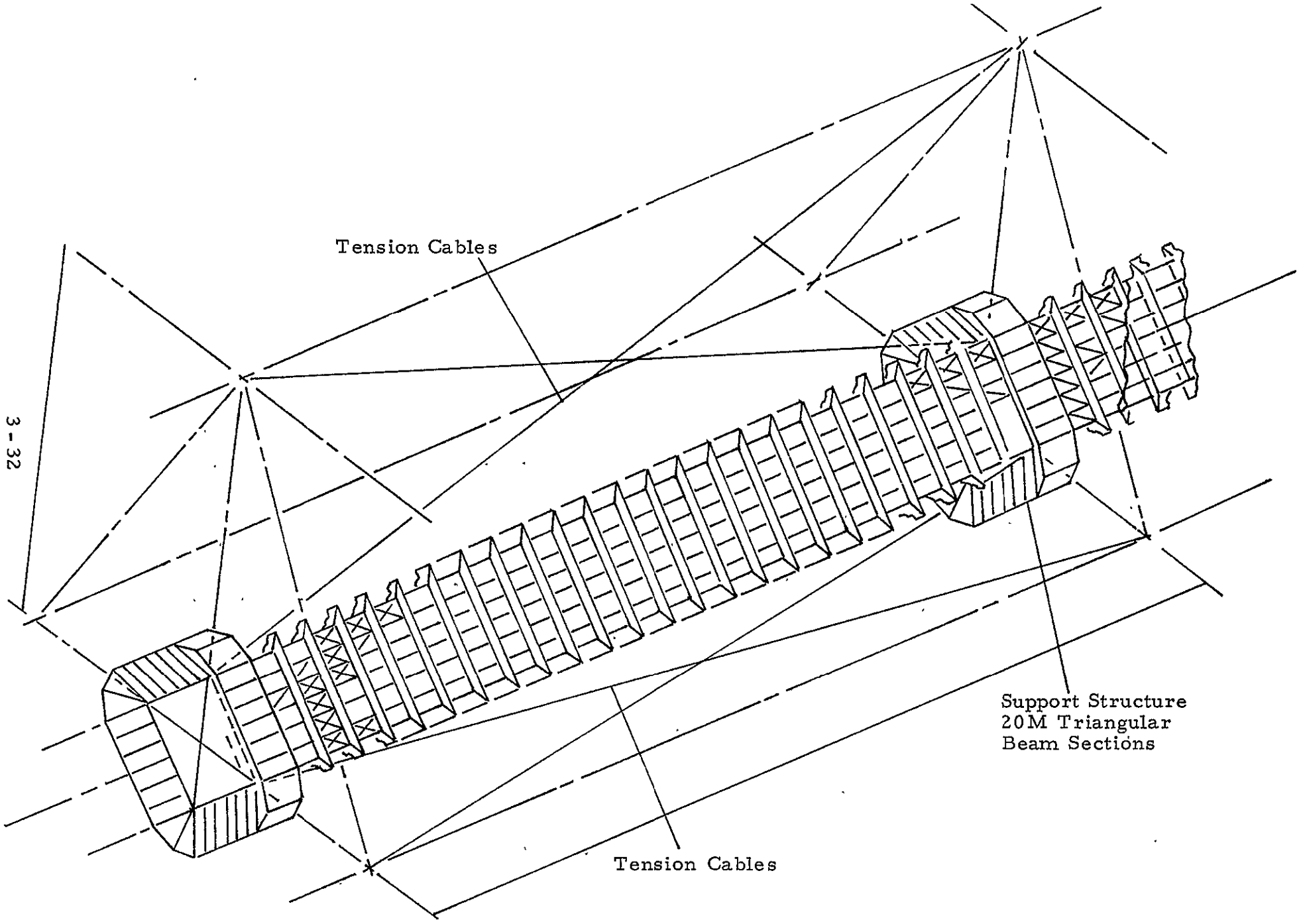

FIGURE 3.11 CONDUCTING MAST CONFIGURATION (FIGURE SUPPLIED BY GRUMMAN)

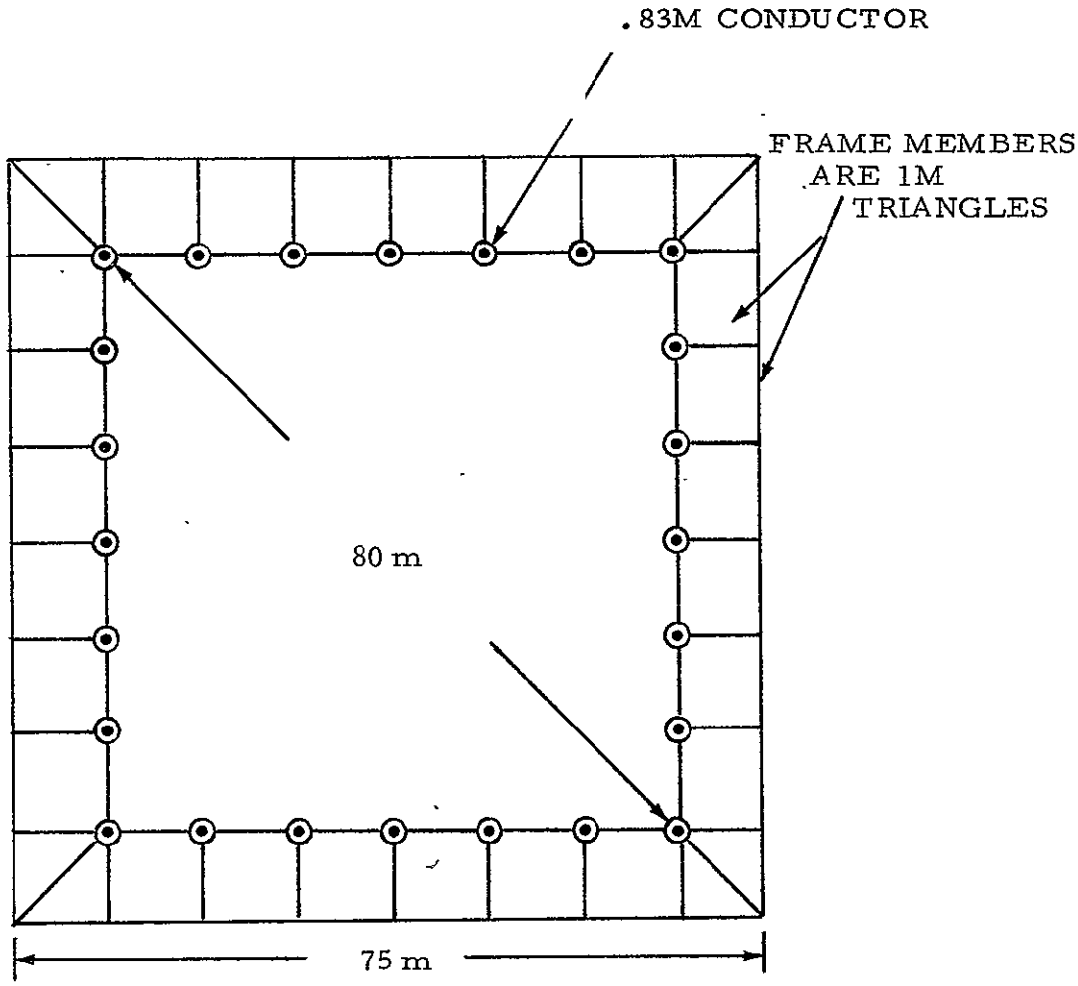

FIGURE 3.12 MAST CROSS-SECTION

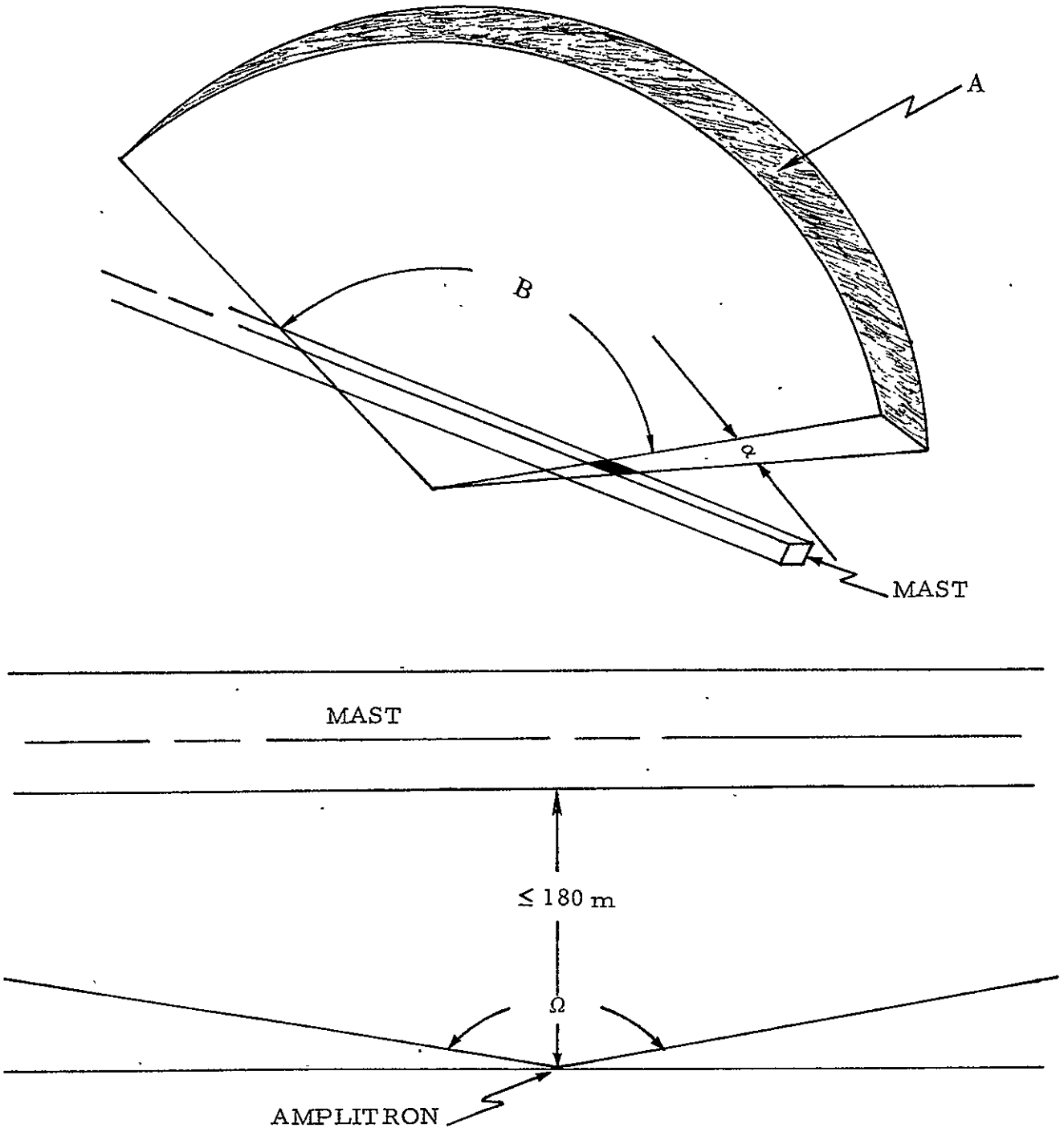

FIGURE 3.13 MAST BLOCKAGE

The angle β is defined by the mast length seen by the Amplitron. For a 160° field of view, the entire mast length of 1017m is in view. The angle β is then 141°. The solid angle obstruction is then computed to be;

$$\Omega_{mast} = (2\pi)\left(\frac{141}{180}\right)\left(\frac{6.24}{180}\right)$$

$$= .054\pi \text{ steradians}$$

3.3.3 FLEX JOINT

The baseline configuration of the SSPS (Figure 3.4.2 of reference 14) shows the flex joint which allows the antenna to nod in elevation over a range of ±4° to be located at a distance of approximately 80 meters from the Amplitron bed on the antenna. The flex joint will be comprised of conductors of size sufficient to carry current from both the solar array panels as well as the supporting structure for these conductors. The largest blockage allowed for the flex joint would be on the order of the 5% blockage total previously assumed for the baseline design.

The Amplitrons radiate into a conical region of 160°. This represents a solid angle of $\Omega \cong 1.653\pi$ steradians. At a distance of 80 meters, the flex joint could be approximately 46 meters in diameter as a maximum. The blockage effect of the flex joint would increase if its diameter increased or if the structure were to be closer than 80 meters from the Amplitrons, or a combination of both effects. For example, a flex joint 20 meters in diameter at a distance of 40 meters would contribute a solid angle blockage of $\Omega = .06\pi$ steradians.

3.3.4 CLOSE-IN STRUCTURAL BLOCKAGE

The blockage contribution due to close-in structure is comprised of electrical equipment required by the MPTS and the support structure for the antenna and the antenna subarrays. The blockage for this condition is shown in Figure 3.12. An optimal placement of electrical equipment required by the antenna such as:

(a) switch gear units

(b) crowbar units

(c) phase front control

would be to locate these equipments on the 108-meter bay support structure as high up as possible, which for the baseline configuration is 40 meters. The resulting blockage of these equipment items are then approximately .004π steradians for each of these items.

As shown in Figure 3.12, Amplitrons located at the edges of the subarray will be blocked significantly by the screw jack and motor equipment used to control the displacement of the subarrays in the vertical direction. The blockage due to this equipment for the sizes assumed and shown in Figure 3.12 is .056π steradians.

There are four switch gear units, four crowbar units, and one phase control unit per subarray or approximately 95 phase control units, for the central region of the antenna. The phase control unit has an assumed cross section of approximately .1 m^2 from the side.

3.3.5 SUMMARY

As one equipment may shield other equipment items, the sum of the individual blockage angles for each equipment is not simply summed together. Possible blockage configurations are the following:

(a) Amplitron located directly in center of antenna adjacent to a subarray screw jack/support structure.

(b) Amplitron located in center region of antenna not blocked by subarray support structure.

In the first case, the analysis does not include the fact that the screw jack/support structure will partially shield a portion of the flex joint and the mast; therefore, the estimate is somewhat conservative. A total blockage summary for this situation would be;

Screw-jack and drive motors	$\cong$	$.056\,\pi$
Mast	$\cong$	$.054\,\pi$
Flex joint	$\cong$	$.083\,\pi$
Phase control units	$\cong$	$.001\,\pi$
Crowbar unit	$\cong$	$.004\,\pi$
	$\Sigma \cong$	$.198\,\pi$ steradians

In the situation described above, three of the crowbar units and three of the switch gear units required for the center region of the antenna were located within the region shielded by the screw jack/motor structure and thus not included in the total.

For the second case, the blockage summary is as follows:

Three crowbar units	$\sim$	$.012\,\pi$
Three switch gear units	$\sim$	$.012\,\pi$
Mast	$\sim$	$.054\,\pi$
Flex joint	$\sim$	$.083\,\pi$
Phase control units	$\sim$	$.001\,\pi$
	$\Sigma \sim$	$.162\,\pi$

The increase in antenna area required by these two situations is 7 % and 5%, respectively.

In all likelihood, the figures given above will increase as the SSPS design progresses and structural designs are further refined. What this study points out, at this stage of development, is that if a passive heat radiation system for the Amplitrons is chosen, the penalties due to blockage have a direct effect on the antenna size, which in turn will be reflected in increased cost and weight penalties for the overall SSPS baseline configuration.

A conclusion to be drawn is that a better thermal design of the overall configuration is required, a design which would allow the MPTS antenna to be more insensitive to the heat dissipation scheme used for the Amplitron waste heat.

3.4 EFFECT OF DIELECTRIC CARRY-THROUGH STRUCTURE

3.4.1 INTRODUCTION

For structural purposes, the two solar arrays of the baseline configuration are connected by the dielectric structure grid network shown in Figure 3.14. In order to minimize the interference due to the carry-through structure on the microwave transmission, the carry-through material is selected on the basis of its poor conducting qualities; i.e., a good dielectric, as well as its structural properties. The material chosen by Grumman is 's glass epoxy' whose electrical properties at a frequency and temperature of approximately 10 GHz (No measurements were available at 2.45 GHz. However, it is expected that the 10 GHz data is representative of the electrical properties of 's glass epoxy' at 2.45 GHz.) and 20° C are given as follows:[23]

$\varepsilon_r \sim 2 \rightarrow 5.$	relative dielectric constant
$p = \tan\delta \sim .007$	loss tangent
$\sigma \sim 3.3 \cdot 10^{-3}$	conductivity, mhos/meter

The principal characteristic phenomena which may affect microwave transmission are (a) phase changes, (b) scattering, and (c) absorption of energy by the obstructing carry-through structure.

The phase change and absorption in transmitting through a dielectric may be analyzed by computing the propagation constant for the medium. Propagation of a plane wave through a dissipative medium is given by a complex phase constant, k, having both a real and imaginary part;

$$k = \beta - j\alpha$$

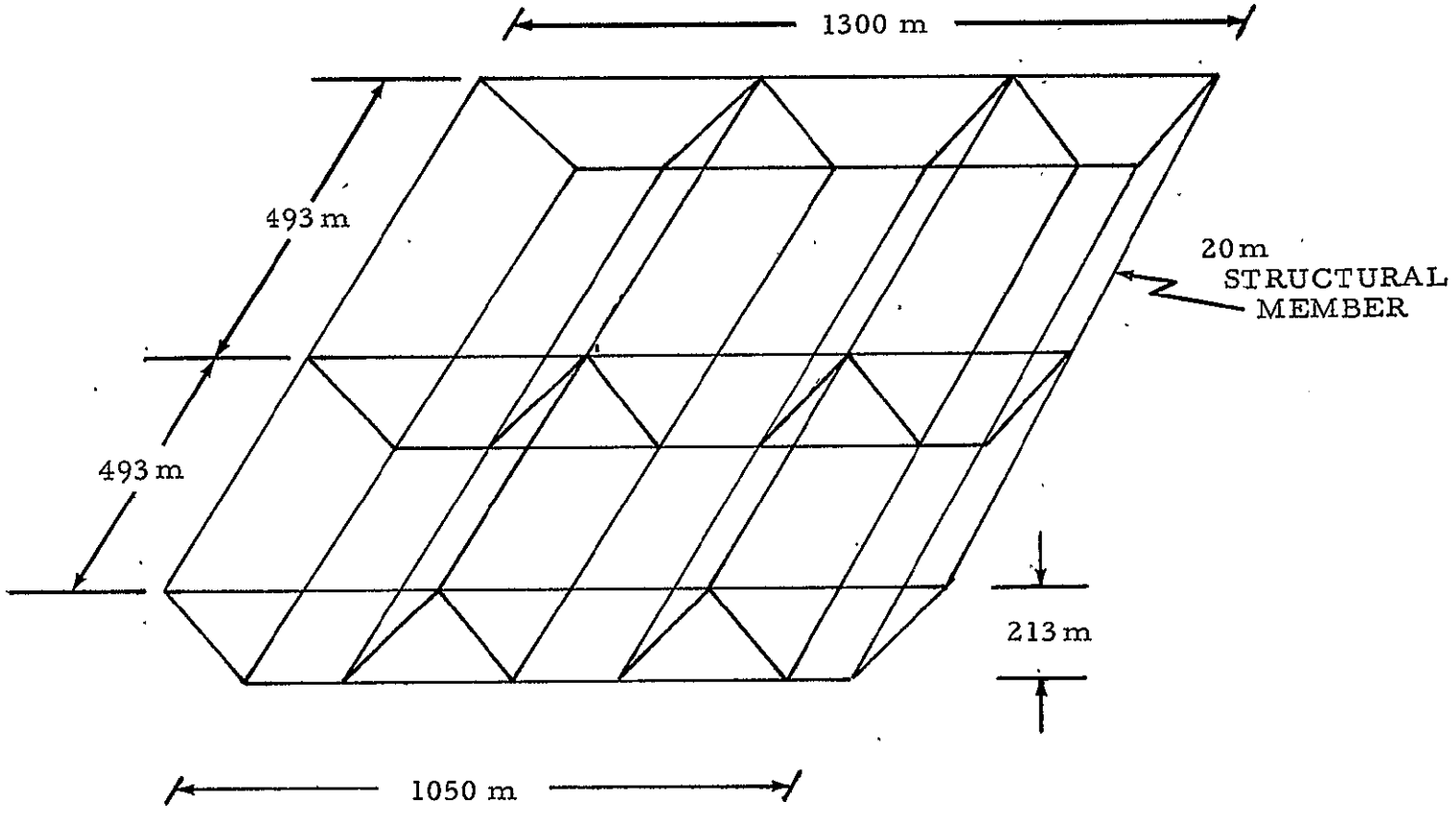

FIGURE 3.14 DIELECTRIC CARRY-THROUGH STRUCTURE OVERALL GEOMETRY

k = complex phase constant

β = phase constant in the medium

α = attenuation constant in the medium

The attenuation and phase constants, α and β, above are in turn a function of the electrical properties of the material such as (a) permeability, (b) dielectric constant, (c) conductivity. Assuming that the permeability of the 's glass epoxy' is that of free space (i.e., that the material is non-magnetic), the complex phase constant becomes:[24]

$$k = \beta - j\alpha = \frac{2\pi}{\lambda_o} \sqrt{\epsilon_r (1 - jp)}$$

The phase constant and attenuation constant are then given by,

$$\beta = \frac{2\pi}{\lambda_o} \sqrt{\epsilon_r f(p)}$$

$$\alpha = \frac{2\pi}{\lambda_o} \sqrt{\epsilon_r g(p)}$$

where the functions g(p) and f(p) represent the real and imaginary parts of the square root of (1 - jp). The functions f(p) and g(p) are tabulated in reference and for a loss tangent of .007 are,

$f(p) = 1.00001$

$g(p) = 0.00375$

The effect of the phase constant β will be to modify the phase of the transmitted energy. And the effect of the attenuation constant α will be to couple the RF energy into heating of the carry-through structure material.

Another effect of the carry-through structure will be that it will act as an impedance mismatch to the antenna causing reflections at any air carry-through structure interface.

These effects will be analyzed in the following three sections.

3.4.2 PHASE CHANGE

The geometry of the microwave transmitting antenna as it relates to the carry-through structure is shown in Figure 3.15. This is an edge view of the antenna looking along the azimuth axis. As the antenna is rotated in azimuth, the effect of the dielectric carry-through structure is to present to the transmitted wavelets regions in which the apparent transmitted path length, causing time delay through the carry-through structure, varies. The phase change associated with the time delay in transmitting through the carry-through structure is defined by the phase constant β in the transmitting medium. The total phase change for a ray is the sum of the phase changes which result in traversing each section of carry-through material:

$$\Delta\phi = \Sigma \beta_i \ell_i$$

$$\beta_i = \beta_o \sqrt{\epsilon_r}$$

ℓ_i = path length through sections of carry-through structure

The relative dielectric constant is computed for the assumption that within the structural members of the carry-through structure there is a homogeneous mix of free-space and 's glass' dielectric material. On this basis, an effective dielectric constant may be computed by comparing the relative volume of the dielectric materials, free space (fs) and 's glass epoxy', within a transmitting volume in the following way:

$$\epsilon_r = 3.5 \left(\frac{V_{dielectric}}{V_{total}} \right) + 1.0 \left(\frac{V_{fs}}{V_{total}} \right)$$

V = volume

The effective dielectric constant in transmitting through a lateral structure member if, $\epsilon_r = 1.000012389$.

A ⟶ J REPRESENT PRIMARY BEAM CAPS

CONNECTING LINES = TRANSVERSE STRUCTURE

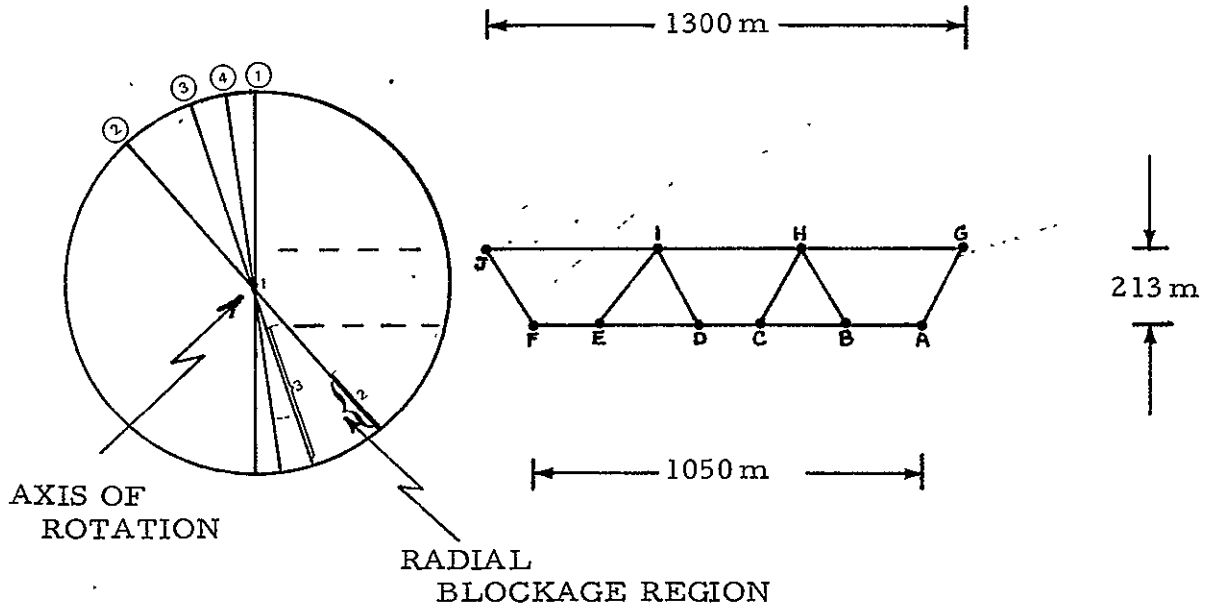

ANTENNA LOCATION

1	θ	=	0
2	θ	=	45
3	θ	=	22.5
4	θ	=	15

FIGURE 3.15 ROTATION EFFECTS OF ANTENNA

Every 493 meters the carry-through structure has vertical ties, composed of interlaced 20 meter triangles. In computing phase changes through the carry-through structure, the number of carry-through structural members must be carefully noted.

Figure 3.16 is a view of the transmitting antenna looking through the carry-through structure at $\theta = 0^\circ$. The effect of rotation of the antenna with respect to the carry-through structure is shown in Figure 3.17. This view represents approximately a 15° rotation and corresponds to the situation noted in Figure 3.15. The area of shading of the antenna by the carry-through structure is increased, because now the lateral structural members do not align but each individually shields a portion of the antenna face.

The ten circular regions shown in both Figures 3.16 and 3.17, represent regions of the antenna in which the transmitted power per unit area, watts/m^2 is constant. In order to shape the antenna beam to have low sidelobes, the antenna has a 10 dB Gaussian taper applied. The taper is applied in ten steps as shown, with the central region having a 21.7 kW/m^2 power density and the outermost ring having 1/10 this value.

The taper was determined to effect the phase change in transmitting through the carry-through structure by weighing the increment of phase change with respect to the power density where the associated obstruction is located. For a given mass of dielectric carry-through material, location of this mass such that it shadows region 10, would be (1/10) that of locating the same mass such that it shadows region one.

The change in amplitude of the main lobe in the far field is then a function of both the amount of shading on the antenna (a function of its location on the antenna face with respect to the different weighted regions) and the total phase change seen by each transmission element (a function of the total amount of associated carry-through material). An expression which describes these effects is shown below.

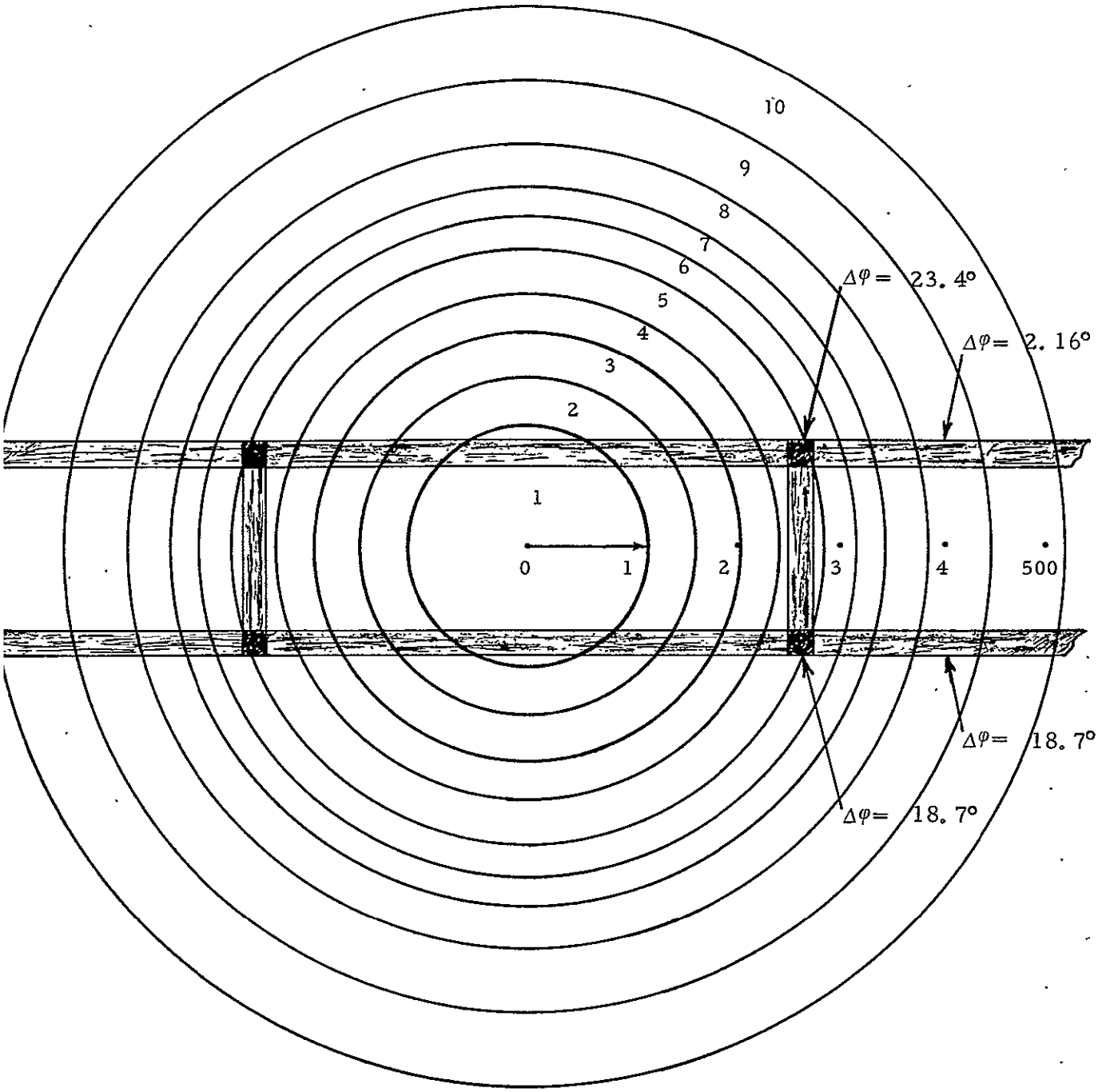

FIGURE 3.16 ANTENNA VIEW ALONG BORESIGHT AT $\theta = 0^{\circ}$

SECTION	NODES
A	1
B	2
C	3
D	4
E	5
F	6
G	6
H	4
I	2
J	1

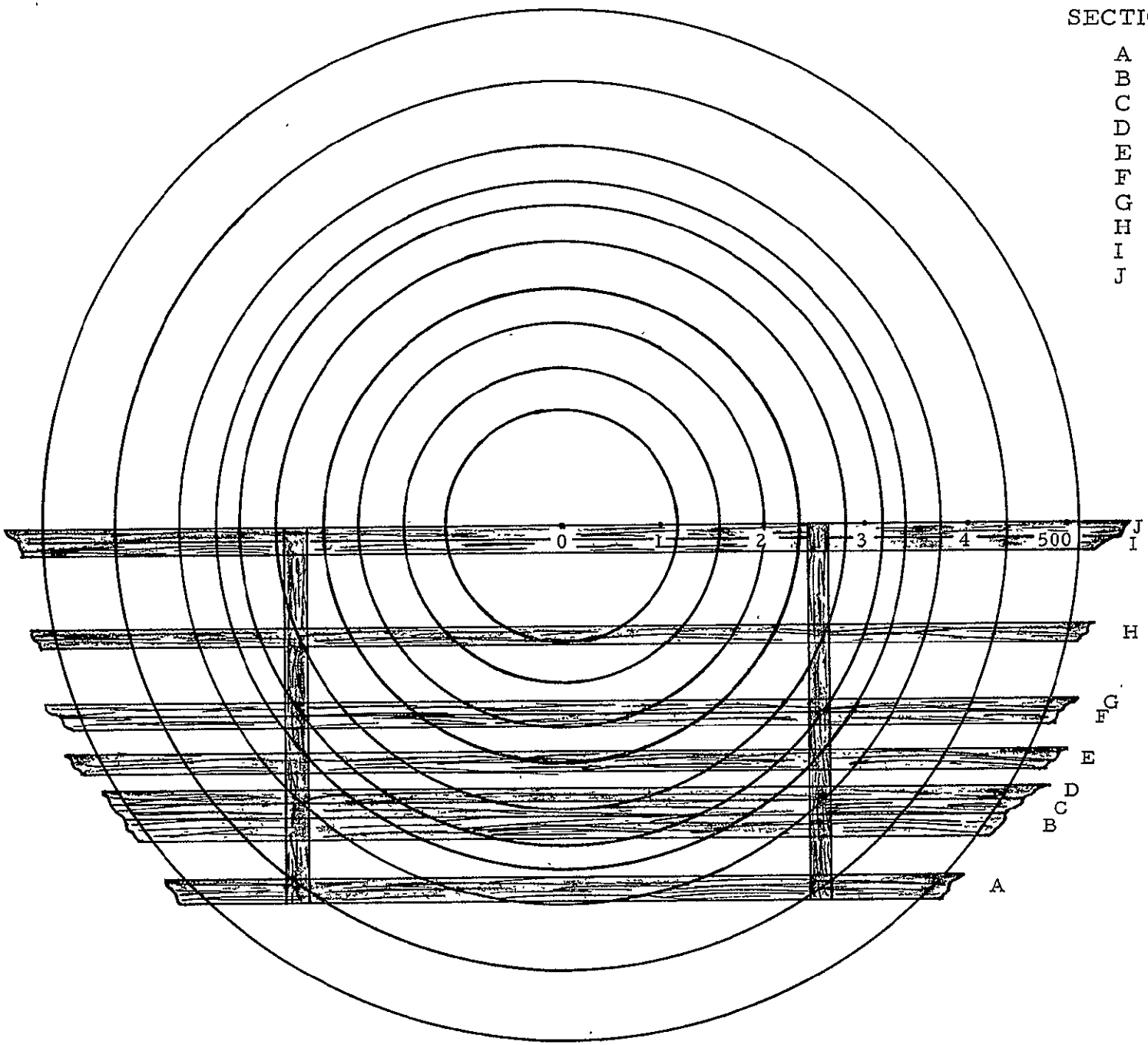

FIGURE 3.17 ANTENNA VIEW ALONG BORESIGHT θ = 15°

$$\frac{E}{E_o} = \frac{\sum_{i=1}^{n} A_i \, W_i \, \text{Cos} \, \Delta\phi_i}{\sum_{j=1}^{10} A_j \, W_j}$$

$\Delta\phi = (\beta_i - \beta_o) \, \Delta\ell$

$\Delta\phi_i$ = phase change as seen by region A_i of antenna as compared to free space

A_i = area of antenna with constant phase shift

W_i = weight given various areas variation 1 to .1

i = subscript which refers to areas of constant phase change

j = subscript which refers to 10 steps of constant power density regions of antenna

E = amplitude of main beam due to shadowing of carry-through structure (volt/m)

E_o = amplitude of main beam with no shadowing (volt/m)

NOTE: When there is no shadowing of the antenna (and therefore no transmission through the carry-through structure), the phase change β is equal to β_o and $\Delta\phi_i = 0$. In this situation the ratio $(E/E_o) = 1.0$.

The weights W_i used for the 10 regions of the antenna are listed below:

Region	Weight
1	1.0
2	.9
3	.8
4	.7
5	.6
6	.5
7	.4
8	.3
9	.2
10	.1

The results of the performed calculation outlined above for the condition of the antenna transmitting through the carry-through structure as shown in Figures 3.16 and 3.17 are tabulated in Table 3-8.

The loss due to the out-of-phase addition of the shadowed antenna transmitting elements is greater for the $\theta = 0^\circ$ case reflecting the higher combination of weighted shadowed area and transmission path length through the carry-through structure.

The power sidelobe level for a 10 dB Gaussian tapered antenna is -25 dB below the peak of the main lobe. If it is assumed that the primary effect of the out-of-phase wavelet addition is to modify the first sidelobe of the antenna beam, the new sidelobe level would rise to the values shown.

TABLE 3-8. AFFECT OF CARRY-THROUGH STRUCTURE SHADOWING OF ANTENNA ON MAIN BEAM AMPLITUDE

	Transmission Angle	
	$\theta = 0^\circ$ (6 AM and 6 PM)	$\theta = 15^\circ$ (5 & 5 AM, 5 & 7 PM)
E/E_o	.999779	.9999305
$1-(E/E_o)^2$	-33.546 dB	-38.57 dB
New Sidelobe	-24.707 dB	-24.905 dB
Sidelobe for $(E/E_o) = 1$	-25.0 dB	-25.0 dB
Associated Loss from Main Beam	0.35%	0.2%

The effect then of the carry-through structure for the two transmitting geometries considered is to modify the first sidelobes by approximately 7% and 2%, respectively. As the first sidelobes contain approximately 5% of the power in the transmitted beam, the effect of the out-of-phase beam addition is to lower the power in the main beam by approximately .35% and .1% for the two cases. It appears that accepting these losses (.35% maximum) at the local times shown would be reasonable and the dielectric carry-through structure does not therefore appear to create a significant problem with respect to the MPTS.

Furthermore, power loss due to out-of-phase addition because of transmission through the carry-through structure is being continuously reduced still further by the reference beam from the ground. Each subarray is continuously having its phase front corrected through the phase control electronics which is referenced by a pilot beam transmitted from Earth.

The transmission path for the phase reference through the carry-through structure is essentially the same as that from the reverse path, consequently the phase change problem of the carry-through structure is reduced to a negligible effect.

There is a question as to how much the response time requirements of the phase control system should be constrained to compensate for the passage of the dielectric carry-through structure. This analysis indicates that there should be no such constraint.

The analysis described shows that in the absence of a phase correcting system for the carry-through structure, approximately a .4% reduction in delivered power would occur early in the morning and again late in the afternoon, local time. It also indicates that power densities at the sidelobes would be increased periodically, and the associated ecological issues therefore will require further analysis and possibly demonstrations as the configuration and system characteristics are matured.

3.4.3 HEATING DUE TO CARRY-THROUGH STRUCTURE

There are two RF heating effects caused by the presence of the dielectric carry-through structure, these are:

(a) the carry-through structure may absorb the microwave energy and thus heat up

(b) the reflected power from the carry-through structure may cause the antenna to heat up with resulting undesired thermal deflections

The coupling of microwave energy to heating of the carry-through structure is a function both of its electrical conductivity and dielectric constant. The absorbed heat is directly proportional to electric conductivity, which is quite low, and inversely proportional to its dielectric constant.

The heating of the antenna due to reflections from the carry-through structure is proportional to the square root of the dielectric constant, as well as the total reflection surface area.

Both these heating effects will be considered in the following sections.

3.4.3.1 Estimate of Microwave Heating Due to Carry-Through Structure

The ability of the carry-through material to absorb the impinging microwave energy is directly proportional to its electrical conductivity, σ, and the square of the electric field strength within the dielectric carry-through material. In turn, the electric field within the 's glass epoxy' is inversely proportional to the square root of its relative dielectric constant. Once this electric field strength is determined, the heating rate of 's glass epoxy' may be computed. The maximum power density is in the center region of the antenna and is 21.7 kW/m^2. The field strength corresponding to this power level is:

$$E_o = \sqrt{(377) \cdot (21.7 \cdot 10^3) \frac{\text{watts}}{m^2} \cdot \text{ohm}}$$

where 377 is the impedance of free space in ohms

$$E_o = 2.8337 \cdot 10^3 \text{ volts/meter}$$

The field strength in the 's glass epoxy' structural members is inversely proportional to the dielectric constant of the medium and for constant power becomes:

$$E = (E_o/\sqrt{\epsilon_r})$$

$$E = 1.5147 \cdot 10^3 \text{ volts/meter}$$

The loss tangent, given earlier for the 's glass' material of .007 corresponds at 2.45 GHz to a conductivity of

$$\sigma = 3.3 \cdot 10^{-3} \text{ mho/m}$$

Using this value, the maximum heating (assuming that the RF is 100% thermally coupled) may be computed. This heating, in watts/m^3 is given by the expression σE^2, and computed to be 7.571×10^3 watts/m^3. The total mass of the carry-through structure is calculated to be approximately 72,575 kg. The total volume of dielectric material assuming a specific gravity of 1.2 is $\approx$ 60 cubic meters. The heat absorbed by the 's glass' material is then 4.5426×10^5 watts or $\sim$ 6.2 watts/kg. The total surface area of the carry-through structure may be estimated on the basis that the thickest members of the structure are the connecting pieces of the one meter triangles (which represents the basic building block of the structure). The thickness of these members are .034 cm. A volume of 60 m^3 would then have a surface area of approximately 1.7647×10^5 m^2. This is equivalent to an irradiance level on the structure of less than 10 w/m^2 and is trivial compared to the solar irradiance of 1353 w/m^2.

This temperature is much lower than the 120° C equilibrium temperature condition computed for the Solar Power Satellite due to solar heating and therefore not considered to be a problem.

3.4.3.2 Heat Load on Antenna Due to Carry-Through Structure

The reflection coefficient from a dielectric slab is given by the following formula from transmission line theory:

$$\rho = \frac{Z_i - Z_o}{Z_i + Z_o}$$

where

Z_i = impedance load of carry-through structure

Z_o = impedance of free space ~ 377 ohms

The impedance of the 's glass epoxy' material is a function of the inverse square root of its relative dielectric constant;

$$Z_L = \left(Z_o / \sqrt{\epsilon_r}\right)$$

Assuming a dielectric constant variation of 2 - 5, the resulting reflection coefficient due to the impedance mismatch of the 's glass epoxy' is as shown in Figure 3.18. As shown, the closer the dielectric material which is used to construct the carry-through structure is matched to free space; i.e., $\epsilon_r = 1.0$, the less reflection there is. The range of dielectric constant for the 's glass epoxy' assumed has been $2. < \epsilon_r < 5$, taking a value of 3.5, the normal reflection coefficient for this value of dielectric constant is $\rho = .303$.

The carry-through structure is made up of a series of one meter triangles, the largest reflective surfaces are represented by the triangular caps which are 6.6 cm wide (see Figure 3.19). The power incident on these structural elements is at a varying incident angle which depends both on the makeup of the structural members (the orientation of the structural caps with respect to the incident power), and the relative orientation with respect to the antenna. These

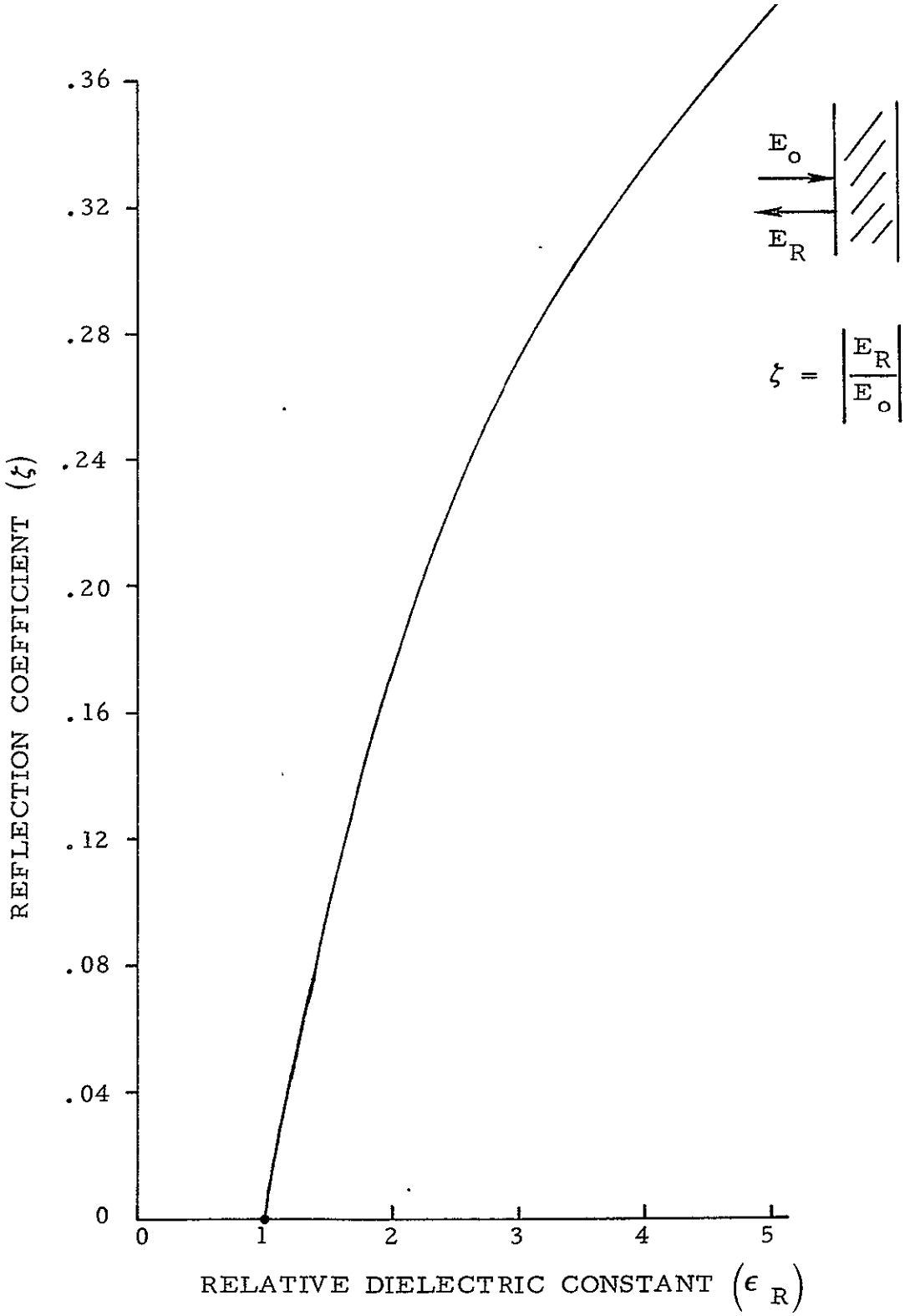

FIGURE 3.18 REFLECTION COEFFICIENT FROM SLAB OF DIELECTRIC MATERIAL

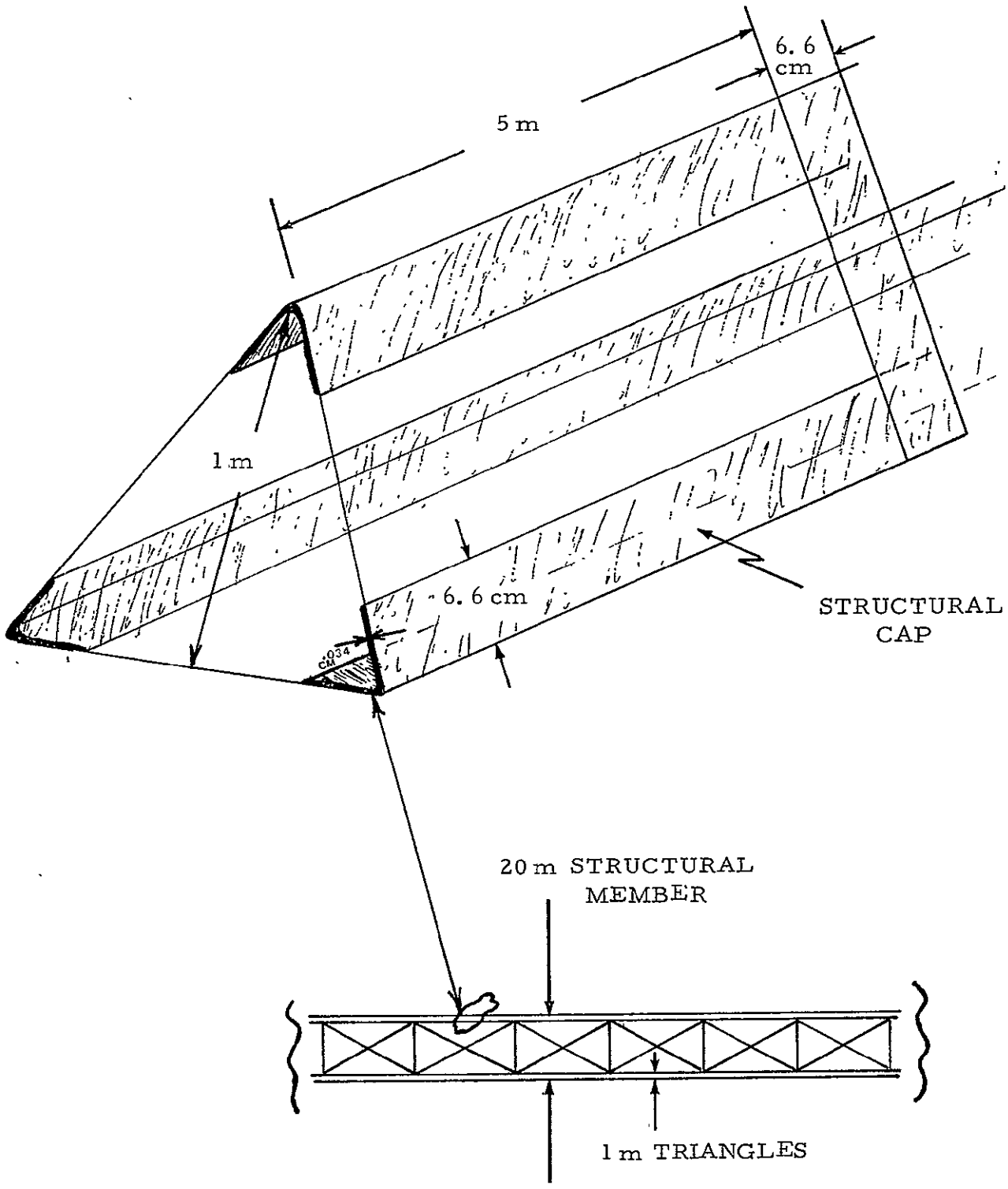

FIGURE 3.19 BLOW UP OF 20 M STRUCTURAL ELEMENT

considerations should reduce the reflection coefficient considerably.

In order to compute the total reflected power, the total area blockage due to the structural caps must be determined. Parametrically, the total reflected power on the antenna is a function of the following parameters:

$P_R = A_s \cdot W_s \cdot P_o \cdot F \cdot \rho^2$ watts.

A_s = total area shielded by carry-through structure

W_s = weight factor, range of 1.0 to .1 for a 10 dB power density tapered antenna

P_o = peak power density of antenna 21.7 kW/meter^2

ρ^2 = power reflection coefficient

F = factor which defines the ratio of total dielectric material seen within a 20m x 20m structural member

The maximum blockage for the antenna occurs when the relative orientation of the antenna and the carry-through structure is at approximately $\theta = 15^\circ$ as indicated in Figures 3.15 and 3.17. The weighted blockage area for this situation (previously computed for the phase calculations) is:

$$A_s W_w = 71,735 m^2$$

This represents approximately 23% of the total weighted surface area of the antenna. The product of $A_s W_s \rho^2 P_o$ is equal to 1.429×10^8. In order to compute the cross-sectional area of a 20 meter square section of dielectric structure, the layout of a section as shown in Figure 3.19 is required. The primary contribution is from the cap structure used to fabricate the one meter triangle building block for the 20 meter structural members. In every 20 meter square section, there is a reflection surface area of approximately $8.448 m^2$.

This is computed based on structure in the 20 by 20 meter section. The ratio of reflective surface area within a 20 meter square structural member is then .02112. The total power reflected onto the antenna structure is then computed to be:

$$P_R = (71,735 m^2)(21.7\ kW/m^2)(.02112)(.303)^2 = 3.018 \times 10^6 \text{ watts}$$

This RF load is effective over an antenna surface area of $\sim$ 180,000m^2 and represents an additional heat flux of 16 watts/m^2, which must be dissipated by the antenna structure.

The waveguide of the antenna is aluminum with an assumed emissivity of .85. The temperature of the waveguide is approximately 40° C and the radiated heat at this temperature, emissivity, condition is 469 watts/meter^2. The reflected power represents 3.4% of this, the majority of which would be reradiated as RF. The waveguide temperature rise would be less than 1° C.

The assumption that the reflected power would be reflected back onto the antenna is a highly pessimistic one. In all likelihood, there will be a significant amount of forward scattering as the impinging RF energy on the carry-through structure will occur at other than 90° incidence. However, even if the power density computed were to be too high by a factor of 100 or more, this reflected energy could have a significant effect on sensitive electronics such as the phase control circuitry.

3.4.4 EFFECTS OF REFLECTED RF POWER ON RF SYSTEMS DUE TO CARRY-THROUGH STRUCTURE

The RF power reflected from the dielectric carry-through structure back to the RF radiating surface on the antenna has been estimated at 16 W/m^2. The uncertainty in this estimate is very large particularly if it is interpreted as the peak value that may interact with a particular RF sensitive set of electronics. Even if it is high by tens of dB, it would still be large compared to the pilot beam control signals at near the same frequency and the problem of isolation of the reflected power from the control electronics would be great.

In depth analysis of pilot beam power, aperture and signal isolation requirements must be conducted in future studies. Early in such studies, reflected RF power from all potential sources should be established and tradeoffs should be evaluated to establish configuration and system constraints. The judgement at this point is that configuration approaches using dielectric or other structure in the field of the MPTS power beam and control signals could be a viable alternate.

3.5 MATERIAL SUBLIMATION EFFECT ON AMPLITRON

3.5.1 INTRODUCTION

The Amplitron when used in a high-pressure environment (i.e., 14.7 PSI) has a glass enclosure surrounding; the cathode and anode, in which a vacuum pressure of approximately 10^{-4} to 10^{-5} TORR is maintained. The low vacuum of space eliminates the need for this glass enclosure as the pressures are on the order of 10^{-13} TORR. A problem may arise, however, if a sufficient number of particles collect in the vicinity of the cathode and thereby increase the local pressure there to 10^{-4} - 10^{-5} TORR. The question to be resolved then is what are the total sublimation products from the MPTS materials, and will they affect the operation and life of the Amplitron?

The results of the study are that for the baseline configuration of the MPTS, the pressure increase due to the collection of sublimation products in the vicinity of the Amplitron is,

(a) primarily due to the materials in the cathode/anode region of the Amplitron; and,

(b) if sufficient venting is provided for these sublimation products in the design of the Amplitron, there is no problem associated with any pressure increase due to sublimation products.

3.5.2 ANALYSIS

The sublimation rate for a material[25] is given by:

$$S = 1.85 \times 10^{6} \frac{P}{\rho} \sqrt{\frac{M}{T}} \quad (cm/yr)$$

P = vapor pressure (TORR)

T = temperature (°K)

M = molecular weight

ρ = density (gm/cc)

As the pressure limitation of 10^{-4} - 10^{-5} TORR for the Amplitron is that measured at the cathode, this fact limits the materials which can be considered to be a problem to be those immediately adjacent to the cathode. Materials considered have been the following:

Copper
Platinum
Pyrolytic Graphite
Aluminum

The platinum and copper represent the cathode and anode of the Amplitron, respectively. Pyrolytic graphite is the material of which the Amplitron heat radiator is made, and aluminum represents the antenna waveguide.

Note the above equation represents a modified form of the state equation for the gaseous or molecular products of the sublimating material. As such, the pressure which is used in computing the sublimation rate is that which corresponds to the temperature of the gas. The vapor pressure, temperature equilibrium relationship for the materials which will be considered here have been experimentally determined and are presented in the reference cited.

Figure 3.20 shows the present Amplitron design. Previous thermal analyses[14] showed that with this design, the maximum temperatures of the various materials was:

Pyrolytic Graphite	~	635° C
Platinum	~	635° C
Copper	~	349° C
Aluminum	~	52° C

The temperatures were determined by specifying a maximum temperature at the cathode of 650° C and anode, 350° C and solving heat balance equations iteratively to reach a temperature equilibrium. The final temperatures for the Amplitron are shown in Table 3-9, corresponding to the points noted in Figure 3.20.

TABLE 3-9. RESULTS OF PREVIOUS COMPUTER THERMAL ANALYSIS OF AMPLITRON

Location	Temperature (°C)
A	635.
B	591.
C	570.
D	349.
E	305.
F	282.
G	265.
H	52.
I	49.
J	48.
K	46.
L	39.
M	40.
N	41.
P	41.

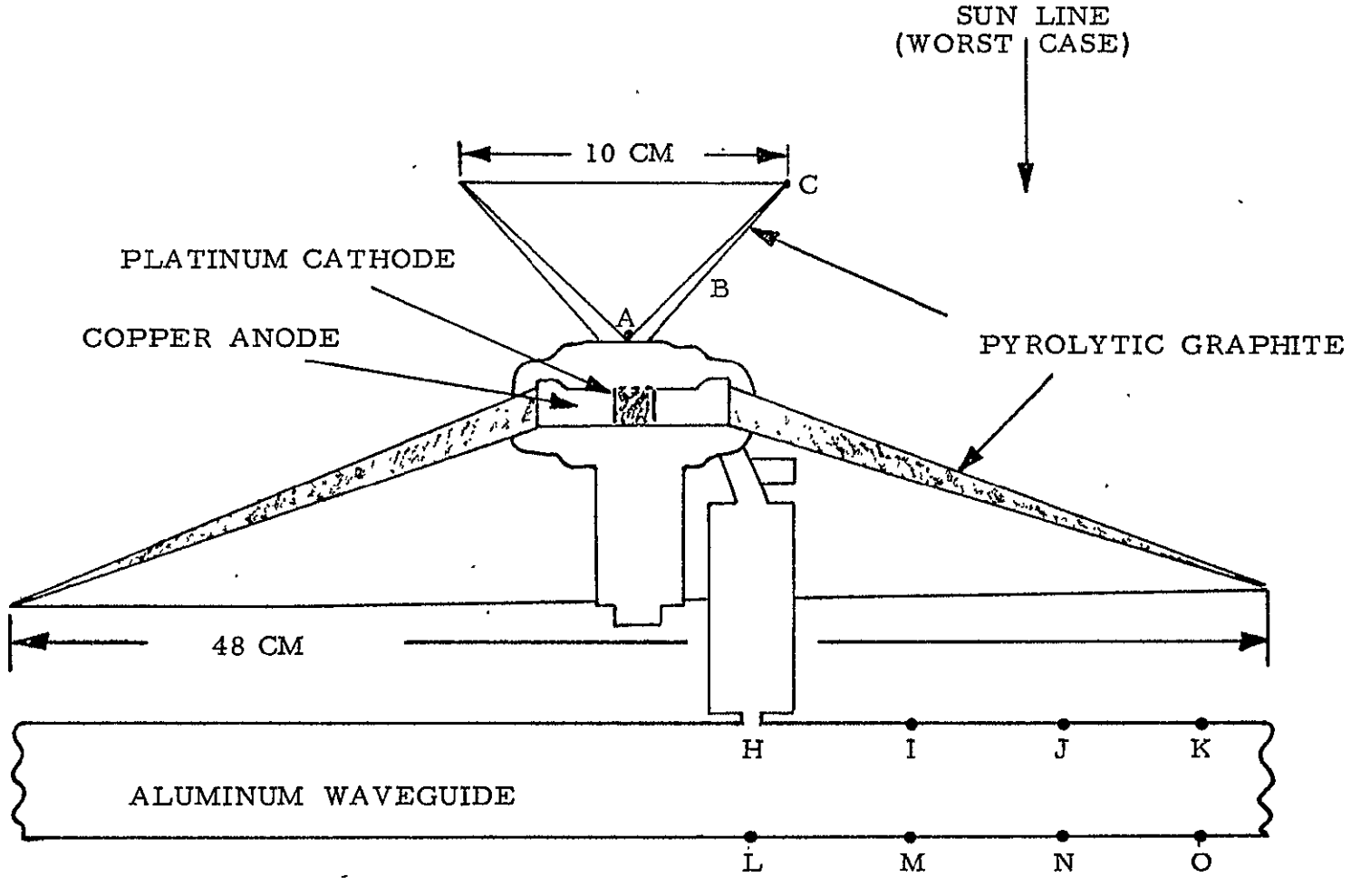

FIGURE 3.20 AMPLITRON CONFIGURATION

Using the experimental pressure temperature relationship defined in reference (25), the sublimation rate of these materials was computed. (Carbon was chosen as representative of pyrolytic graphite for which no vapor pressure/ temperature relationship could be found.) These results are shown plotted in Figure 3.21. Copper represents the material which is most likely to affect the operation of the Amplitron. This is so for the following reasons. Of the sublimation rates of the materials shown plotted in Figure 3.21, at the temperatures computed for the Amplitron; Copper at 349° C shows the highest rate by a factor of at least 10^3 over the Aluminum waveguide, the platinum cathode, and the pyrolytic graphite radiators. Furthermore, the copper sublimation products are in a region critical to the Amplitron operation. For these reasons, only the sublimation products of the copper anode were considered in the study.

In order to compute a concentration of copper particles, the total surface area of copper which could sublime at the computed rate was calculated to be approximately 70 cm^2. A weight equal to the molecular weight of copper subliming provides 6.023×10^{23} particles. If the sublimation rate for copper at a temperature of 349° C is used, along with the total surface area of copper which is subliming, the weight of copper sublimated may be computed.

This weight total using Avogadro's number results in a total number of particles subliming. The concentration of copper particles is computed by determining the volume in the cathode/anode region of the Amplitron. The results of this calculation are shown in Table 3-10. The calculation has assumed the sublimation rate for copper at 349° C to be constant for the period of time varying from one year to thirty years. The pressure calculated is that assuming the worst possible condition that all the copper sublimed remains trapped within a confined volume adjacent to the cathode.

The likelihood of leakage of particles to space, in which the pressure is approximately 10^{-13} TORR or lower, is high. On this basis, the Amplitron design should be such as to ensure that this leakage occurs. The Amplitron then would be unaffected by sublimation products.

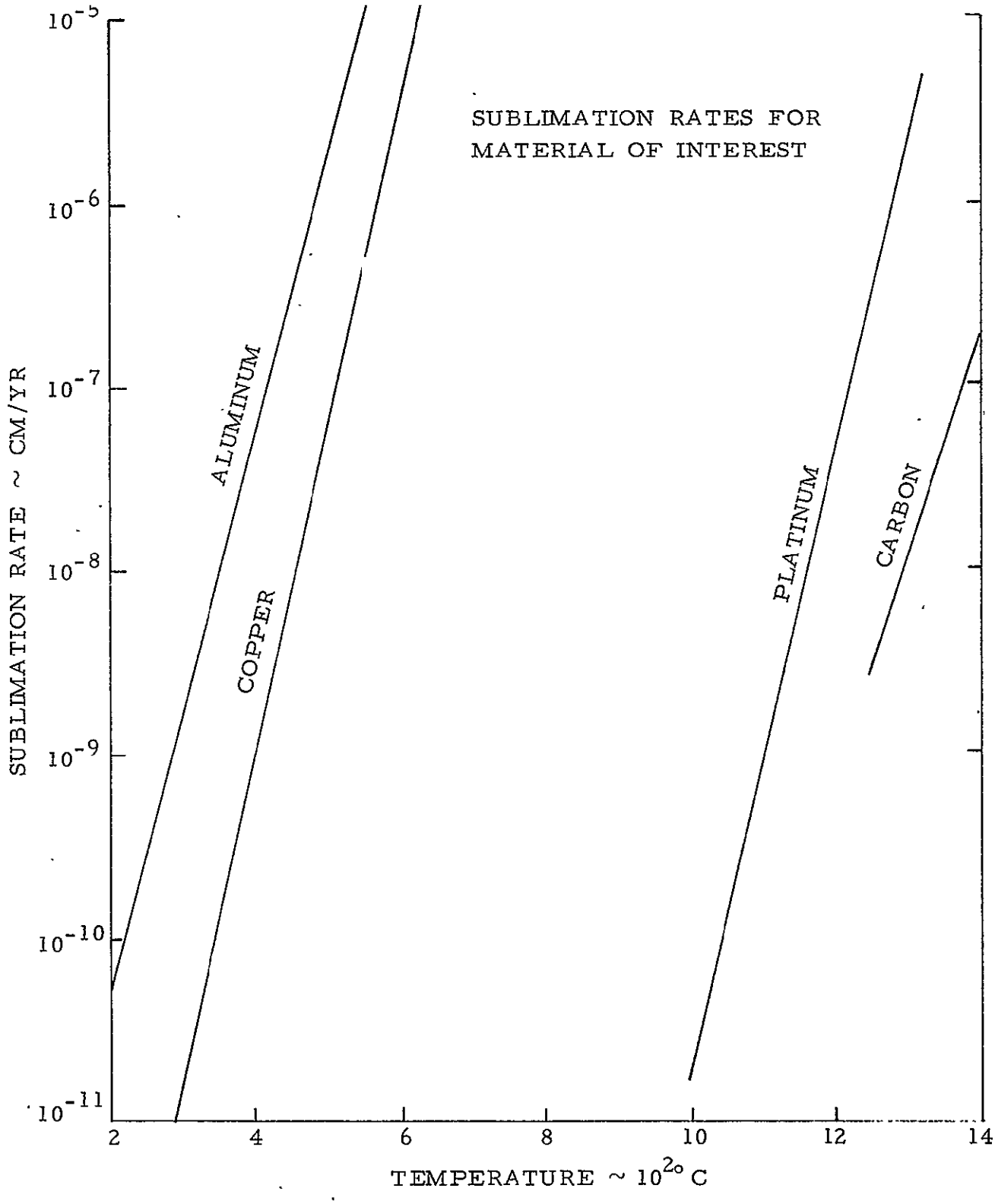

FIGURE 3.21 SUBLIMATION RATE AS A FUNCTION OF TEMPERATURE

TABLE 3-10 SUMMARY OF SUBLIMATION OF COPPER ANODE (T = 349° C)

Year	No. of Particles	Concentration	Pressure ~ TORR
1	2.72×10^{14}	5.44×10^{12} no/cc	7×10^{-5}
10	2.72×10^{15}	5.44×10^{13} no/cc	6.3×10^{-4}
20	5.505×10^{15}	1.01×10^{14} no/cc	1.01×10^{-3}
30	1.651×10^{16}	3.302×10^{14} no/cc	2.4×10^{-3}

Amplitron operating pressure limit given as $\approx 10^{-5} - 10^{-4}$ TORR

3.6 SUMMARY & RECOMMENDED DEVELOPMENT PLAN

3.6.1 CONCLUSIONS OF PRESENT STUDY

The following conclusions may be drawn from the present study:

- A 40 kV Amplitron at 5 kW output power represents a cost and weight penalty over the 20 kV, 5 kW tube.
- A 40 kV dc power distribution system operating with two, 20 kV, 5 kW Amplitrons in series represents a weight and cost saving. However, there is a subarray isolation problem which must be analyzed further.
- The system requires further design effort to eliminate the need to enlarge the antenna due to a thermal blockage of Amplitrons located adjacent to the 108m bay structure and directly in the center of the antenna.
- The carry-through structure does not appear, from preliminary calculations, to be a problem, both in terms of transmission losses, and structural heating. However, because of the complex nature of this problem, further experimental efforts are recommended particularly with respect to the phase control circuitry. This requirement, of course, depends on the final design configuration. It is recognized that a design configuration could be selected which will not include structures which interfere with the MPTS.
- Sublimation of materials adjacent to the Amplitron does not appear to have significant effect on successful operation of the Amplitron.

The effect of the carry-through structure has been shown to be small in terms of modification of the transmitted beam resulting only in .3 dB sidelobe rise for the assumed conditions. However, both experiments and computer

simulations should be developed to certify the design concept before a satellite is placed in orbit. To this end, a plan has been outlined and will be described in the following sections to resolve this problem. Also, the phase control circuitry should be analyzed to determine if the reflected RF background interferes with the pilot beam signal from Earth.

Sublimation of material in space in terms of affecting the operation of the Amplitron is not considered a problem and therefore no tasks have been scheduled to pursue this subject.

The present configuration of the satellite presents a thermal blockage problem for the Amplitrons. Consequently, a better method of dissipating the Amplitron waste heat will have to be developed to obviate the need for increasing the antenna or system configurations should be developed to reduce the blockage.

Further design work is required in order to have a 40 kV antenna power transmission system. A 40 kV, 5 kW Amplitron presents a weight and cost penalty which may completely eliminate its consideration. The system of 20 kV, 5 kW Amplitrons in series presents approximately a 25% weight and cost saving for the power distribution system. However, the problems associated with isolating the subarrays will have to be investigated in depth.

A schedule and task description recommended to resolve these issues is presented in the following sections.

3.6.2 DEVELOPMENT PLAN

3.6.2.1 Dielectric Carry-Through Structure

The tasks to be performed are noted in Figure 3.22 along with the schedule for their performance. The primary emphasis for these tasks are to ensure that if the satellite design consists of a dielectric carry-through structure that any transmission problems are resolved prior to system concept commitment.

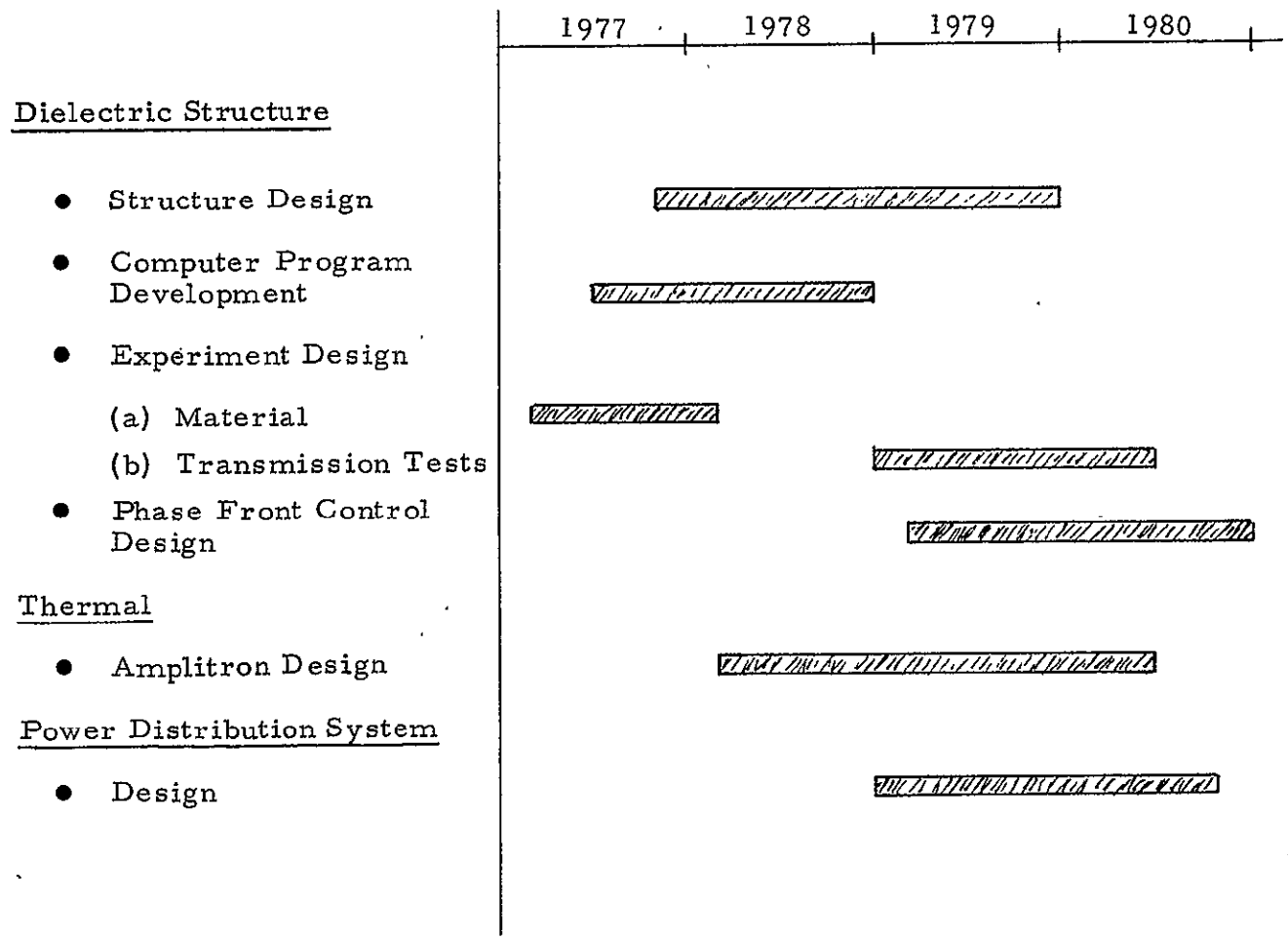

FIGURE 3.22 TASKS/SCHEDULE

A logical procedure or sequence for the tasks are to; a) refine the design of the carry-through structure as much as possible; b) develop a computer program which may be used to extend knowledge in areas which may not be experimentally modelled, as well as to assist in the understanding of the experimental data; c) settle on a material for the carry-through structure; and, d) design experiments to determine the electrical properties of the carry-through material, and design an experiment in which a properly scaled antenna and carry-through structure is tested.

The structure design effort should attempt to arrange the carry-through structure such that higher power density regions of the antenna are less shadowed. The material tests may be done at University Laboratories (e.g., Laboratory for Insulation Research at MIT, and will determine the electrical conductivity, dielectric constant and loss tangent at 2.45 GHz for a range of material suitable for the carry-through structure.

The RF blockage effect of the carry-through structure has not been shown to be a significant problem. However, experimental tests and computer simulations should confirm this.

An exact scaling of the carry-through structure to the experimental test antenna is not possible on a practical basis. Furthermore, the preliminary calculations presented here demonstrate that the effect of the RF blockage due to carry-through structure does not warrant this type of test. What is envisioned is that models of the carry-through structure will be made approximately representing the same volimetric blockage of the space antenna. These models could be inserted in the near field of the 2.45 GHz transmitting antenna. The beam pattern in the far field could then be measured and compared with the unobstructed antenna patterns from this antenna.

The developed computer program would aid in understanding and reducing the beam pattern measurements taken, and once confidence is established, be used to extrapolate to conditions in which experimental data is not available.

The results of this aspect of the study will be to either accept the concept carry-through structure design with or without modifications, or point the way to alternate schemes.

The reflected RF signal computed is significantly higher than the pilot beam signal from the ground. Consequently, unless there is an adequate frequency or polarity separation of the pilot beam signal from the reflected RF as well as adequate filtering on the phase control circuitry, this reflected RF may be a problem for the RF circuitry. The phase front control circuitry should be further refined to resolve this aspect of the dielectric carry-through structure.

3.6.2.2 DEVELOPMENT THERMAL BLOCKAGE

The structure required to rotate the antenna both in azimuth and elevation, as well as the bay structure for the subarrays, and the cabling and equipment requirement for the microwave transmitting system all contribute to a thermal blockage of the Amplitrons. This blockage exceeds that previously assumed in the design of the Amplitron heat radiation cones. Some of the blockage may be decreased or eliminated by judicious design. However, the requirements of moving a large, massive structure will always be present and with it some blockage of the Amplitrons. Thermal analyses are required in conjunction with the design of the antenna and its connecting structure to the solar panels which will obviate the need to increase the antenna as a direct function of the thermal blockage of the Amplitrons. Recognizing that this blockage may exist, a method of curing the problem by either conducting heat from 'problem' Amplitrons to other radiating elements or other more direct cooling schemes for these Amplitrons should be developed.

3.6.2.3 POWER DISTRIBUTION SYSTEM

The satellite power distribution system has many obvious advantages when operation is at high voltages. For a given power level, the current varies inversely with voltage. And, as current is a key parameter in sizing of cabling and electrical hardware, it would be advantageous to operate at high voltages. The two 40 kV Amplitron configurations investigated in the present study pointed out that an isolation problem exists for a 40 kV system having 20 kV Amplitrons in series.

The effect of this isolation problem on the overall system design remains to be studied. Further, the usage of a 40 kV, higher power Amplitron, though inefficient on a cost and weight basis for the microwave power distribution system, may be justified on an overall system basis. Other approaches to achieve lower cost and weight for power distribution should be investigated.

4.0 COST MODEL INPUT DATA

The work carried out under this portion of the study had an impact on the previous estimate of cost and risk. This section describes the Raytheon provided changes to the ECON cost model and their basis.

4.1 VARIABLE SYSTEM POWER

In order to investigate the cost relations for higher and lower parts, it was necessary to provide an equation relating rectenna area to power output at the ground bus after five years. This is:

Revise first two terms of equation $C_{GRD-STA}$ to be a single term;

$$C_{RECT}\ A_{RECT}$$

where

C_{RECT} = Specific cost of rectenna, real estate, and site preparation in \$/Hectare (1 Hectare ~ 2 Acres)

$$A_{RECT} = \frac{\pi}{4}\ \frac{5}{P_{5\,YR}}\ x\ \frac{10^4}{SIN\ E}$$ (Ground area of rectenna, hectares)

E = Elevation angle (for SW Site 50°)

$$P_{5\,YR}(GW) = P_{OUT(GW)}\ \frac{5}{5.258}$$

	Best	Most Likely	Worst
C_{RECT} (\$/HECTARE)	73,700	109,800	160,600

4.2 ANTENNA ILLUMINATION TAPER

The amplitude taper across the antenna was changed from 5 dB to 10 dB to improve sidelobe level. This required the use of a larger antenna in order to allow the heat generated in the central portion of the array to be dissipated.

The heat radiators were already packed as tightly as possible at the center so the only way to get the taper was to increase aperture. The items in the cost model which were changed were:

- The basic diameter of the antenna (D_{ANT}) is increased from 0.83 KM to 1.027 KM to account for the change in amplitude taper from 5 dB to 10 dB.
- Change terms in C_{ANT} equation as follows to account for increased MPTS antenna area due to using a 10 dB taper not 5 dB.

	Best	Most Likely	Worst
$C_{PD}(\$/KW)$	6.00	6.59	12.52
C_{PCE}	25.77	28.63	56.80
C_{WG}	12.13	13.47	26.95
C_{ST}	12.40	13.78	27.56

- Change the following specific Mass terms to account for larger antenna area:

	Best	Most Likely	Worst
$m_{ANTS}(KG/KW)$	.1228	.1364	.1500
m_{WG} (KG/KW)	.3786	.4207	.8415

4.3 40 kV -VS- 20 kV POWER DISTRIBUTION

Previously, Raytheon had assumed a 20 kV Amplitron configuration with 20 kV power distribution. Use of 40 kV distribution can reduce the cost and mass of the distribution system. It does have a negative effect on cost and mass of the DC to RF converters (Amplitrons). This is discussed in Section 3.0 of this report. Two alternate configurations were investigated. One used 40 kV Amplitrons and the other series connections of two 20 kV Amplitrons.

- 40 kV Amplitrons

C_{DC-RF} ($/KW) increases	(Amplitron)
m_{DC-RF} (KG/KW) increases	(Amplitron)
C_{PD} ($/KW) decreases	(Power distribution)
$m_{ANT\ PD}$ (KG/KW) decreases	(Power distribution)

	Best	Most Likely	Worst
C_{DC-RF} ($/KW)	20.70	23.00	46.00
m_{DC-RF} (KG/KW)	0.468	0.520	0.852
C_{PD} ($/KW)	3.91	4.29	8.15
$m_{ANT\ PD} = \frac{M_{ANT\ PD}}{P_{ANT}}$	0.0315	0.0350	0.0700

- Series 20 kV Amplitrons (use two 20 kV Amplitrons in series to allow 40 kV distribution):

C_{DC-RF}	unchanged, same Amplitrons
m_{DC-RF}	unchanged, same Amplitrons
C_{PD} & $m_{ANT\ PD}$	decrease because lower current means smaller, less costly power distribution
C_{WG}, m_{WG}	increase because insulated spacing and structure is needed

	Best	Most Likely	Worst
C_{PD}	3.91	4.29	8.15
$m_{ANT\ PD}$	0.0315	0.0350	0.0700
C_{WG}	12.74	14.14	28.30
m_{WG}	0.4013	0.4459	0.8920

4.4 POWER DISTRIBUTION

Further work on the power distribution resulted in changes to the cost model.

- The design of the power distribution system was refined making it lighter and less costly than previously estimated. The degree of risk in the cost of the power distribution is estimated to be slightly reduced; also, as reflected in the best and worst. This figure takes into account the change in D_{ANT} from 0.83 KM to 1.027 KM, and the improved collection efficiency term.

	Best	Most Likely	Worst
C_{PD}(\$/KW)	6.00	6.59	12.52

- Add a term to the M_{ANT} equation to account for Power Distribution:

$$M_{ANT\,PD} = m_{ANT\,PD}\, P_{ANT}$$

$m_{ANT\,PD}\left(\frac{KG}{KW}\right)$ =	Best	Most Likely	Worst
	0.0470	0.0522	0.1044

Based on new efficiency numbers and a new $M_{ANT\,PD}$ = 440×10^3 KG (Most Likely)

4.5 EFFICIENCIES

Some refinements were made to the efficiency terms.

- Modify efficiencies as follows:

	Best	Most Likely	Worst
η_{PC}	.96	.95	.94
η_{BC}	.97	.95	.93
η_{RF-DC}	.91	.88	.85
$\eta_{RECT-PD}$	.96	.95	.94

5.0 REFERENCES

1. A special issue of Radio Science 9, 881-1090 (1974) contains papers summarizing the important aspects of the ionosphere modification experiments.

2. Goldman, M. V.: Review of Non-Linear Theory of Ionospheric Interaction. University of Colorado, Report UC1003, 1973.

3. Holway, L. H., Jr. and Meltz, G.: Excitation of Parametric Instabilities by Non-Monochromatic HF Fields. Proceedings of the IVORY CORAL 1973 Technical Review Meeting, sponsored by DARPA, pp. 215-232, 1973.

4. Meltz, G. and Holway, L. H., Jr.: Theoretical Studies of Ionospheric Heating by Powerful Radio Waves. Final Technical Report RADC-TR-73, sponsored by DARPA, 1974.

5. Meltz, G. and LeLevier, R. E.: Heating of the F-Region by Deviative Absorption of Radio Waves. J. Geophys. Research 75, 6406-16, 1970.

6. Holway, L. H., Jr., and Meltz, G.: Heating of the Lower Ionosphere of Powerful Radio Waves. J. Geophys. Research 78, 8402-08, 1973.

7. Holway, L. H., Jr., and Meltz, G.: Modification of the Lower Ionosphere by High Power HF Transmissions. Raytheon Research Division Report T-984. Also presented at the 1974 URSI Annual Meeting, University of Colorado, Boulder, Colorado, October 14-17, 1974.

8. Meltz, G. and Holway, L. H., Jr., and Tomljanovich, N. M.: Ionospheric Heating by Powerful Radio Waves. Radio Science 9, 1049-64, 1974.

9. Sen, H. K. and Wyller, A. A.: On the Generalization of the Appleton-Hartree Magnetoionic Formulas. J. Geophys. Research 65, 3931-3950, 1960.

10. Holway, L. H., Jr.: High Frequency Breakdown in Ionic Crystals. J. Appl. Phys. 45, 677, 1974.

11. Dalgarno, A.: Collisions in the Ionosphere in Advances in Atomic Molecular Physics, Vol. 4, editied by D. R. Bates, pp. 381-410, Academic, New York, 1968.

12. Leu, M. T., Biondi, M. A. and Johnson, R.: Measurement of the Recombination of Electrons with $H_3O^+(H_2O)_n$ Series Ions. Phys. Rev. A7, 292, 1973.

13. Utlaut, W. F.: Ionospheric Modification Induced by High-Power HF Transmitters. Proc. IEEE 63, 1022-43, 1975.

14. Microwave Power Transmission Systems Studies, Vol. II. Report NASA CR-134886. Raytheon Company, Equipment Division, Advanced Development Laboratory, Sudbury, Mass.

15. Perkins, F. W. and Valeo, E. J.: Thermal Self-Focusing of Electromagnetic Waves in Plasmas. Phys. Rev. Letters 32, 1234, 1974.

16. Perkins, F. W.: personal communication.

17. Gordon, W. E.: Personal communication.

18. Stevens, G. H.: NASA Lewis Research Center memorandum, October 12, 1976.

19. Burgess, B.: Propagation of VLF Waves Under Disturbed Conditions. Radio Science, Vol. 68D, No. 1, January 1964.

20. Matsushita, S.: A Study of the Morphology of Ionospheric Storm. J. Geophys. Res., 64, 305, 1959.

21. Aarons, Jules: Equational Scintillations. A Review, AFGL-TR-76-0076, April 1976.

22. Van Name: Modern Physics

23. Plastics for Aerospace Vehicles. MIL-HDBK-17A, January 1971 (Table 2-6 Properties of E-Glass and S-Glass).

24. Jackson, J. D.: Classical Electrodynamics, Wiley Publishers, 1962.

25. Jaffe, L. D. and Rittenhouse, J. B.: Evaporation Effects on Materials in Space, Chapter 9 of Materials for Missiles and Spacecraft, Univ. of California, Engineering and Sciences Extension Series, McGraw-Hill Book Co., 1963.

(THIS PAGE INTENTIONALLY LEFT BLANK)

APPENDIX A

MICROWAVE POWER TRANSMISSION SYSTEM (MPTS) CHARACTERISTICS

P_o = Peak power density at transmitting antenna
= 21,700 W/m^2

dB = Taper of truncated Gaussian power distribution at transmitting antenna
= 10. i.e. Power density at edge = 2,170. W/m^2 and it is accomplished in ten steps.

A_T = Area of transmitting antenna (m^2)

η_d = Antenna aperture efficiency

$$= \frac{2\left[1 - 10^{-\frac{dB}{20}}\right]^2}{\left[1 - 10^{-\frac{dB}{10}}\right]_{0.115\ dB}}$$

P_D = Maximum power density at main lobe at range R(m) through environment with propagation efficiency η_a and beam forming efficiency η_b at wavelength λ (m)

$$= \frac{P_o A_T^2}{R^2 \lambda^2} \left[\frac{1 - 10^{-\frac{dB}{20}}}{0.115\ dB}\right]^2 \eta_b \eta_a$$

A_R = Area of aperture normal to boresite at Range R(m), wavelength λ(m) from a transmitting antenna aperture A_T (m^2).

$$3.1648 \frac{\lambda^2 R^2}{A_T} \quad \& \quad D_{R_{minor}} = \sqrt{\frac{346.96}{P_G}}\ R, \quad D_{R_{major}} = \frac{D_{R_{minor}}}{\sin 50^\circ} \left(\begin{matrix}\text{SW} \\ \text{location}\end{matrix}\right)$$

η = MPTS efficiency end to end $\left(\frac{\text{dc out of Rectenna}}{\text{dc out of Orbital Power Source}}\right)$

$= \eta_t\ \eta_b\ \eta_a\ \eta_s\ \eta_r\ \eta_d$

$= .8202 \times 0.95 \times 0.9875 \times 0.95 \times 0.8406 \times 0.903$ for $\lambda = .1225$m ($f = 2.45$ GHz), Southwest ground site.

$= .5549$

$P_{in} = 10,340\ A_T$ (W) dc input power to antenna

$P_T = 8,480\ A_T$ (W) rf output power from antenna

$P_G = 5,732\ A_T$ (W) dc output power from rectenna ($R = 37 \times 10^6$m)

$P_D = 0.51123 \times 10^6 \dfrac{A_T^2}{R_R^2}\ \eta_b\ \eta_a$ (W/m^2) power density maximum at ground

$P_{D_{S.L.}} = P_D \times 10^{-2.4}$ (W/m^2) power density maximum at sidelobes (with nominal outage)

For $\lambda = 0.1225$ m

$$\eta_d = \frac{\left[2\pi \int_o^a f(\rho)\ \rho\, d\rho\right]^2}{A_T 2\pi \int_o^a f^2(\rho)\ \rho\, d\rho}$$

where $f(\rho) = \tau\, e^{-K\left(\frac{\rho}{a}\right)^2}$

and $K = \dfrac{dB}{20} \ln 0$

$= 0.115$ dB

a = transmitting antenna maximum radius

ρ = radius to element within the antenna

$$= \frac{\left[2\pi \int_o^a e^{-K\left(\frac{\rho}{a}\right)^2} \rho\, d\rho\right]^2}{A_T 2\pi \int_o^a e^{-2K\left(\frac{\rho}{a}\right)^2} \rho\, d\rho}$$

$$= \frac{\left[2\pi \cdot e^{-K\left(\frac{\rho}{a}\right)^2}\right]_o^a}{A_T 2\pi \dfrac{e^{-2K\left(\frac{\rho}{a}\right)^2}}{4K/a^2}} = 2 \frac{\left[1 - e^{-K}\right]^2}{\left[1 - e^{-2K}\right]} \times \frac{1}{K}$$

$$\frac{2\left[1 - 10^{-\frac{dB}{20}}\right]^2}{\left[1 - 10^{-\frac{dB}{10}}\right] 0.115\ dB}$$

$$P_T = P_o A_T \left[\frac{1 - 10^{-\frac{dB}{10}}}{0.23\ dB}\right]$$

$$P_D = \frac{P_T \eta \frac{4\pi A}{\lambda^2}}{4\pi R^2} \eta_b = \frac{P_T \eta A_T \eta_b}{R^2 \lambda^2}$$

where R = distance from transmitter (meters)

η_b = phase control beam forming efficiency

= 0.95

$$= \frac{P_o A_T^2}{R^2 \lambda^2} \left[\frac{1 - 10^{-\frac{dB}{10}}}{0.23\ dB}\right] \frac{2\left[1 - 10^{-\frac{dB}{20}}\right]^2}{\left[1 - 10^{-\frac{dB}{10}}\right] 0.115\ dB} \eta_b$$

$$P_D = \frac{P_o A_T^2}{R^2 \lambda^2} \left[\frac{1 - 10^{-\frac{dB}{20}}}{0.115\ dB}\right]^2 \eta_b$$

$$\eta = \eta_t \eta_b \eta_a \eta_s \eta_r \eta_d$$

η_t = Efficiency of power transmission, conditioning, conversion (dc - rf) waveguide transmission and radiation out the waveguide slots.

= $1.845 - e^{0.01f}$ for the Amplitron (See p. 12-13 & 12-9 of Ref. 14) where f = frequency in GHz

= 0.8202 for f = 2.45 GHz

η_b = Efficiency of beam formation by the transmitting antenna including effects of phase errors.

= 0.95

η_a = Efficiency of propagation through the atmosphere and ionosphere. (See p. 12-3 & 8 of Ref. 14)

= $1.99 - e^{0.001f}$ for southwest location = 0.9875

= $1.98 - e^{0.002f}$ for northeast location = 0.975

η_s = Beam interception at rectenna

= 0.95 for 10 dB taper

$\frac{\sqrt{A_T A_R}}{\lambda R}$ = r = 1.78 (See Figure 12-3, pg. 12-7 of Ref. 14)

η_r = rf to dc conversion efficiency including losses associated with reflected power and interface to power grid.

= $1.896 - e^{0.022f}$ = 0.8406

$A_R = \frac{\lambda^2 R^2}{A_T} \times 3.1684$

$P_G = P_T \eta_a \eta_b \eta_s \eta_r \eta_d$

η_a = 0.9875 for southwest location

η_b = 0.95

η_s = 0.95

η_r = 0.8406

η_d = 0.903

P_G = 0.676 P_T

$$\eta_d = \frac{2\left[1 - 10^{-\frac{dB}{20}}\right]^2}{\left[1 - 10^{-\frac{dB}{10}}\right] 0.115\ dB}$$

for dB = 10

$$\eta_d = \frac{2\left[1 - 10^{-.5}\right]^2}{(1 - .1) \times 1.15}$$

= 0.903

$$P_{in} = \frac{P_T}{t}$$

$$\eta_t = 0.8202$$

$$P_{in} = 1.219\, P_T$$

$$P_T = 0.391\, P_o\, A_T \quad \text{and for } P_o = 21.7 \times 10^3 \text{ W/m}^2$$

$$P_T = 8480\, A_T$$

$$P_{in} = 10340\, A_T$$

$$P_G = 5732\, A_T$$

$$P_D = 0.51123 \times 10^6 \frac{A_T^2}{R^2}\, \eta_b$$

$$\left\{ \begin{aligned} P_D &= \frac{P_o\, A_T^2}{R^2\, \lambda^2} \left[\frac{1 - 10^{-\frac{dB}{20}}}{0.115\ dB} \right]^2 \eta_b \\ &\equiv \frac{21.7 \times 10^3\, A_T^2}{0.1225^2\, R^2} \left[\frac{1 - 10^{-\frac{10}{20}}}{1.15} \right]^2 \eta_b \\ &= 1.446 \times 10^6 \times .3535\, \eta_b \frac{A_T^2}{R^2} \\ &= 0.51123 \times 10^6 \frac{A_T^2}{R^2}\, \eta_b \end{aligned} \right.$$

$$A_R = 272.5 \frac{R^2}{P_G} \quad \text{(normal to boresite)}$$

$$\left\{ \begin{aligned} A_R &= 3.1684 \frac{\lambda^2 R^2}{A_T} = \frac{3.1684 \times .1225^2 R^2}{P_G/5732} \\ &= 272.5 \frac{R^2}{P_G} \end{aligned} \right.$$

$$D_R = \sqrt{\frac{346.96}{P_G}}\, R \quad \text{(minor axis)}$$

$$A_T = 174.4 \times 10^{-6}\, P_G$$

$$D_T = 0.0149 \sqrt{P_G}$$

PARAMETERS OF MICROWAVE SYSTEMS AS A FUNCTION OF P_G

D_S = 3 dB Spot Size at $R = 37 \times 10^6$ m Km $\frac{1.2\lambda}{D_T} \times 36,608$	P_G = GW	A_T = $157.4 \times 10^{-6} P_G$ m^2	D_T = $0.14157\sqrt{P_G}$ m	A_R = $301.97 \frac{R^2}{P_G}$ (m^2 normal to boresite)	D_R = $\sqrt{\frac{384.96}{P_G}} R$ (minor axis)	$P_D = 511,230 \frac{A_T^2}{R^2} \eta_b \eta_a$ Mainlobe			$P_D \times 10^{-2.4}$ Sidelobes	
						At Ground $\eta_a = 0.9875$ mw/cm^2	At "F" Layer $\eta_a = 1$ mw/cm^2	At "D" Layer $\eta_a = 1$ mw/cm^2	At Ground mw/cm^2 dB Down .24	At Ground mw/cm^2 dB Down 18.5
6.0	4	629,600.	895.	103.349×10^6	10,921.	13.8	13.8	13.9	.055	.2
5.4	5	787,000.	1,001.	82.679×10^6	10,260.	21.7	21.5	21.8	.087	.31
5.2	5.258	827,600.	1,027.	78.622×10^6	10,005.	24.0	23.8	24.1	.096	.34
4.9	6	944,400.	1,096.	68.899×10^6	8,916.	31.2	30.9	31.4	.123	.44
4.5	7	1,101,800.	1,185	57.948×10^6	8,255.	42.5	42.1	42.8	.169	.60
4.2	8	1,259,200.	1,267.	51.674×10^6	7,722.	55.6	55.0	56.0	.222	.78
4.0	9	1,416,600.	1,343.	45.933×10^6	7,281.	70.3	69.7	70.9	.280	.99
3.8	10	1,574,000.	1,416.	41.339×10^6	6,907.	86.7	86.0	87.4	.345	1.22
3.6	11	1,731,400.	1,484.	37.581×10^6	6,848.	105.0	104.2	105.8	.418	1.48

$\eta_b = 0.95, \quad \eta_a = 0.9875$

For 10 dB taper, 10 steps:

First sidelobe is $\simeq$ 26 dB down without outage (Figure 6-14 of NASA CR-134886)

Considering outage to cost 2 to 7.5 dB (Figure 6-15) gives 24 to 18.5 dB down

Limits of theory for Ionospheric effects

"D" region up to $\simeq 3000°K$

equivalent P_D = 40 to 50 mw/cm^2

"F" region

equivalent P_D = 60.to 70 mw/cm^2 (S. W)

> 200 mw/cm^2 (N. E)

Most significant effects are at "F" region

$\therefore$ Limit of theory 70 to 200 mw/cm^2

Projected limits for biological effects at sidelobes = 0.1 to 0.5 and possibly 1.0 mw/cm^2

APPENDIX B

THE EFFECT OF HIGH POWER MICROWAVES ON ION CHEMISTRY

The large increase in electron temperature predicted for power fluxes of 20 mW/cm^2 and greater is likely to cause a significant, noticeable change in the rates of several important ionic reactions. Changes in the neutral chemistry may also occur as a result of the vibrational excitation of nitrogen by thermal electrons.

Dissociative recombination is a process which is known to be effected directly by the increase in temperature. The rate coefficients, α_1, and α_2, for

$$e + NO^+ \xrightarrow{\alpha_1} N + O \qquad \text{(B-1)}$$

and

$$e + O_2^+ \xrightarrow{\alpha_2} O + O \quad , \qquad \text{(B-2)}$$

reactions which play a key role in determining the electron concentration in the E and F-layer, are both inversely proportional to T_e. LeLevier (1970)[1] has shown that long before density changes develop as a result of hydrodynamic effects, modifications in the dominant recombination rates will produce an increase in the electron concentration. If the change in electron temperature δT_e is modeled by an exponential increase

$$\delta T_e / T_{eo} = f \left[1 - e^{-t/t_1}\right] \quad , \qquad \text{(B-3)}$$

where f is the steady state fractional increase, then the change in density will be given by

$$\delta N_e / N_{eo} = f \frac{[M^+]}{\{N_e + [M^+]\}} \cdot \left[1 + \left(t_1 e^{-t/t_1} - t_2 e^{-t/t_2} \right) \Big/ \left(t_2 - t_1 \right) \right] \quad , \tag{B-4}$$

where

$t_2^{-1} = \alpha_{1,2} \left\{ N_e + [M^+] \right\}$. The quantity $[M^+]$ is the combined density of NO^+ and O_2^+ . The rate coefficients for (B-1) and (B-2) are (Banks and Kockarts, 1973A)[2]

$$\alpha_1 = 5 \times 10^{-7} \ (300^\circ \text{ K}/T_e) \quad \text{cm}^3 \ \text{sec}^{-1}$$

and

$$\alpha_2 = 2 \times 10^{-7} \ (300^\circ \text{ K}/T_e) \quad \text{cm}^3 \ \text{sec}^{-1}$$

The density of molecular ions is altitude dependent, varying from 7×10^2 to 3×10^3 cm^{-3} at midnight between 150 and 240 km, and from 1×10^5 to 2×10^4 cm^{-3} at midday over the same range of altitudes. Since the two rates are nearly equal, we can simplify our analysis by considering a two component system of electrons and molecular ions with a single mole fraction weighted reaction rate coefficient, having a value of $3 \times 10^{-7} \ (300^\circ \text{ K}/T_e)$. Equations (B-3) and (B-4) can be used with the results presented in Section 2 and a representative model for the molecular ion concentration (Banks and Kockarts, 1973B)[2] to predict the increase in N_e due to a modification of the dissociative recombination loss process. The results are shown in the Table B-I below:

TABLE B-I. PERCENTAGE INCREASE IN ELECTRON DENSITY FOLLOWING 200 SEC OF HEATING

ALTITUDE (km)	SITE POWER FLUX (mW/cm^2)	NIGHT NORTHEAST 20	NIGHT NORTHEAST 80	NIGHT NORTHEAST 320	NIGHT SOUTHWEST 20	NIGHT SOUTHWEST 80	NIGHT SOUTHWEST 320	DAY SOUTHWEST 20	DAY SOUTHWEST 80	DAY SOUTHWEST 320
210		1.1	3.4	5.1	4.1	5.4	6.6	0.5	1.2	2.7
230		0.3	0.7	1.3	0.9	1.4	1.9	0.2	0.5	1.2
250		0.2	0.3	0.8	0.5	0.8	1.3	0.3	0.6	1.3

It is seen that a few percent increase in electron concentration is expected below the F-layer peak. The net change in N_e consists of this increase and an increase (or decrease, depending on geometry and altitude) due to the hydrodynamic expansion. An additional increase of 2 to 5 percent is expected at altitudes of about 200 km due to hydrodynamic effects alone. The combined effect may produce as much as a 10 percent increase at the base of the F-2 layer. Accurate estimates will require an extension of the existing codes to include the important dissociative recombination processes described earlier. The necessary changes in the ionospheric heating code are straightforward but involved.

A more important effect of microwave heating of the ionosphere may occur as a result of the vibrational and electronic excitation of the neutral components. It is known that excitation of reactants will increase chemical activity (Taylor, 1974)[3] throughout the atmosphere. In particular, impact excitation of the vibrational modes in molecular nitrogen by hot thermal electrons can (Newton et al, 1974)[5] accelerate the production of NO^+ ions through the important reaction

$$O^+ + N_2 \xrightarrow{\gamma_1} NO^+ + N \qquad \text{(B-5)}$$

If the N_2 vibrational temperature T_{VIB} exceeds 1200° K, then a rapid increase occurs in the rate of (B-5), raising its value by an order of magnitude between 1000° K and 3500° K. The increased production of NO^+ ions supplants the slow creation of O_2^+ through the charge-exchange process

$$O^+ + O_2 \xrightarrow{\gamma_2} O_2^+ + O \qquad \text{(B-6)}$$

As a result, electrons now recombine with NO^+ ions as well, accelerating ionization loss by

$$NO^+ + e \xrightarrow{\gamma_1} N + O \qquad \text{(B-7}$$

At the lower electron temperatures in the ambient mid-latitude ionosphere recombination occurs (in the F-layer) through

$$O_2^+ + e \xrightarrow{\gamma_2} O + O \quad , \qquad \text{(B-8)}$$

where molecular oxygen ions are supplied by the charge exchange process (B-6). The rate limiting step is the ion exchange reaction. The rate coefficient for this process (Banks and Kockarts, 1973 A)[2] is

$$\gamma_2 = 1 \times 10^{-11} \sqrt{900^\circ K/T} \quad cm^3\ sec^{-1}$$

while the accelerated rate coefficient for the production of NO^+ is (Newton and Walker, 1975)

$$\gamma_1 = 1 \times 10^{-11} \left(T_{VIB}/3500^\circ K\right)^2 \ cm^3\ sec^{-1}$$

The concentration of NO^+ increases due to electron heating and a density depletion occurs. This may be a far-reaching effect since the vibrational states of N_2 are metastable with very long lifetimes. At F-layer heights, the principal loss of vibrationally excited nitrogen N_2^* is diffusion. Below 200 km the atomic oxygen concentration is large enough to quench N_2^* at a rate that equals or exceeds the diffusion loss process. High velocity winds will transport the vibrationally excited species, N_2 and possibly O_2, far from the region of microwave heating, leaving a wake of depleted ion concentration. Schunk and Banks (1975)[6] estimate the effective lifetime of N_2^* to be 5000 sec. at altitudes above 200 km. If the wind is of order 100 m sec^{-1}, then the excited N_2 molecules will travel approximately 4° of latitude before being quenched by atomic oxygen - a distance of nearly 450 km. This mechanism has been put forth as one of the causes of the trough in electron concentration seen near the equatorward edge of the auroral oval.

It is not possible within the scope of this effort to provide an accurate appraisal of the impact of this change in ion chemistry. We have used the results of Newton and Walker (1975)[5], who calculated the electron density decreases in auroral red arcs due to vibrationally excited nitrogen, to estimate the change in N_e due to this mechanism. Figures B-1 and B-2 illustrate the large decrease in N_e that might be expected for sustained heating in the absence of convective cooling. The results of Newton et al (1974)[4] suggest that it may take hundreds of seconds for the vibrational states to be populated at the altitude of maximum heating. These results may not be representative, in regard to the time constant, in our case inasmuch as the maximum electron temperature in their example was 3500° K. The effect of electron temperature T_e on the electron density depletion at several heights is shown in Figure B-3. The results described in Section 2 predicted temperatures well in excess of 3000° K for a Southwest site geometry. Thus, the results presented herein are considered to be illustrative only. An accurate investigation of the effect of high power microwave transmission on chemistry will require further study. In particular, possible changes in the D-layer neutral temperature and composition must be examined as vibrational excitation of molecules will be far more efficient at these altitudes as shown in Section 2.

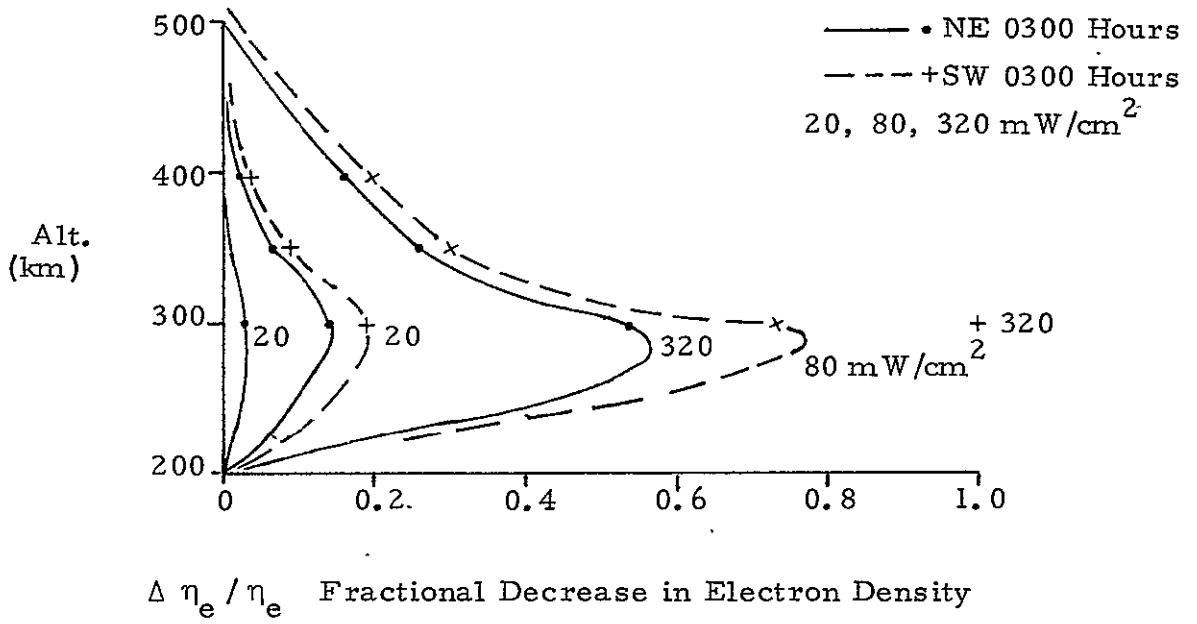

FIGURE B-1. Electron density depletion as a function of altitude for various power fluxes at a typical Northeast (NE) and Southwest (SW) location. The large change in density is due to an accelerated recombination brought about by an increase in the rate of NO^+ production.

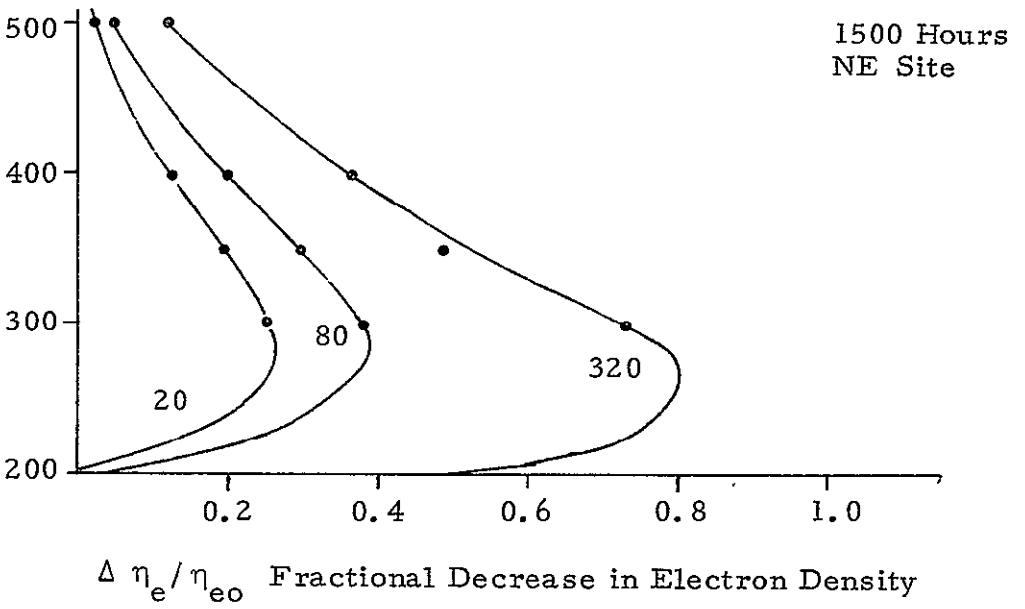

FIGURE B-2. Electron density depletion as a function of altitude at midday for three power fluxes. A Northeast (NE) site geometry is assumed. An increase in NO^+ production produces the indesited decreases.

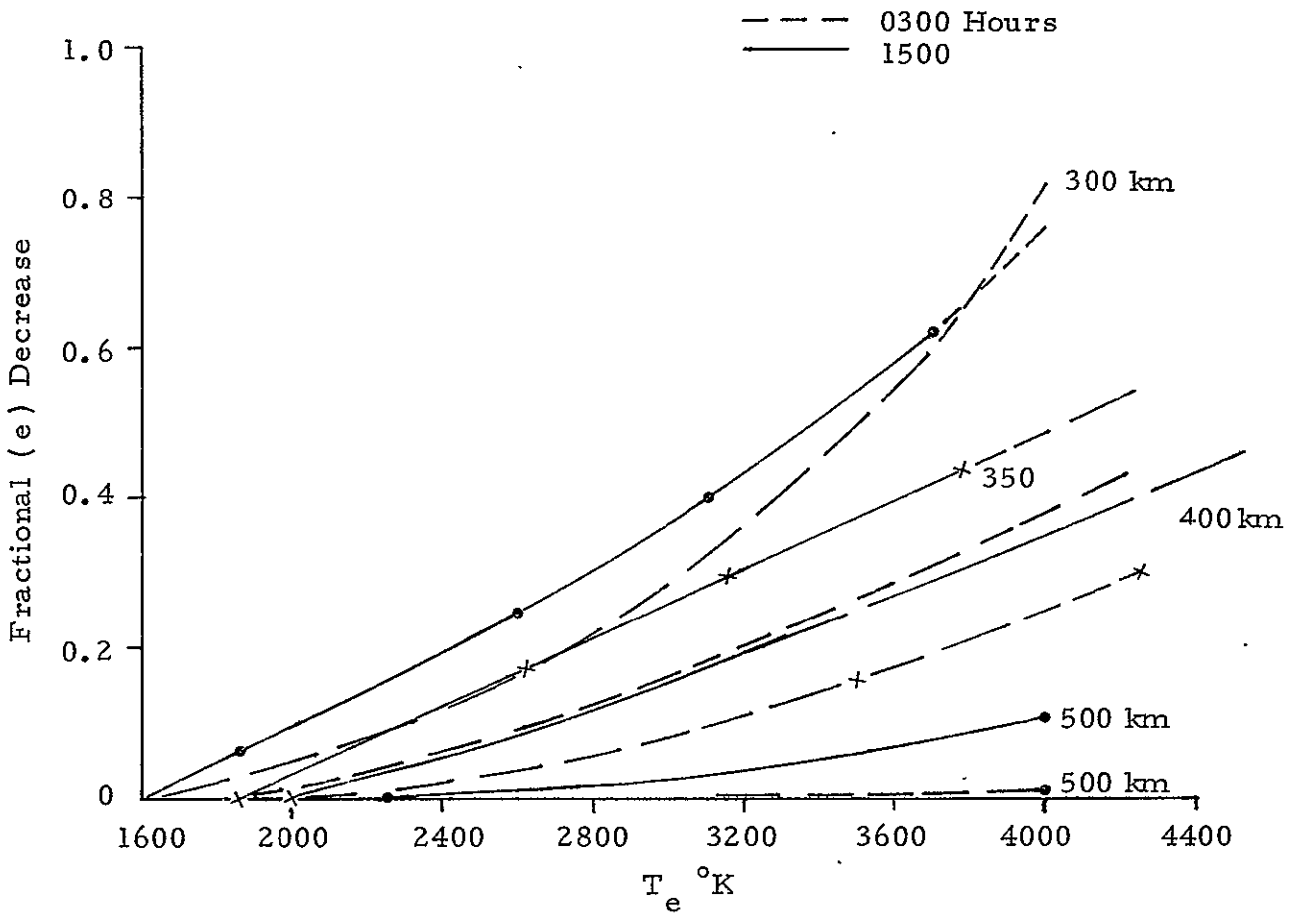

FIGURE B-3. Fractional electron density decreases as a function of electron temperature T_e at the peak of the F-layer and above. Results are shown for night (0300 hours) and midday conditions (1500 hours).

APPENDIX B

REFERENCES

(1) LeLevier, R. E., "Artifical Heating of the Ionosphere - Early Time Phenomena", J. Geophys. Res. 75: 6419 (1970)

(2) Banks, P. M. and Kockarts, G., "Aeronomy", Academic Press, New York, Part A, (1973 A); Part B, (1973 B).

(3) Taylor, R. L., "Energy Transfer Processes in the Stratosphere", Can. J. Chem. 52: 1436 (1974)

(4) Newton, G. P., Walker, J. C. G. and Meijer, P. H. E., "Vibrationally Excited Nitrogen in Stable Auroral Red Arcs and its Effect on Ionospheric Recombination", J. Geophys. Res. 79: 3807 (1974)

(5) Newton, G. P. and Walker, J. G. C., "Electron Density Decrease in SAR Arcs Resulting from Vibrationally Excited Nitrogen", J. Geophys. Res. 80: 1325 (1975)

(6) Schunk, R. W. and Banks, P. M., "Auroral N_2 Vibrational Excitation and the Electron Density Trough", Geophys. Res. Letters 2: 239 (1975)

(THIS PAGE INTENTIONALLY LEFT BLANK)


RAYTHEON
RAYTHEON COMPANY
EQUIPMENT DIVISION